U.PORTO
FEUP FACULDADE DE ENGENHARIA
UNIVERSIDADE DO PORTO

The use of antisense nucleic acid mimics for suppressing microRNAs involved in Gastric Cancer

Joana Filipa Torrinha Ferreira Lima

Dissertation submitted to obtain the degree of

Doctor of Philosophy in Chemical and Biological Engineering

Porto, Mai 2018

The use of antisense nucleic acid mimics for suppressing microRNAs involved in Gastric Cancer

Joana Filipa Torrinha Ferreira Lima

Industrial PhD

Developed in collaboration with Biomode, S.A.

Supervisor:

Nuno Filipe Ribeiro Pinto de Oliveira Azevedo (PhD), LEPABE, Department of Chemical Engineering, Faculty of Engineering, University of Porto.

Co-supervisors:

Laura Isabel Macieira Cerqueira (PhD), Biomode 2, S.A.

Maria do Céu Fontes Herdeiro Figueiredo (PhD), i3S Instituto de Inovação e Investigação em Saúde, University of Porto.

Porto, Mai 2018

This work was financially supported by: Project POCI-01-0145-FEDER-006939 - Laboratory for Process Engineering, Environment, Biotechnology and Energy – LEPABE – funded by FEDER funds through COMPETE2020 – Programa Operacional Competitividade e Internacionalização (POCI) – and by national funds through FCT – Fundação para a Ciência e a Tecnologia and Biomode 2, S.A - Scholarship in Industry SFRH/BDE/51909/2012.



“Imagination is more important than knowledge.
For knowledge is limited, whereas imagination embraces the entire world,
stimulating progress, giving birth to evolution.
It is, strictly speaking, a real factor in scientific research.”

Albert Einstein, 1931

Acknowledgements

First of all, my thanks go to my supervisor, Prof. Nuno Filipe Azevedo, for all the suggestions, ideas and the assistance in improving the structure of this document. I would like to add further thanks to my co-supervisors, Laura Cerqueira and Prof. Céu Figueiredo, who greatly helped me keep the whole thesis in the right course, providing the essential tools to develop this work.

My acknowledgements to both Prof. Carla Oliveira and Joana Carvalho for the suggestions and help in the miRNA field, which laid the foundation of this thesis.

A word of appreciation to Prof. Jesper Wengel for providing me important assistance in the design and synthesis of the nucleic acid mimics.

My gratitude to all my colleagues in i3S, especially to the EPithelial Interactions in Cancer group. Marina Leite, thank you for all the scientific support, advice and challenging conversations. To Joana Marques for being my tutor, and for all the time dedicated during the animal science course. Miguel Marques, thank you for assisting me with the fluorescence microscope. To Inês Ribeiro, the master of the western blots, who greatly contribute for the beautiful blots in this work. To Joana Melo, thank you to be always available to help in every situation. To you all, with no exception, thank you truly for all the support, friendship and good moments shared in i3S/IPATIMUP. You are indeed EPIC!

I would like to acknowledge Gabriela Almeida for the supervision and Carla Pereira for aiding me in the *in vivo* experimental work.

My sincere gratitude to all my colleagues in the Biological Engineering Lab at FEUP for all the help given and the cheerful times. Especially to Anabela Borges, thank you for your support, friendship, and positivism in difficult moments. To Ana Catarina Meireles and Ana Luísa Gonçalves, for sharing this road with me.

Thank you to all the FISH group, especially to Andreia Azevedo and Silvia Fontenete for aiding me in the design of the nucleic acid mimics and above all for your friendship. I also cannot thank

Rita Sobral Santos enough, who greatly help me to keep this thesis on the right path. Thank you for all the trivial conversation and the most profound scientific discussions. For being a dreamer and making me believe that everything was possible. May we continue to share good moments with a good pack of laughs.

My warmest thank goes to the family Biomode. I have been part of this project since the beginning and without a doubt, it was one of the most rewarding experiences at all the levels. Carina Almeida, thank you for all your constant ideas and reviews. Mário Sousa thank you for all the hilarious moments, you are truly a master on choosing Christmas gifts. I particularly thank Rui Rocha with whom I shared since the very beginning this journey at Biomode.

I would like to express my deep gratitude to my family for their love and support, at all times.

To my dearest friends, for their understanding in all my absences. Thank you for being the best!

Finally, my warmest thanks to Aurélien Foissier, who greatly helped me with constant motivation. Thank you for the long and quiet waiting, and most importantly, your love.

To everyone who have contributed to this thesis, both directly and indirectly.

Joana Filipa Lima

Scientific Outputs

Within the scope of this thesis, the following manuscripts have been partially published/submitted in scientific periodicals with referees:

- **Lima, J. F.**, Cerqueira, L., Figueiredo, C., Oliveira, C. & Azevedo, N. F., 2018. Anti-miRNA oligonucleotides: A comprehensive guide for design. *RNA Biology*. (doi: 10.1080/15476286.2018.1445959);
- **Lima, J. F.**, Carvalho, J., Pinto-Ribeiro, I., Almeida, C., Wengel, J., Cerqueira, L., Figueiredo, C., Oliveira, C. & Azevedo, N. F., 2018. Targeting miR-9 in gastric cancer cells using Locked Nucleic Acid Oligonucleotides. Submitted to BMC Molecular Biology Journal;
- **Lima, J. F.**, Maia, P., Cerqueira, L. & Azevedo, N. F., 2018. Comprehensive model for the hybridization dynamics of molecular probes in FISH. In preparation.

Other Scientific Outputs

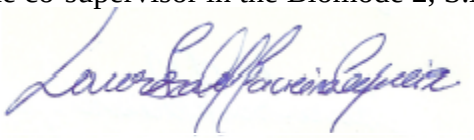
- **Lima, J. F.**, Carvalho, J., Oliveira, C., Cerqueira, L., Figueiredo, C. & Azevedo, N. F. "The Targeting of oncomicroRNAs using Locked Nucleic Acid Oligonucleotides". COST Action 2014, Istanbul, Turkey.

The student	The supervisor
	
Joana Filipa Lima	Nuno Filipe Azevedo

Industrial Outputs

This thesis was developed in collaboration with the company Biomode 2, S.A. where the following relevant outputs were achieved:

- Implementation of a Quality Management System based on ISO 9001:2008 and ISO 13485:2003, 2015-2016;
- Certification by AENOR in both referential systems, 2016;
- Company's product presentation at IAFP *Annual Meeting*, Jun 31 – Aug 3 2016, St. Louis, Missouri, USA.

The student	The co-supervisor in the Biomode 2, S.A.
	
Joana Filipa Lima	Laura Cerqueira

Abstract

Gastric cancer (GC) is one the most incident cancers worldwide and the third leading cause of cancer mortality. It has been demonstrated that in GC, like in most epithelial cancers, the E-cadherin expression is dysregulated. E-cadherin impairment is often associated to invasiveness and metastization and there is increasing evidence that E-cadherin impairment, among other causes, might be due to the activity of overexpressed microRNAs (miRNAs).

MiRNAs are small, non-coding RNA molecules that post-transcriptionally regulate gene expression. They target the 3'untranslated region (3´UTR) of mRNAs, causing essentially its deadenylation and/or translation repression. Overexpressed miRNAs are often associated with the downregulation of several tumor suppressor proteins, and thus being implicated in the pathogenesis of several human diseases, including cancer. There is evidence that miRNA-9 (miR-9) is overexpressed in GC. Also, recent studies show that miR-9 directly influences the E-cadherin protein expression by targeting the 3'UTR mRNA region responsible for the expression of the E-cadherin encoding gene, *CDH1*. However, in order to develop new strategies for cancer treatment a complete study that intensely discloses the role of miRNAs in cancer, and particularly miR-9, is still missing.

Numerous works were published in the past decades showing the potential of anti-miRNA oligonucleotides (AMOs) to target specific miRNAs. Different chemical configurations of antisense oligonucleotides can be used to improve the performance and potency of AMOs, namely by increasing resistance to nucleases and improving target affinity. Moreover, the new generation of AMOs has a great potential to be used *in vivo* in many detection and therapeutic strategies.

This thesis is focused on the role of miR-9 in GC and its influence on the expression of the E-cadherin gene. Several types of LNA anti-miR oligonucleotides (LNA-AMOs) with a complementary sequences to miR-9 were designed and tested regarding their potential to detect miRNAs *in vitro* and *in vivo* using FISH (Fluorescence *in situ* Hybridization) and to silence miR-9.

Abstract

As a result, it was possible to identify and visualize the *in vitro* uptake of low-dosing LNA-based AMOs without any carrier or transfection agent as early as 2h after the application of the AMOs in the media. Furthermore, it was also possible to assess the silencing potential of miR-9 using different LNA anti-miR designs and the consequent effect on E-cadherin expression. Even in a gymnotic setting and applying a relatively low AMO concentration, all the configurations tested were able to rapidly silence to some extent their target, causing a re-expression of E-cadherin.

Keywords: Gastric cancer, miRNAs, anti-miRNA oligonucleotides, LNA-AMOs, E-cadherin, FISH, nucleic acid mimics, miR-9.

.

Resumo

O Cancro Gástrico (CG) é um dos cancros com maior taxa incidência a nível mundial e é a terceira causa de morte mais comum relacionada com cancro. À semelhança de outros cancros epiteliais, a expressão da caderina-E no GC encontra-se alterada. A perda de função desta proteína de adesão celular está frequentemente associada ao aumento da invasão e metastização. Recentemente, foi demonstrado que no CG as células exibem perfis de expressão de microARN (miARN) específicos, capazes de regular negativamente a expressão da caderina-E.

MiARNs são pequenas moléculas de ARN de cadeia simples, não-codificantes, que regulam a expressão genética a um nível pós-transcripcional. Estas moléculas ligam-se de forma complementar à região 3'UTR do ARN mensageiro (ARNm) alvo causando, maioritariamente, a sua repressão e/ou deadenilação. No CG, descobriu-se recentemente que o miARN-9 influencia diretamente a expressão do gene da caderina-E, reprimindo a sua tradução pela ligação à região do ARNm que codifica o gene da caderina (*CDH1*). No entanto, as funções exatas e mecanismos subjacentes ao miR-9 ainda não estão bem estabelecidas, faltando um estudo abrangente a fim de se poder delinear novas estratégias no tratamento do cancro.

Uma abordagem promissora no controlo genético pós-transcripcional para a evolução de novas terapias contra o cancro, prende-se no desenvolvimento de sequências anti-sense tendo por alvo miARNs negativamente regulados. Os anti-miARNs (AMOs) podem atuar como inibidores competitivos de miARNs, negando a sua capacidade de interagir com o ARNm alvo. Novas configurações químicas, como alternativa ao desenho de sequências de ADN, podem ser usadas para melhorar o desempenho e a potência dos AMOs. Estas novas moléculas, usualmente chamadas de mímicos de ácidos nucleicos, devido à sua estrutura química apresentam uma maior estabilidade térmica e poder seletivo relativamente ao seu alvo. Moléculas como o *Locked Nuclei Acid* (LNA) apresentam baixos níveis de toxicidade, podendo ser utilizadas *in vivo* para localização *in situ* de miARNs em células e tecidos.

A fim de determinar as implicações futuras do uso de AMOs para controlo de genes a um nível pós-transcricional, é fundamental avaliar a capacidade destas moléculas para suprimir miARNs

maduros de cadeia simples. Neste trabalho, teve-se especial atenção ao papel do miR-9 no cancro gástrico e à sua influência sobre a expressão do gene da caderina-E. Várias moléculas anti-miARN, contendo especialmente modificações de LNA, foram desenhadas e testadas em relação às suas propriedades para detetar, aplicando FISH, e silenciar *in vitro* e *in vivo* o miR- 9 alvo. Como principal resultado, foi possível identificar e visualizar a internalização *in vitro* de AMOs modificados, utilizando uma concentração relativamente baixa e sem qualquer tipo de moléculas ou agentes de transfeção a assistirem o transporte. Adicionalmente, a internalização destas moléculas foi detetada 2h depois de se aplicar uma solução de hibridação contendo AMOs diretamente ao meio de cultura. Além disso, foi possível também avaliar o potencial dos LNA-AMOs na repressão dos níveis de expressão do miR-9. Todas as configurações de AMOs usadas neste trabalho foram capazes de silenciar o miR-9 e consequentemente afectar a expressão da caderina-E, observando-se um ligeiro aumento na expressão.

Palavras-Chave: Cancro gástrico, miARN, ARN, anti-miARN, LNA-AMOs, caderina-E, FISH, mimicos de ácidos nucleicos, miR-9.

Table of Contents

Acknowledgements ix

Scientific Outputs xi

Industrial Outputs xiii

Abstract xv

Resumo xvii

List of Figures xxiii

List of Tables xxix

Nomenclature xxxi

Chapter 1 Introduction 1

1.1 Problem statement and motivation 1

1.2 Main objectives 3

1.3 Document structure 5

2 Chapter 2 7

Chapter 2 Literature review 7

2.1 MicroRNA biogenesis and function 7

2.2 MiRNAs in GC 11

2.2.1 Cellular function of miRNAs in GC 17

2.2.2 Clinical applications of miRNAs in GC 20

2.3 Controlling miRNAs activity 23

2.3.1 Gain-of-function strategies 23

2.3.2 Loss-of-function strategies 24

2.4 The design of Anti-miRNAs 26

2.4.1 Chemical modifications – AMOs evolution 27

2.4.2 Design Strategies of AMOs 34

2.5 miRNA detection using AMOs 39

2.6 Summary 41

Chapter 3 Materials and methods 43

3.1 Theoretical assessment of a comprehensive model for the hybridization dynamics of molecular probes in FISH 43

3.2 Cell culture and transfection 44

3.3 LNA anti-miR design 45

3.4 LNA anti-miR synthesis 46

3.5 Cellular uptake 47

3.6 Image Quantification 48

3.7 Viability assay 48

3.8 Total RNA extraction 48

3.9 Reverse transcription 49

3.10 Quantitative Real-time PCR 49

3.11 Western Blot analysis 50

3.12 *In vivo* assays 50

3.13 Statistical Analysis 51

Chapter 4 Results and discussion 53

4.1 Theoretical assessment of a comprehensive model for the hybridization dynamics of molecular probes in FISH 53

4.1.1 The journey: from the medium to the target RNA site 55

4.1.2 Diffusion of the MPs in the bulk liquid 59

4.1.3 Diffusion of the molecular probes through the cell membrane and envelope 67

4.1.4 Transport through the cell cytoplasm until the reaction site 71

4.1.5 Reaction of MP with RNA molecules available at the reaction site 73

4.1.6 Summary 75

4.2 Anti-miRNA oligonucleotides design and testing 78

4.2.1 Antisense oligonucleotides design and synthesis 78

4.2.2 Screening of the cell lines for miR-9 content 80

4.2.3 Cellular uptake of AMOs and their effect on cell viability 81

4.2.4 Effect of Anti-miR oligonucleotides in cell viability 85

4.3 Anti-miRNA activity assessment 87

4.3.1 miR-9 relative quantification 87

4.3.2 *CDH1* relative quantification and E-cadherin expression 90

4.4 *In vivo* detection of miR-9..... 92

Chapter 5 Concluding remarks and future perspectives 95

5.1 General conclusions 95

5.2 Future perspectives..... 98

References 101

List of Figures

Chapter 1

Figure 1.1. Schematic representation of the strategy applied in this thesis. A) Design and synthesis of the different chemical configurations used in this thesis; B) uptake and cytotoxic assessment of LNA-based-AMOs in cancer cell lines by Fluorescence in situ hybridization (FISH) and MTT assay, respectively; C) in vitro silencing effect of the developed AMOs to the target miR-9 and its consequences on the expression of the CDH1 mRNA and protein expression by real-time PCR and western blot analysis; D) in vivo testing: silencing effect of the AMOs on the tumor development and miRNA in vivo detection. 5

Chapter 2

Figure 2.1. MiRNA biogenesis. Formation of a primary miRNA structure (pri-miRNA) by RNA polymerase II and III (Pol II/III), followed by Drosha's cleavage, resulting in a pre-miRNA. The pre-miRNA is then exported to the cytoplasm by Exportin-5/Ran complex (Exportin), where it is transformed in a loop-free homoduplex miRNA by the action of Dicer-TRBP. After association of the RLC complex comprised essentially by Dicer-TRBP-Ago2, the ds-miRNA is loaded into Ago2 (mediated by Hsp90), where is further processed to a mature single-stranded miRNA (guide strand). The RISC complex is then guided by the miRNA to the target complementary mRNA, leading to mRNA cleavage, translational repression or deadenylation. Upon RISC binding, other important proteins may associate to the Ago2, like GW182, to assist on the silence of the mRNA. DGCR8: Microprocessor complex subunit DGCR8 (DiGeorge syndrome critical region 8); Dicer: Double-strand-specific ribonuclease; TRBP: Trans-activation-responsive RNA-binding protein; Ago2: protein argonaute-2; Hsp90: Heat shock protein 90-KDa; RLC: RISC-loading complex; RISC: RNA-induced silencing complex; (n)AAAAA: poly-A tail of RNA; m7GpppN: 7-methyl guanosine cap structure of RNA. 9

Figure 2.2. Different functional roles of miRNA. A) Overexpression of miRNAs (oncomiR) targeting mRNAs that regulate the translation of tumor suppressor proteins promotes cancer development. B) Under-expression of miRNA with a tumor-suppressing profile leads to an increase of oncoproteins (red squares), also responsible for tumor formation. The question marks represent any perturbation on miRNA levels, which can occur at any stage of the miRNA biogenesis, leading either to its overproduction or degradation. TSGene: tumor suppressor gene; $_{(n)}$AAAAA: poly-A tail of RNA; m7GpppN: 7-methyl guanosine cap structure of RNA (adapted from Esquela-Kerscher et al.[72])..... 12

Figure 2.3. Loss-of-function strategies: miRNA sponges (A), miRNA Masking (B) and anti-miRNA oligonucleotides (C).ORF-Open Reading Frame..... 24

Figure 2.4. Chemical modifications applied in the AMOs design. Unmodified nucleotides – DNA: deoxyribonucleic acid, RNA: ribonucleic acid; Sugar modifications - 2'-OMe: 2'-O-methyl, 2'-F: 2'-fluoro-RNA, LNA: Locked Nucleic Acid, UNA: Unlocked Nucleic Acid, and 2'-MOE: 2'-O-methoxyethyl; Backbone modifications – PO: phosphodiester, PS: phosphorothioate, PACE: phosphonoacetate, PMO: Phosphorodiamidate Morpholino Oligomers, and PNA: Peptide Nucleic Acid. In red is highlighted the site and the type of modification..... 27

Figure 2.5. AMOs design flowchart: from the identification of target miRNA to the validation of anti-miRNA oligonucleotides. 36

Chapter 3

Figure 3.1. Representative images of the different cell lines used in the assay. HEK293 cell line (A); HeLa (B) and MKN74 (C) cell lines; all images were acquired with x100 amplification. .. 44

Chapter 4

Figure 4.1. Analogy between the oxygen transfer model and the diffusion/reaction model. (A) Oxygen transfer from the gas bubble to the cell cytoplasm and subsequent reaction: (1) Transfer

from the interior of the bubble to the gas–liquid interface; (2) Movement across the gas–liquid interface; (3) Diffusion through the relatively stagnant liquid film surrounding the bubble; (4) Transport through the bulk liquid; (5) Diffusion through the relatively stagnant liquid film surrounding the cells; (6) Movement across the liquid–cell interface; (7) Transport through the cytoplasm till the site where the reactions take place; (8) Biochemical reactions involving oxygen consumption. Adapted from Blanch and Clark10; (B) Molecular probe transport model in FISH: (1) MP diffusion through the medium until the cell membrane; (2) Membrane uptake of MP; (3) Cytoplasm diffusion within the cells until the nucleus; (4) Reaction between MP and target RNA. 56

Figure 4.2. Representation of the Brownian motion in one-dimension. A) MP random walk along th x axis with equal probability to move a distance δ or – δ at each time-step. B) Probability (p(x,t)) to find a particle in a time interval at a distance δ from its origin. 60

Figure 4.3. Schematic representation of the MP diffusion in the bulk. l is the mean distance between the cell-centers, where the maximum distance for a MP to encounter a cell is l/2. This distance was further corrected by removing the diameter of each cell-type, considering the cell in the center of the cube, in a vertical or in a horizontal orientation (for non-spherical cells). Considering a three-dimensional movement of MPs, the mean square displacement ($< r (n)^2 >$) is the hypotenuse of Pythagoras's theorem for the given geometric volume ($r(n)^2 = ((l /2)^2 + h^2)$). . 64

Figure 4.4. Variation of the diffusional characteristic time (s) of a 10bp MP with the cellular size of most bacteria and animal cells (in radius, μm) and the bulk cellular concentrations (cells/mL). 66

Figure 4.5. Cellular membrane differences between gram-negative and gram-positive bacteria, and animal cells. The schematic representation is at scale considering the cell sizes displayed in Table 3. The bacterial cells are represented 5 times bigger than their real size. 68

Figure 4.6. Representative output of a miR-9 versus gene of interest query using the TargetScan database. 78

Figure 4.7. Expression profile of miR-9 (A) and E-cadherin (B) in the cell lines used in this study; * represents a statistically significant difference from the control ($p < 0.05$). 80

Figure 4.8. Representative images of the FISH assays using MKN74 cells treated with AM_LNA_PS sequence at different concentrations (FAM_AM_LNA_PS/5nM; FAM_AM_LNA_PS/50nM and FAM_AM_LNA_PS/100nM) in a hybridization solution containing 0.5M of urea. The hybridization step was performed at 37 ºC for 2 hours, followed by a washing step during 30 minutes. Cells without any sequence were used as a negative control (control). All images were acquired using an x200 amplification (A). Average fluorescence intensity for the FAM_AM_LNA_PS sequence at 5nM, 50nM, and 100 nM (B); the fluorescent signal intensity is expressed in arbitrary fluorescent units (AFU); * significantly different from control (*P < 0.05, **P<0.01, ***P<0.001); ns – not significantly different from control (P>0.05). 82

Figure 4.9. Representative images of the FISH assays using MKN74 cells treated with SC_LNA_PS_50nM sequence at different concentrations of urea in the hybridization solution, and washing times (SC_LNA_PS_0.5M/30min; SC_LNA_PS_0.5M/60min; SC_LNA_PS_2M/30min, and SC_LNA_PS_2M/60min). The hybridization step was performed at 37 ºC for 2 hours. All images were acquired using an x200 amplification (A). Average fluorescence intensity for the SC_LNA_PS sequence using different concentrations of urea in the hybridization solution (0.5M and 2M) and different washing times (30 min and 60 min) (B); the fluorescent signal intensity is expressed in arbitrary fluorescent units (AFU); * significantly different from control (*P < 0.05, **P<0.01, ***P<0.001); ns – not significantly different from control (P>0.05). 83

Figure 4.10. FAM_AM_LNA_PS at 100 nM applied directly into the medium after2h (A), 4h (B), 8h (C) and 48h (D) of hybridization. The image was acquired using an x400 amplification and a ZEISS ApoTome.2 with a medium grid for optical sections of the fluorescent image. 84

Figure 4.11. MTT viability assay results for the three different cell lines treated with different concentrations of FAM_AM_LNA_PS oligonucleotide sequence (A) and FAM_SC_LNA_PS sequence (B). The control is related to the cells without any Anti-miR oligonucleotide treatment. Error bars correspond to the standard deviation of the mean determined for three independent

experiments. No statistically significant differences were found regarding cells treated with AM_LNA_PS or SC_LNA_PS and the control (p>0.05)..... 86

Figure 4.12. MTT viability assay result for MKN74 cells treated with higher concentrations of FAM_AM_LNA_PS sequence. Error bars correspond to the standard deviation of the mean determined for two independent experiments. No statistically significant differences were found regarding cells treated with FAM_AM_LNA_PS or FAM_SC_LNA_PS and the control (p>0.05). 87

Figure 4.13. Relative quantification of miR-9 expression by qRT-PCR for the MKN74 cells treated with the control sequences: SC_LNA_PS and GN_LNA_PS (A) and AM_LNA_PS, AM_LNA_2OMe_PS, AM_LNA_Pal_PS (B) sequences. Error bars correspond to the standard deviation of the mean determined for three independent experiments. *significantly different from control (*P < 0.05, **P<0.01, ***P<0.001). 88

Figure 4.14. Relative quantification of CDH1 mRNA levels by qRT-PCR for the MKN74 cells treated with AM_LNA_PS, AM_LNA_2OMe_PS, AM_LNA_Pal_PS and SC_LNA_PS sequences after 4, 8, 12 and 24h of incubation (A). E-Cadherin protein level measured by western blotting, extracted from MKN74 cells subjected to the same conditions above (B). All the results were normalized against the situation without any treatment (MKN74 WT) and the respective endogenous control; *significantly different from control (*P < 0.05, **P<0.01, ***P<0.001). 91

Figure 4.15 *In vivo* imaging using AM_LNA_PS sequence at 2μM in a hybridization solution containing 0.5M of urea in 900 mM of NaCl (A). MKN45 cell in a 24-well plate incubated with FAM_AM_LNA_PS sequence at 2μM (red square); the white square is the control with MKN45 cells incubated a PBS solution (B). The imagens were acquired using an IVIS Lumina series III microscope. The scale bar indicates the epi-fluorescence intensity: dark red corresponds to high fluorescence signal and yellow low fluorescence signal. 93

Figure 4.16. Representative images of FISH in depparafinized tumors. The left tumor corresponds to the control situation with PBS (A) and in the right tumor an AM_LNA_PS at 2μM in a hybridization solution containing 0.5M of urea was administrated (B). The images were acquired

using an x200 amplification using a ZEISS ApoTome.2. All images were taken at equal exposure times, with overlapping of the DAPI channel, to stain the nucleus. 94

List of Tables

Chapter 2

Table 2.1 Dysregulated miRNAs in tissues validated for GC 13

Table 2.2 Role of miR-9 and its validated targets in different cancer types 16

Table 2.3 Properties of the different chemical modifications applied to AMOs……..37

Chapter 4

Table 4.1 Direct comparison between the different steps proposed in the oxygen uptake model and the MP diffusion model, presented in this work 58

Table 4.2 Characteristic diffusional times in the bulk solution..... 65

Table 4.3 Size of the different layers for Bacteria and animal cells, using E. coli as a model for Gram negative bacteria, B. subtilis for Gram positive and HeLa for animal cells 69

Table 4.4 Summary of the characteristic times given for 10bp and 40 bp MPs in each diffusional barrier 75

Table 4.5 Anti-miR sequences used in this work and respective theoretical melting temperatures. LNA nucleotide monomers are represented by the symbol + before the nucleotide, 2'-OMe-RNA monomers in small caps letters, DNA nucleotides in capital letters, and palmitoyl-amino-LNA by the symbol*, FAM-fluorescein. 79

Nomenclature

Acronyms

2’F	Fluorine 2’-hydroxyl group
2’MOE	Methoxyethylated 2’-hydroxyl group
2’OMe	Methylated 2’-hydroxyl group
3’UTR	3’Untranslated Region
AA	Amino acids
Ago2	Argonaut protein-2
AJ	Adherens junctions
Akt	Protein kinase B
AMO	Anti-miRNA Oligonucleotide
APD	Photo-diode detector
ASGPR	Asialoglycoprotein receptor
ASO	Antisense Oligonucleotide
Bcl-2	B-cell lymphoma 2 apoptosis regulator protein
BCL2L11	Bim-encoding gene
Bim	Bcl-2-like protein 11
bp	base-pair
CA	California State
CCND2	Cyclin D2-encoding gene
CCR4-NOT	Transcription complex subunit
CDH1	E-cadherin-encoding gene
CDK	Cyclin-dependent kinase
CDKN1	Cyclin-dependent kinase inhibitor 1
CpG	Deoxycytidine-deoxyguanosine
CPP	Cell-Penetrate Peptides
DAPI	4',6-Diamidino-2-Phenylindole, Dihydrochloride dye
DCP2	m^7GpppN-mRNA decapping Protein 2
DGC	Diffuse gastric cancer
DGCR8	DiGeorge syndrome Critical Region 8
DMSO	Dimethyl sulfoxide
DNA	Deoxyribonucleic Acid

Nomenclature

ds-miRNA	Double-stranded miRNA
E-Cadherin	Epithelial cadherin protein
EGC	Early gastric cancer
elF-4E	Eukaryotic translation initiation factor 4E
EMT	Epithelial-mesenchymal transition
EZH2	Enhancer of Zeste Homolog 2–encoding gene
FAM	Fluorescein
FDA	Food and Drug Administration
FISH	Fluorescence *in situ* Hybridization
FRAP	Fluorescence recovery after photobleaching
G1/G2	Growth-phase 1/2
GalNAc	N-Acetylgalactosamine
GAPDH	Glyceraldehyde 3-phosphate dehydrogenase
GC	Gastric Cancer
GFP	Green fluorescent protein
HCV	Hepatitis C virus
HDGC	Hereditary Diffuse Gastric Cancer
Hsp90	heat shock protein 90-kDa
ISH	*in situ* hybridization
LNA	Locked Nucleic Acid
LPS	Lipopolysaccharide
M phase	Mitotic phase
m^7GpppN	7-methyl guanosine cap structure
MA	Massachusetts State
MET	Mesenchymal-epithelial transition
miRNA/miR	microRNA
MMP	Matrix metalloproteinase
mRNA	Messenger RNA
MTT	3-(4,5-Dimethylthiazol-2-yl)-2,5-Diphenyltetrazolium Bromide
MSD	Mean-square displacement
MP	Molecular Probe
NIR	Near-infrared fluorescence
nt	Nucleotides
ORF	Open reading frame
OTR	Oxygen transfer rate

OUR	Oxygen uptake rate
PABPC	Cytoplasmic poly(A)-binding Protein
PACE	Phosphonoacetate
PAN2-PAN3	PAB-dependent poly(A) specific ribonuclease
PBS	Phosphate-buffered saline
PDCD4	Programmed cell dead protein 4
PI3K	Phosphatidylinositol 3-kinase
PMO	Phosphorodiamidate Morpholino Oligomer
PNA	Peptide Nucleic Acid
PO	Phosphodiester
pre-miRNA	precursor miRNA
pri-miRNA	primary miRNA
PS	Phosphorothioate
PT	Portugal
PTEN	Phosphatase and tensin homolog
RECK	Reversion-inducing cysteine-rich protein with Kazal motifs
RISC	RNA-induced silencing complex
RLC	RISC-loading complex
RNA	Ribonucleic Acid
RNAi	RNA interference
RUNX3	Runt-related transcription factor 3-encoding gene
S phase	DNA replication phase
shRNA	Short-harpun RNA
TLR9	Toll-like receptor-9 gene
TRBP	RNA-binding domain proten
TX	Texas State
UNA	Unlocked Nucleic Acid
USA	United States of America
VCSEL	Vertical cavity surface emitting laser
VEGF	Vascular Endothelial Growth Factor
XRN1	Cytoplasmic 5’-to-3’ exoribonuclease
ZEB	Zinc finger E-box-binding homeobox encoding gene
ZEN	N, N-diethyl-4-(4-nitronaphthalen-1-ylazo)-phenylamine

Symbols

a	Motion characterization constant
C^*_{O2}	Relative to equilibrium concentration of oxygen
C_{O2}	Concentration of O_2 (kgm^{-3} or $molm^{-3}$)
D	Diffusion coefficient ($m^2\ s^{-1}$)
D’	Diffusion coefficient inside the membrane ($m^2\ s^{-1}$)
D_0	Diffusion coefficient in water ($m^2\ s^{-1}$)
D_{cyto}	Diffusion coefficient in cytoplasm ($m^2\ s^{-1}$)
D_{peri}	Diffusion coefficient in periplasm ($m^2\ s^{-1}$)
K	Boltzmman’s constant ($m^2.Kg.s^{-2}.K^{-1}$)
k_1	Association reaction constant of second order kinetics ($M^{-1}s^{-1}$)
k_2	Dissociation reaction constant of first order (s^{-1})
KLa	Volumetric oxygen mass transfer coefficient (s^{-1})
M_w	Molecular weight (kg/mol)
n_{MP}	Number of molecules
q_{MP}	Specific MP uptake rate (mol MP kg−1 s−1)
Rh	Average hydrodynamic radius of the biggest crowders
rh	Average hydrodynamic radius
rp	Hydrodynamic radius of the spherical particle
T	Temperature (K or ºC)
t	Time Period (s or min)
T_H	Hybridization temperature (ºC)
T_m	Melting temperature (ºC)
V	Volume for diffusion (m^3)
δ	Displacement
ΔG^o	Free Gibbs Energy (J)
η	Solvent viscosity (Pa·s)
η_0	Viscosity in water (Pa·s)
ξ	Average distance between the surfaces of proteins

Chapter 1

Introduction

1.1 Problem statement and motivation

Gastric Cancer (GC) is the third leading cause of cancer-related mortality worldwide[1]. The development of GC is highly associated with the accumulation of genetic and epigenetic changes in combination with environmental factors[2]. Indeed, the diffuse gastric cancer (DGC) results mainly from the deregulation of E-cadherin due to genetic or epigenetic alterations, whereas the intestinal type is often associated with infection by *Helicobater pylori (H. pylori)*, and environmental factors such as obesity, dietary factors, and smoking. The ability of cancer cells to separate from the main tumor and evade adjacent tissues is intimately related to the loss of E-cadherin expression[3–5]. E-cadherin is a transmembrane protein and the major component of the adherent junctions, which plays a central role in the establishment and maintenance of epithelial cell-cell adhesion[6]. Emerging evidence established E-cadherin as a tumor suppressor and the functional loss of E-cadherin is regarded as a major factor in tumor progression and invasion in

epithelial cancers, including gastric cancer[7–9]. Indeed, E-cadherin inactivation is the most well-established defect in GC. In hereditary diffuse-type of GC (HDGC) and in sporadic GC with a diffuse component, the mechanisms that contribute to E-cadherin impairment are associated mostly with intragenic mutations, E-cadherin-encoding gene (*CDH1)* locus deletions and promoter methylation. In fact, over 40% of HDGC cases present a germline mutation on *CDH1* gene, and almost 50% of the diffuse gastric carcinomas present *CDH1* somatic mutations[10–12] Germline mutations in *CDH1* occurs in most GCs of both diffuse and intestinal type, and other mechanisms may occur to explain the overall defects on E-cadherin expression, such as miRNA posttranscriptional regulation.

GC cells have been shown to display a specific miRNA expression profile, where in an analysis of a miRNA profile of 37 GC specimens and 4 normal gastric mucosas, miR-9 was found to be overexpressed[13]. Moreover, there is accumulating evidence that miR-9 overexpression may be repressing the *CDH1* gene, leading to tumor progression and invasion.[14].

Taking into consideration these evidences, the work presented in here aimed to study specifically the relationship between miR-9 overexpression and E-cadherin dysregulation by using the model of gastric cancer as a proof-of-concept.

The potential of miRNAs as a tool for the detection and therapeutics in gastric cancer has been highlighted by a number of studies[15–18]. These findings opened an opportunity to develop innovative strategies for a better understanding of the mechanics behind the miRNA role in several biological functions and more specifically in cancer deregulation occurrences. One of the most promising approaches to control miRNA expression is linked to the use of antisense oligonucleotides to target dysfunctional miRNAs. AMOs can act as competitive inhibitors of miRNAs, denying their ability to interact with and repress target mRNAs[19].

Many studies using various types of chemically-modified antisense oligonucleotides, such as Locked Nucleic Acid (LNA), have been reported[20–24] as good candidates to be used in therapeutics and detection strategies involving miRNAs, due to their improved chemical structure[22,25,26]. LNAs are characterized by increased thermal stability, resistance to nucleases and improved target affinity towards the RNA target. Depending on the sequence design, LNA also show low toxicity effects, being prone to be used *in vivo*[20,24,27].

Here, an approach that targets miR-9 involved in GC using nucleic acid mimics was pursued. Complementary sequences to miR-9 were developed and tested using *in vitro* and *in vivo* models to assess their ability to inhibit single miRNAs with important implications for future development of target therapeutics.

This thesis is integrated in a broader project that aims to develop new diagnostic methods based on nucleic acid mimics technology. So far, the work has led to the publication of several papers, patents and the foundation of a spin-off – Biomode, S.A – that now acts as a partner of this PhD project. The main supervisor, Nuno F. Azevedo, is one of the founders of Biomode and he is now involved in the COST Action TD1004 on theragnostics, funded by the European Community. Céu Figueiredo (co-supervisor, i3S/IPATIMUP) has expertise in *H. pylori* and gastric cell culture techniques and Laura Cerqueira (co-supervisor and co-founder of Biomode) on hybridization methods of nucleic acid mimics. The work plan also benefited from synergies established with leading European researchers such as Jesper Wengel (University of Southern Denmark), expert in the synthesis and design of nucleic acid mimics; and Carla Oliveira (i3S/IPATIMUP) expert in miRNAs and in the molecular determinants of sporadic and hereditary forms of gastrointestinal cancer.

1.2 Main objectives

The main goal of this work was to develop AMOs to target specifically overexpressed miR-9 believed to be involved in the downregulation of E-cadherin in GC. This study aimed to test the ability of the designed AMOs to detect the target miRNA and their potency to silence miR-9 activity.

Prior to the experimental work, a comprehensive model for the hybridization dynamics of molecular probes (MPs) in FISH was developed. The main goal of this extensive study was to define the limiting step for diffusion of the MPs by calculating the characteristic time associated to each diffusional barrier encountered by the molecular probes in a FISH procedure.

In order to achieve the experimental goals proposed in this thesis the following strategy was settled as represented in the figure 1.1.

Introduction

A. Design and synthesis of different anti-miRNA oligonucleotide sequences

The first task of the experimental work was to design and develop different oligonucleotide sequences complementary to the miR-9 that specifically targets the 3'UTR (untranslated region) mRNA that encodes the E-cadherin gene (Figure 1.1 A). Complementary AMOs were designed taking into consideration optimal sequence length, specificity to the target and theoretical melting temperature.

B. Cellular uptake and cytotoxicity assessment

After the design, the synthesized sequences were tested to assess their ability to enter the cells and detect specifically the target miRNA by placing miR-9-positive cells in the presence of the AMOs. The cellular uptake was monitored by fluorescence microscopy at different time points (Figure 1.1 B). In this task, the cytotoxic profile of the synthesized AMOs was also assessed by preforming a cell viability assay, using different concentrations of AMOs (Figure 1.1 B).

C. Silencing effect of anti-miR oligonucleotides

MiR-9-positive cell lines were treated with the AMOs and the expression of both miR-9 and *CDH1* mRNA were evaluated by qRT-PCR to assess the silencing effect of the developed AMOs (Figure 1.1 C). Furthermore, the E-cadherin protein expression was analyzed by Western Blot to monitor the effect of miR-9 silencing. It was expected that the developed AMOs would be able to effectively reduce the miR-9 expression levels on the cell models used, and consequently lead to a re-expression of E-cadherin.

D. *In vivo* assessment

Although extremely valuable to address simple biological questions, *in vitro* systems such as mono-cellular cultures are limited for the understanding of cellular behavior and tissue interactions. Therefore, nude mice models were used in this study to further highlight the potential use of AMOs for the *in vivo* detection of miRNAs and to observe the effect of AMOs-mediated miR-9 knockdown on tumor formation and metastasis (Figure 1.1 D).

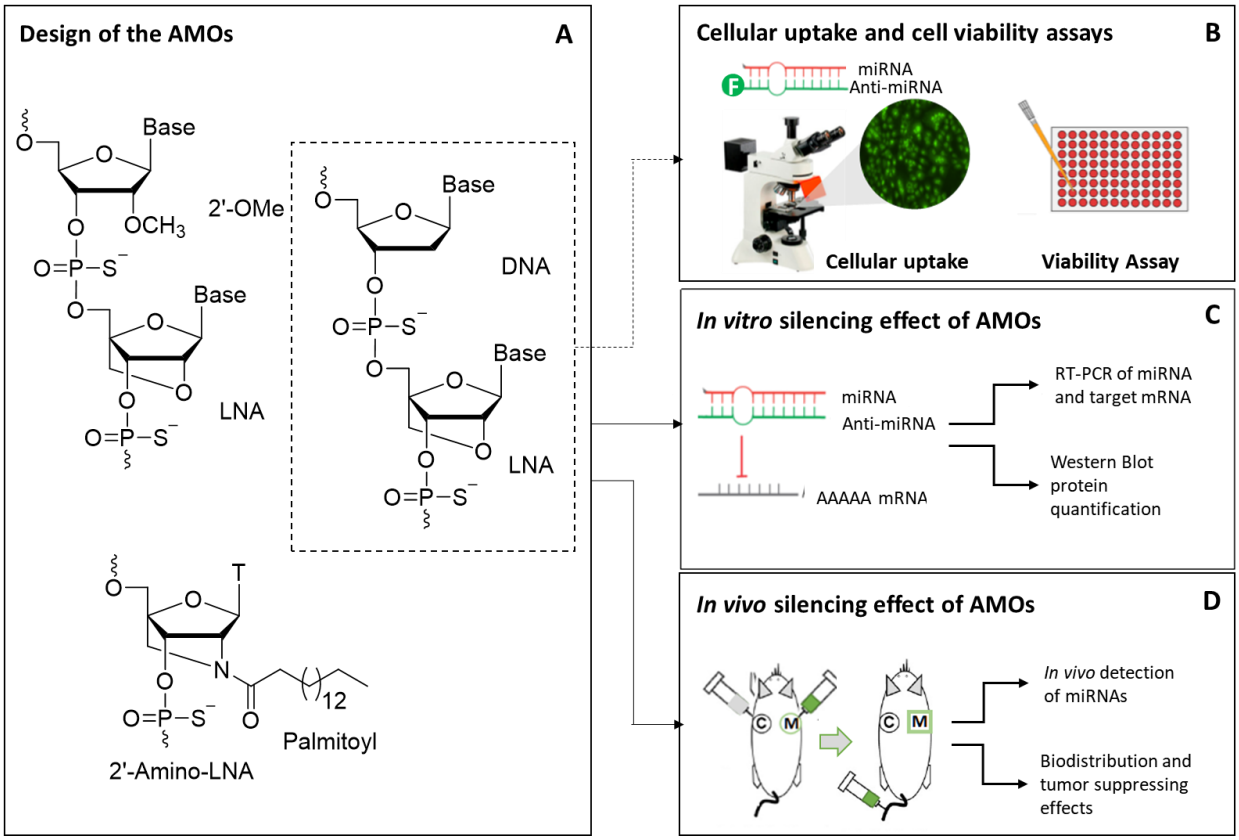


Figure 1.1. Schematic representation of the strategy applied in this thesis. A) Design and synthesis of the different AMOs used in this thesis; B) uptake and cytotoxic assessment of LNA-based-AMOs in cancer cell lines by Fluorescence in situ hybridization (FISH) and MTT, respectively; C) in vitro silencing effect of the developed AMOs to the target miR-9 and its consequences on the expression of the CDH1 mRNA and protein expression by real-time PCR and western blot analysis; D) in vivo testing: silencing effect of the AMOs on the tumor development and miRNA in vivo detection.

1.3 Document structure

The thesis is divided in 5 chapters. In the first and current chapter are stated the main goals, motivation and the overall organization of this manuscript.

The following chapter is a literature review describing the state-of-the-art on miRNAs biogenesis and function, as well the latest advances on AMO designs for detection and therapeutics.

Chapter 3 includes all the materials and methods used to develop this work and in chapter 4 is discussed the main results achieved, highlighting the potential of AMOs to be applied both *in vitro* and *in vivo* for the detection and silencing of miRNAs.

The last chapter is dedicated to the general conclusions of this work and to the future perspectives identified within the course of this thesis.

Chapter 2

Literature review

2.1 MicroRNA biogenesis and function

MiRNAs are small, single-stranded and noncoding RNAs, with approximately 21 nucleotides (nt) that regulate gene expression at a posttranscriptional level. They complementarily bind to the 3'UTR of their target messenger RNAs (mRNAs) causing their degradation, translational repression, and/or deadenylation (Figure 2.1) [28–30].

In most eukaryotic cells, the miRNA processing unleashes a silencing response specific to a target RNA sequence, so-called RNA interference (RNAi). The RNAi pathway is an important cellular process to control gene expression, triggered endogenously by the conversion of double-stranded RNA sequences into miRNAs[31]. MiRNA transcription starts in the nucleus, typically from intronic or intergenic regions of DNA, with the formation of a primary structure called pri-miRNA as a result of the action of RNA polymerase II or RNA polymerase III [32,33] (Figure 2.1). The pri-miRNA

has a long stem and loop structure that is shortened to a precursor miRNA (pre-miRNA) with ~60 nt by ribonuclease-III Drosha together with the DGCR8 protein (Microprocessor complex subunit DGCR8: DiGeorge syndrome critical region 8)[34,35]. The pre-miRNA is then exported to the cytoplasm via the Exportin-5/Ran complex[36,37], where it is further processed by another ribonuclease-III enzyme named Dicer (Double-strand-specific ribonuclease)[38–41] into an imperfect miRNA duplex with unpaired nucleotides (Figure 2.1). In the cytoplasm, the pre-miRNA is recognized and cleaved by Dicer with the assistance of TRBP (Transactivation-responsive RNA-binding proteins), forming a smaller double-stranded miRNA (ds-miRNA) with 21-27nt. After the cleavage, the ds-miRNA dissociates from and re-associates with Dicer at a different position with the help of TRBP. Although there are some studies reporting that TRBP is not absolutely necessary for miRNA biogenesis, recent evidences reinforce that the TRBP increases the RNA-binding affinity of Dicer and enhances cleavage accuracy, especially in a crowded environment[42]. The protein argonaute-2 (Ago2)[43] is further associated to this complex, forming a loading complex (RLC)[44], which assists in the assembling of an RNA-induced silencing complex (RISC). The ds-miRNA is then transferred to the Ago2 in a process mediated by Hsp90 (heat shock protein 90-KDa), which maintains the Ago2 in an open conformation in order to receive the miRNA, forming a pre-RISC complex. Inside Ago2, the two miRNA strands are separated and the passenger strand is removed. The selection of the guide strand from a ds-miRNA is not arbitrary. The strand whose 5’ end is less stable serves as guide, whereas the other is discarded (the so called “asymmetry rule”). It is believed that TRBP senses the asymmetry of the ds-miRNA, and positions the miRNA in an orientation that allows a correct strand selection and loading into the Ago2 proteins.

Finally, the RISC complex is then directed by the mature miRNA to the complementary mRNA[45] (Figure 2.1). In the case in which the RISC binding is perfectly complementary to the target mRNA, the mRNA will be cleaved by Ago2. This process is frequently found in plants, where miRNAs share high homology to the 3’UTR of mRNAs. Conversely, in mammals, the RISC normally binds partially to the complementary mRNA. The seed region at positions 2-7 from the 5’-end of the miRNA sequence, is often fully paired and essential for the interaction. Due to this partial complementarity, translation repression and/or mRNA deadenylation pathways (Figure 2.1)[29,46,47] are preferred rather than mRNA cleavage[48]. After silencing, the miRNA remains intact and able to target other mRNA molecules with the same complementarity degree.

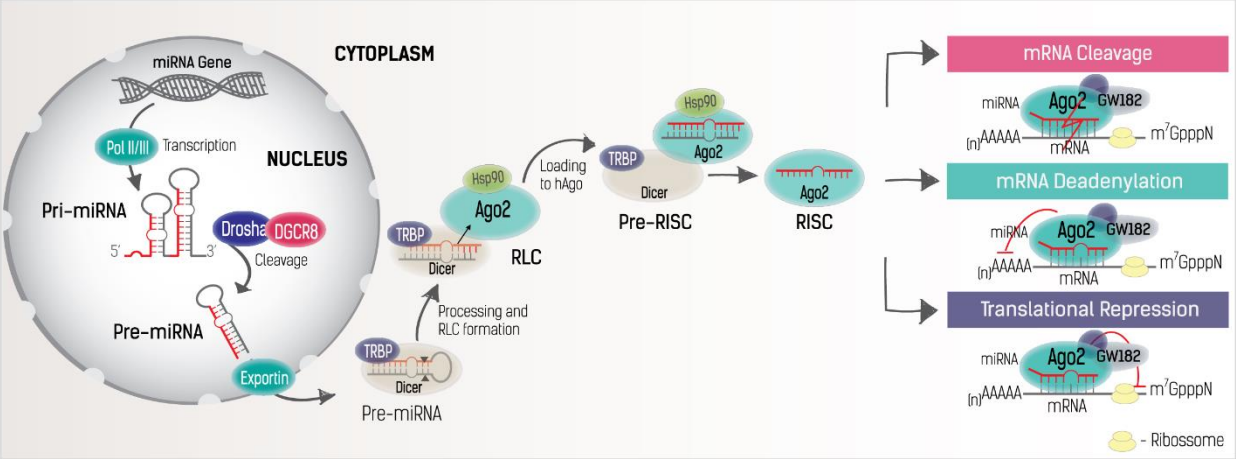


Figure 2.1 MiRNA biogenesis. Formation of a primary miRNA structure (pri-miRNA) by RNA polymerase II and III (Pol II/III), followed by Drosha's cleavage, resulting in a pre-miRNA. The pre-miRNA is then exported to the cytoplasm by Exportin-5/Ran complex (Exportin), where it is transformed in a loop-free homoduplex miRNA by the action of Dicer-TRBP. After association of the RLC complex comprised essentially by Dicer-TRBP-Ago2, the ds-miRNA is loaded into Ago2 (mediated by Hsp90), where is further processed to a mature single-stranded miRNA (guide strand). The RISC complex is then guided by the miRNA to the target complementary mRNA, leading to mRNA cleavage, translational repression or deadenylation. Upon RISC binding, other important proteins may associate to the Ago2, like GW182, to assist on the silence of the mRNA. DGCR8: Microprocessor complex subunit DGCR8 (DiGeorge syndrome critical region 8); Dicer: Double-strand-specific ribonuclease; TRBP: Trans-activation-responsive RNA-binding protein; Ago2: protein argonaute-2; Hsp90: Heat shock protein 90-KDa; RLC: RISC-loading complex; RISC: RNA-induced silencing complex; (n)AAAAA: poly-A tail of RNA; m7GpppN: 7-methyl guanosine cap structure of RNA.

Translation repression and/or mRNA deadenylation processes are intimately connected and although the precise translation repression mechanism is still unclear, the deadenylation and consequent mRNA decay mediated by miRNA are better understood. The RISC complex of miRNAs can trigger mRNA deadenylation that leads to decapping and ultimately to mRNA decay. The deadenylation process starts with the association of Ago2 proteins present in the RISC complex to a GW182 protein which is responsible for the recruitment of cytoplasmic deadenylase complexes: PAN2–PAN3 (PAB-dependent poly(A)-specific ribonuclease subunit PAN2 and PAN3) and CCR4–NOT (transcription complex subunit)[49]. Deadenylated mRNAs are then

decapped by DCP2 (m^7GpppN-mRNA hydrolase)[50]. Without the protection of the poly-A tail, mRNAs are ultimately degraded by the cytoplasmic 5′-to-3′ exoribonuclease, XRN1.

To understand how miRNAs might repress translation and consequently lead to mRNA decay, it is desirable to go a step back and have a short overview of the normal mRNA translation mechanism. Translation is a multistep process beginning with the recruitment of ribosomal subunits to the mRNA, leading to the initiation, elongation, and termination of the translation. A cap-dependent translation, which is the most frequent process for translation, requires an mRNA with a 5'-cap and a poly-A tail. The 5'-cap is recognized by the cap-binding protein, eIF4E (Eukaryotic translation initiation factor 4E), part of the eIF-4F initiation complex. The eIF-4F complex is responsible for recruiting the 40s ribosomal subunit to the mRNA, which is then checked for the initiation codon to start translation. The assembly of the 60s subunit is then followed by the elongation phase. The cytoplasmic poly-A-binding protein (PABPC) also play an important role in the translation. PABPC proteins recognize the poly-A tail and interact with eIF4F complex, forming a circular structure essential to protect the mRNA from degradation and thus leading to an effective translation.

Several studies are trying to elucidate how miRNA interact with the mRNA translation machinery and its correlation with mRNA deadenylation and decay[51–55]. A common ground of understanding is that miRNAs can inhibit cap-dependent translation at the initiation phase. More likely, miRNAs seem to interfere with the 5'-cap elF4F complex. The first studies indicate that deadenylation is the cause of the translation depression. Deadenylated mRNAs fail to assume the circular conformation due to the action of GW182 proteins on PABPC[56,57] and therefore contribute to the repression and decay of mRNA. However, in 2006[54], it was demonstrated that although the two mechanisms are intimately connected, deadenylation and translation repression can function independently[54]. MiRNAs can repress the translation before the deadenylation step occurs, albeit the extension of the repression on deadenylated mRNAs seem to be higher comparison to the one observed in mRNAs containing the poly-A tail [55].

It is evident that miRNAs work together in a regulatory network, where clearly their mechanism of post-transcriptional regulation plays an important role in the control of mRNA levels. Up to now, more than 35,000 mature miRNAs have been identified across 223 species, from which 2603

entries (from 1881 hairpin miRNA precursors) belong to *Homo sapiens*[58–61]. It is believed that at least 60% of human genes are regulated by miRNAs, and that they are involved in the regulation of almost every biological process[62]. It comes with no surprise that many miRNAs are associated with several human diseases and have already been identified in different pathologies including neurological disorders, cardiovascular diseases, inflammatory processes, and cancer[63]. In the latter case, more than half of the miRNA genes are located in specific genomic regions frequently associated with cancer development and progression[64]. MiRNAs are able to control the expression levels of oncogenes and tumor suppressor genes, modulating apoptosis, cell migration, and angiogenesis.

2.2 MiRNAs in GC

In cancer, miRNAs can act both as oncomiRs and as tumor suppressors (Figure 2.2)[65–68] depending on their target gene. Several miRNAs have been reported to be dysregulated in GC (Table 2.1.), where carcinogenesis is promoted either by the overexpression of miRNAs with oncogenic activity (oncomirs) (Figure 2.2 A) or by the low expression of miRNAs with tumor suppressor activity (Figure 2.2, B)[69–74].

The overexpression of oncomiRs results in the repression of tumor suppressor genes. Silencing overexpressed miRNAs has been reported to reduce proliferation, induce apoptosis, and to hinder the invasive and metastatic potential of cancer cells. Conversely, the under-expression of miRNAs with tumor suppressor activity results in the expression of oncoproteins. Restoring the miRNA levels to a normal expression profile leads, as well, to a regression of the carcinogenesis both *in vivo* and *in vitro*.

In Table 2.1 is provided an extensive list of validated overexpressed and under-expressed miRNAs in GC, among which onco-miR-21 and tumor suppressor-miR-200 family are discussed as an example of key miRNAs associated with GC. Further examples are revised in the next sections to demonstrate the impact of miRNA regulation in cancer, according to the cellular function of the genes they control, and their clinical significance in GC.

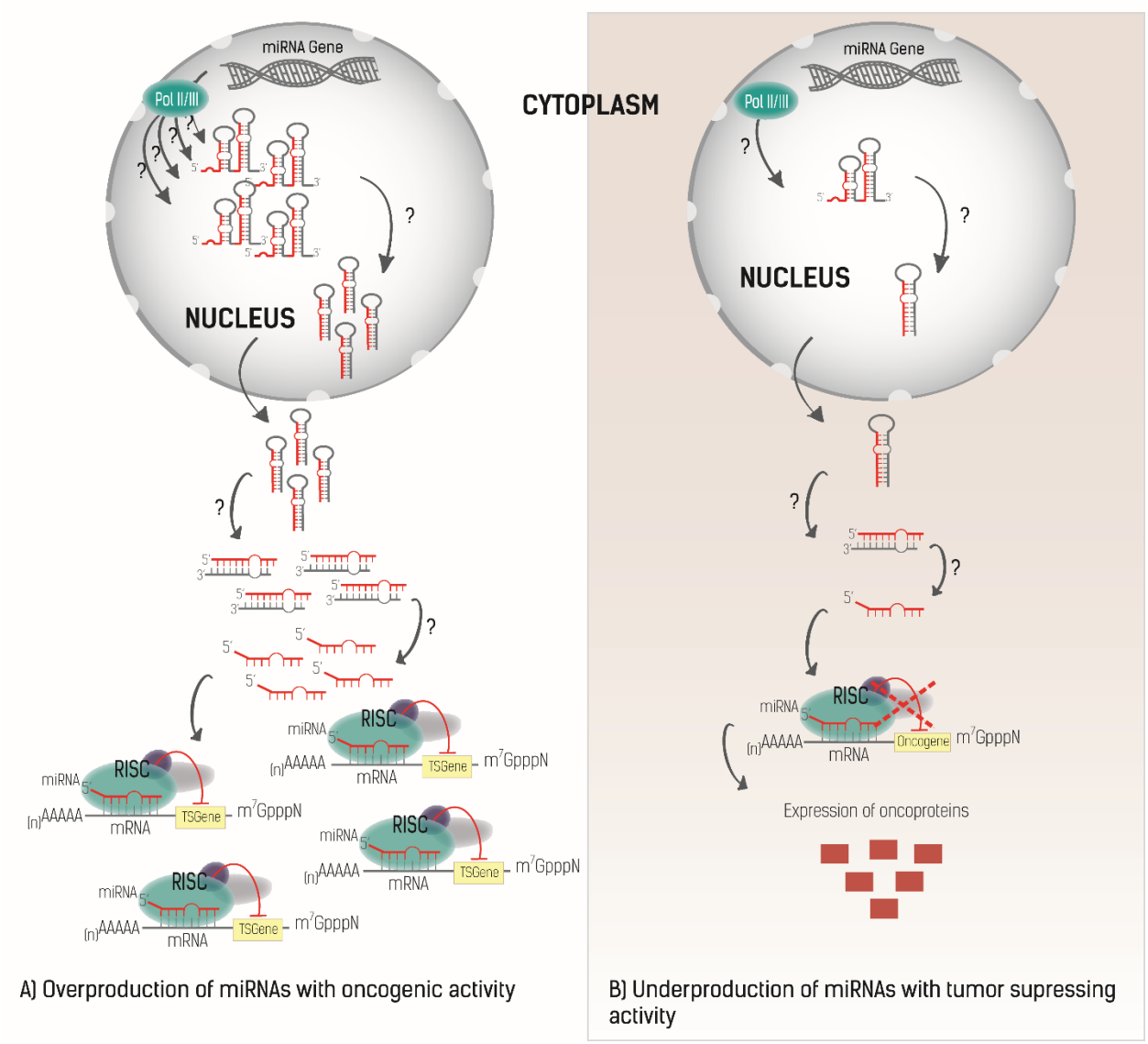


Figure 2.2. Different functional roles of miRNA. A) Overexpression of miRNAs (oncomiR) targeting mRNAs that regulate the translation of tumor suppressor proteins promotes cancer development. B) Under-expression of miRNA with a tumor-suppressing profile leads to an increase of oncoproteins (red squares), also responsible for tumor formation. The question marks represent any perturbation on miRNA levels, which can occur at any stage of the miRNA biogenesis, leading either to its overproduction or degradation. TSGene: tumor suppressor gene; $_{(n)}$AAAAA: poly-A tail of RNA; m7GpppN: 7-methyl guanosine cap structure of RNA (adapted from Esquela-Kerscher et al.[71]*).*

Table 2.1 Dysregulated miRNAs in tissues validated for GC

miRNA Role	miRNAs in GC	References
OncomiR (overexpressed)	miR-15b-5p, -17-5p/20a, miR-17-92 cluster, -18 a, -20, -21, -23a/b, -25	[15,75–97]
	miR-27a, -92, -93, -106a, miR-106b~93~25 cluster, -107, -125b, -130b	
	miR—145, 148a, -150, -181b/c, 196a/b, -196a-5p, -199a-3p, -199a-5p	
	miR_-215, miR-221~222 cluster, -223, -362, -370, -423-5p	
Tumor suppressor miRNA (under-expressed)	let-7a, miR-1, -16, -22, -24, -27b, -29 family, -30a-5p, -31, -33b-5p	[98–117]
	miR-34b/c, -34c-5p, -101, -124/a, -125a-3p/-5p, -126, -128b, -129	
	miR-129-2, -132-3p, -137, -142-5p, -143, -148a/b, -155, -185, -193b	
	miR-195, -200 family, -204, -204-5p, -206, -210, -212, -219-2-3p	
	miR-219-5p, -320a, -326, -328, -331-3p, -335, -338-3p, -365, -365, -367	
	miR-375, -378, -449, -455, -486, -490-3p, -495, -551a,-503, -516a-3p	
	miR-532, -542-3p, -610, -613, -874, -941, -1207-5p, -1247, -1266	
Double role	miR-9, -10b, -146a, -183, -218, -223	[75,118–125]

The aberrant expression of miR-21 has been identified in several types of cancer, including GC. In GC, overexpressed miR-21 is known to downregulate the following tumor-suppressor genes: *RECK* (reversion-inducing cysteine-rich protein with Kazal motifs), *PDCD4* (programmed cell death protein 4) and *PTEN* (phosphatase and tensin homolog)[89,126–129]. *RECK* negatively regulates the matrix metalloproteinase-9, -2, and -14 (MMP-9, -2, -14) involved in cancer progression by suppressing MMP secretion and enzymatic activity[126]. *PDCD4* is significantly downregulated in various human cancers, and has been associated with a poor patient prognosis[128]. It is also involved in the apoptotic machinery, which suppresses cell transformation, tumorigenesis and invasion. *PTEN* is a well-stablished tumor suppressor that antagonizes the PI3K-AKT/PKB signaling pathway, which regulates cell survival and proliferation via activation of PI3K (phosphatidylinositol 3-kinase) and Akt (Protein Kinase B), and thereby modulating cell cycle progression[127]. It has been demonstrated that by silencing miR-21 it is possible to upregulate the

tumor suppressor genes mentioned above, inhibiting cellular proliferation, apoptosis, invasion and metastasis.

Overall, the reduced expression of the tumor suppressor-family-miR-200 has been associated with metastasis and invasion. The miR-200 family is composed by five members arranged as two clusters: miR-200a/200b/429 and miR-200c/141, and known to target *ZEB1* and *ZEB2* (encoding Zinc finger E-box-binding homeobox 1 and 2, respectively) oncogenes[107,130]. It has been demonstrated that ectopic expression of the miR-200 family, individually or as clusters, hindered EMT (epithelial-mesenchymal transition) progression by downregulating directly both *ZEB1* and *ZEB2* genes, which are well known as transcriptional repressors of E-cadherin. Furthermore, an *in vitro* overexpression of miR-200 family reverted dramatically the EMT process by up-regulating E-cadherin and thus promoting the mesenchymal-epithelial transition (MET) mechanism, where the cellular phenotype morphologically changed from mesenchymal (more mobile and invasive phenotype) to epithelial with formation of adherens junctions[107]. Additionally, the downregulation of the cluster miR-200a/200b/429 has also been implied in multidrug resistance of GC cells. Exogenous expression of miR-200a/200b/429 sensitized human drug-resistant gastric cells to chemical-induced apoptosis, by directly downregulating the anti-apoptotic proteins encoded by *BCL2* and *XIAP*[131].

At a first glance, the regulatory mechanism of miRNAs seems simple: a specific miRNA either is an oncomiR or a tumor suppressor-miRNA. However, in the same tissue there is evidence that miRNAs can present both roles targeting different genes during cancer progression. Furthermore, the events that regulate the carcinogenesis are often transversal to different types of cancer, and this way the same miRNA can be implicated in different tumors, with common regulatory pathways. It is the case of miR-9, which has been described in a myriad of cancers. MiR-9 in humans can be transcribed from three independent genomic loci, resulting in three pri-miRNAs (miR-9-1, miR-9-2 and miR-9-3). Those three pri-miRNAs can be further processed to give rise to two functional mature miRNAs: miR-9-3p and miR-9-5p, being the later the most investigated mature miR-9. Consequently, the expression levels of miR-9-5p is highly variable across cancers, being either upregulated or downregulated. The same miRNA can behave as oncogene or tumor suppressor gene in the same type of cancer, depending on the type of alteration, cell type or transcriptional/posttranscriptional events. Due to their small size, point mutations are less probable

to occur, and the main mechanisms for miRNA inactivation or activation seem to be correlated with homozygous deletions, the combination mutation plus promoter hypermethylation (in case of miRNA inactivation/underexpression) or gene amplification (in case of miRNA activation/overexpression). In GC, miR-9 has been reported to function both as a tumor suppressor and as oncomiR (Table 2.2). As a tumor suppressor, miR-9 targets the oncogenes: *RAB34, NFKB1*, *CCND1*, and *ETS1*; and as an oncomiR targets the *CDX2* gene (Table 2.2)[18,118,132,133]. Hongchun Luo *et al.*[132] showed that the miR-9 expression was directly linked to the *RAB34* gene, encoding the Ras-related protein Rab-34. Rab-34 is a small GTPase protein member of the *RAS* oncogene family that regulates aggregation, junction, and fusion of vesicles in exocytosis and endocytosis. The ectopic expression of miR-9 in gastric cell lines led to a decrease of Rab-34 expression.

The same was observed in the work of Hai-Ying Wan et al.[18], regarding the *NFKB1* gene, which is responsible for the regulation of immune responses, embryo and cell-binding development, cell-cycle progression inflammation, and tumorigenesis. The authors established the relationship between miR-9, *NFKB1* and the vascular endothelial growth factor (VEGF). The re-expression of miR-9 in gastric cell lines, decreased the expression of the NF-kB1 factor, which in its turn downregulated VEGF, resulting in the inhibition of the invasion and metastasis of tumorigenic cells. Overexpression of *CCND1* gene (encoding cyclin D1, an oncoprotein from the family of G1 cyclins (see section 2.2.2.1)) is often associated with carcinogenesis at early stages and is a prognostic indicator of poor survival in cancers like breast cancer[134]. Ets-1 is a transcription factor that directly controls the expression of a wide variety of genes that regulate differentiation, proliferation, and invasion[135]. Restoring the expression levels of miR-9 in GC cells, attenuated the proliferation, migration, and invasion of cancer cells, by knocking down the expression of cyclin D1 and Ets-1[133].

Regarding the oncogenic activity of miR-9, Rotkrua *et al.*[118] suggested that the downregulation of *CDX2* by miR-9 might contribute to cell proliferation in GC. The *CDX2* gene encodes a caudal-type homeobox protein 2 involved in the differentiation and maintenance of the intestinal epithelial lining[136].

Table 2.2 Role of miR-9 and its validated targets in different cancer types

miR-9 role	Type of cancer	miR-9 targets	References
Onco-miRNA	Colorectal Cancer	*CTNNA1*	[137]
	Breast Cancer	*CDH1*	[14,138,139]
	Gastric Cancer	*CDX2*	[118]
	Liver Cancer	*TLN1*, *CDH1*, *KLF17*	[140–142]
	Bladder Cancer	*LASS2*	[143]
	Leukemia	*HES1*, *MLL*	[144,145]
	Osteosarcoma	*GCIP*	[146]
	Glioblastoma Multiforme (GBM)	*MAPKAP/MAPK14/MAPKAP3*	[147]
	Squamous cell carcinoma: Esophageal Cancer and Skin Cancer, respectively	*CDH1*, *CTNNA1*	[120,148]
Tumor Suppressor	Colorectal cancer	*TM4SF1*, *UHRF1*	[149,150]
	Breast Cancer	*NOTCH1*	[151]
	Gastric Cancer	*NFKB1*, *RAB34*, *CCND1* and *ETS1*	[18,120,132]
	Liver Cancer	*WWTR1*, *IL6*, *AP3B1*, *TC10*, *ONECUT2*, *IGF2BP1*, *MYO1D*, *ANXA2*	[152,153]
	Cervical Cancer	*CKAP2*, *HSPC159*, *IL6*, and *TC10*	[154]
	Lymphoblastic leukemia	*FGFR1* and *CDK6*	[155]
	Ovarian Cancer	*NFKB1*	[156]
	Oral squamous cell carcinoma	*CXCR4*	[157]
	Melanomas	*NFKB1*	[119]
	Medulloblastoma	*HES1*	[158]
	Neuroblastoma	*MMP14*	[159]

The role of *CDX2* in GC is still unclear. At an initial stage, it is reported to function as an oncogene, which expression is associated with the development of intestinal metaplasia, a premalignant lesion with high risk to evolve to a gastric carcinoma[160,161]. During cancer progression, the expression of *CDX2* progressively decreases, suggesting it might function as a tumor suppressor and a prognostic marker[134].

The double role of miRNAs is an interesting example that highlights the importance of carrying out a comprehensive characterization of the role of miRNAs in cancer and their post-transcriptional mechanisms in mRNA regulation. This would allow to develop new strategies in cancer treatment and cutting-edge therapies specifically designed to control oncomirs or to promote the expression of miRNA with tumor suppressing activity.

2.2.1 Cellular function of miRNAs in GC

As seen above, miRNAs are frequently associated with carcinogenesis, and indeed more than half of the miRNA genes are located in specific genomic regions involved in cancer, modulating cell proliferation, apoptosis, cell migration, invasion and metastasis[64]. In the following sections, the main miRNAs involved in the regulation of the different cellular functions in GC are discussed in more detail.

2.2.1.1 Cell proliferation, cell cycle progression and apoptosis

Increased cell proliferation, altered cell cycle progression or dysregulated apoptosis are cellular events that arise from the silencing of genes involved in the cell cycle or apoptotic pathways.

The progression of the cell cycle is regulated by cyclins and cyclin-dependent kinases (CDKs). CDKs are only active when the partner cyclin is present, and are responsible for coordinating the entry of target proteins into the different phases of the cell cycle: growth (G1/G2 phase), DNA replication (S phase), and mitotic phase (M phase)[162]. Cyclin-CDK inhibitors, where the members from the cyclin-dependent kinase inhibitor 1 (*CDKN1A, CDKN1B, CDKN1C*) are included, are able to arrest the cell cycle by binding to, and inactivating, cyclin-CDK complexes. Dysregulated

miRNAs promote tumor progression by upregulating cyclins or by downregulating cyclin-CDK inhibitors. Tumor suppressors, such as miR-29a and miR-206, have been reported to be downregulated in GC leading to the overexpression of oncogenes. MiR-29a targets *SAPCD2*, which encodes a mitosis phase-dependent expression protein, responsible for the G2/M cell cycle progression and proliferation[163]. MiR-206 targets *CCND2* (encoding cyclin D2) responsible for accelerating the cancer progression from the G1 to the S phase. Moreover, cyclin D2 overexpression correlates with GC poor prognosis[164].

On the other hand, two overexpressed miRNAs clusters: miR-106b~93~25 (where miR-106b and miR-93 both directly target *CDKN1A*, and miR-25 targets *CDKN1B*), and miR-221~222 (both known to target *CDKN1B* and *CDKN1C*) have been reported to promote cyclin-CDK activity by downregulating CDK inhibitors of the *CDKN1* family, and thereby stimulating G1 to S phase progression[94]. Moreover, miR-17-5p, -18a, and miR-20 have also been reported as inhibitors of *CDKN1* expression[97].

Apoptosis can be initiated through one of two pathways: an intrinsic pathway regulated by Bcl-2 (B cell lymphoma 2) superfamily; or by an extrinsic pathway, triggered by surrounding cells through the activation of specific pro-apoptotic death receptors on the cell surface. Both apoptotic pathways induce cell death by activating caspases (caspases-3, -6 and -7) that are responsible for the undifferentiated degradation of proteins. In the intrinsic pathway, also called the mitochondrial pathway, the balance between the activity of pro-apoptotic proteins (encoded by *BCL2L11*, *BAX*, *BID, BAK* or *BAD*) and anti-apoptotic proteins (encoded by *BCL2L1* and *BCL2*), members of the Bcl-2 family is a pivotal factor for regulation of the apoptosis[162].

The miR-106b~93~25 cluster is also involved in apoptosis, where miR-25 is responsible for the downregulation of Bim, a pro-apoptotic protein encoded by *BCL2L11*, leading to cell proliferation. Moreover, oncomiR-130b have also been reported to be overexpressed and to inhibit apoptosis by targeting *RUNX3* in GC cells, and consequently suppressing Bim expression[85]. *RUNX3* is known to activate apoptosis by induction of Bim expression.

Conversely, downregulated miRNAs, such as miR-204 and miR-497 have been shown to target directly the anti-apoptotic Bcl-2-like protein 1 (encoded by *BCL2*), and thus positively regulate the apoptosis[99,165,166]. Another miRNA worth mentioning as an apoptotic regulator is the miR-

375, which is one of the most described downregulated miRNAs in GC. MiR-375 is responsible for the regulation of *PDK1*, which encodes a 3-phophoinositide-dependent protein kinase directly involved in the PI3K/Akt signaling pathway[125]. Restoring the expression of miR-375 induces apoptosis by downregulating *PDK1*.

2.2.1.2 Cell migration, invasion and metastasis – the case of E-cadherin dysregulation

Cell migration, invasiveness and metastasis are essential processes for cancer cells to detach from the primary tumor and become mobile and invasive. E-cadherin is an epithelial transmembrane type-I cadherin of approximately 120 kDa responsible for a calcium-dependent cell-cell adhesion[167]. Human E-cadherin is encoded by the *CDH1* gene and is composed by three major domains: a single transmembrane domain, a cytoplasmic domain of about 150 amino acids (AA), and an ectodomain of approximately 550 AA, concealing five tandemly repeated domains[7]. The binding of calcium ions occurs at these domains, conferring to the protein a rigid conformation and thus mediating cell-cell adhesion. Cell-cell adhesion is in this way achieved by extracellular interactions between cadherin proteins of adjacent cells (trans-interaction). The interaction stability of the adhesion is also dependent on a cis-interaction between cadherin molecules within the same cell, partially mediated by the transmembrane domain[168,169]. The cytoplasmic domain interacts with different catenins (α-, β- and γ-) forming a cadherin-catenin complex[170]. The α-catenin is associated with actin filaments, which contributes to the stability of the complex designated as Adherens Junctions (AJ).

Genetic or epigenetic alterations on the E-cadherin gene leading to its functional loss are highly associated with the EMT process, by which tumor cells acquire a motility phenotype. Epithelial cells undergoing EMT with concomitant loss of E-cadherin become invasive, and are able to migrate to different tissues, contributing this way to metastasis[8].

Several miRNAs are implicated in the E-cadherin/EMT process regulation either by directly targeting *CDH1* or by targeting key EMT-inducing transcription factors, which in turn indirectly regulates E-cadherin expression (miR-200 family example presented above). Moreover, Carvalho *et al*.[13] demonstrated that the loss of miR-101 is associated with *EZH2* (enhancer of zeste homolog 2) overexpression, causing the loss of E-cadherin expression, specifically in intestinal-type GC[13].

The *EZH2* gene encodes a histone methyltransferase that is associated with the silencing of tumor suppressor genes, such as *CDH1*.

On the other hand, some miRNAs act as EMT enhancers. Overexpression of miRNA-27 is known to upregulate the EMT-associated genes *ZEB1, ZEB2,* and *SNAI2*, inducing this way EMT, and consequently repressing E-cadherin expression in GC[171].

Additionally, in breast cancer it was reported that the myc and N-myc proto-oncogene proteins, directly induces the miR-9 expression, which in its turn targets the *CDH1* gene. The upregulation of miR-9 leads to the concomitant downregulation of E-cadherin[172], promoting EMT and cell motility/invasiveness. More recently, it has been observed that in GC the myc oncoprotein is also overexpressed, and directly influences the miR-9 expression. It is believed that upregulated miR-9 in GC, contributes to the E-cadherin[173] impairment in the same way as it is observed in breast cancer.

2.2.2 Clinical applications of miRNAs in GC

2.2.2.1 miRNAs as diagnostic and prognosis biomarkers

At early stages, GC patients are often asymptomatic, leading to a late diagnosis of the disease. As a consequence, the diagnosis of an advanced clinical condition hampers the success of treatment and cancer eradication. Moreover, the standard detection practice for GC relies on endoscopy with biopsy, an invasive procedure that patients tend to avoid, contributing this way to a late diagnosis. Also, the current cancer biomarkers present poor specificity, sensitivity, and stability to be used as an efficient and reliable noninvasive methodology for cancer detection. To address these issues, miRNAs are arising as a new class of biomarkers for early cancer detection and prognosis[174]. MiRNAs can be released by exosomes, from the main tumor to the circulating fluids, including blood, urine, and gastric juice. Furthermore, circulating miRNAs are easy to detect, stable in fluids and their expression levels in GC patients have been reported to be significantly different from healthy individuals. All these factors evidence the potential use of miRNAs as diagnostic biomarkers[175].

The first work reporting the expression levels of a group of circulating miRNAs, identified miR-17-5p, miR-21, and miR-106a/b as significantly upregulated, while let-7a as significantly downregulated in the plasma of GC patients[176]. These miRNAs, were subsequently validated as potential GC biomarkers, since high levels of circulating miR-21 are associated with tumor size, histological type, lymph-node metastasis and tumor stage; and the overexpression of miR-17-5p and miR-106a/b in peripheral blood is closely related to high proliferation rate of cancer cells[77,176–178].

Another noteworthy example is the identification of four highly expressed miRNAs, miR-103, miR-107, miR-194, and miR-210 in human diffuse gastric cancer (DGC) serum[179]. High levels of miR-103 and miR-104 were transversely observed during cancer progression, from early to advance stage, implying their used as biomarkers in diagnosing the of DGC stage.

In the intestinal-type of GC, miR-32, miR-182 and miR-143 were also implicated in cancer progression and stage of the tumor, and may be a potential diagnostic biomarkers for this type of cancer[180]. Furthermore, miRNA-199a-3p was identified as a potential biomarker of early gastric cancer (EGC), since miRNA-199a-3p was overexpressed in the plasma of pre-operative EGC patients, compared to healthy individuals, and its levels were dramatically reduced in post-operative patients[81].

The prognosis of GC depends mainly on the probability of recurrence of the disease and on the extension of the metastasis. Li *et al*. reported that a seven-miRNA signature (composed by miR-10b, miR-21, miR-223, let-7a, miR-338, miR-30a-5p and miR-126) is related to relapse-free and overall survival among GC patients[181]. Moreover, high expression of miR-192a-3p and low expression of miR-142-5p are also more likely to indicate relapse or recurrence of GC patients. MiRNA profile studies demonstrated that differentially expressed circulating miRNAs are associated with the prognosis of GC patients. For instance, high expression levels of miR-10b and miR-21 are associated with a high metastasis risk and poor clinical outcomes[84,182]. It was also reported that the probability of survival was significantly lower in patients with high expression levels of miRNA-20b or miRNA-150[183]. Additionally, the downregulation of miR-451, miR-218, miR-145, or miRNA-125a-3p are associated with a poor survival outcomes[104,123,184], and high

levels of miR-20a, miR-25, miR-93, miR-103, miR-106a/b, miR-130b, miR-155, and miR-221~222 are indicative of advanced tumor stage[185].

These miRNAs may be used as biomarkers to predict high risk for invasion, lymph node metastasis, distant metastasis and overall poor long-term survival.

Taken together, these findings consolidate the emerging value of miRNAs as diagnostic and prognostic biomarkers, where the miRNA signature of a patient could be useful to support future medical decisions concerning GC course of treatment.

2.2.2.2 miRNAs as chemoresistance markers

There is accumulating evidence that miRNAs are a key player in the resistance profile of cancer cells to chemotherapy treatment, but the mechanism by which this occurs remains still poorly understood. Nevertheless, future cancer therapies will largely benefit from the use of miRNA expression, since the ability to predict the effects of chemotherapy may help to reduce the use of unnecessary drugs, increasing the chances of a successful treatment. Chemotherapy is a common procedure and the primary treatment against GC. However, the therapy tends to fail due to the increasing resistance of tumors to chemotherapeutic agents.

It has been demonstrated that upregulated miRNAs in drug resistant cell lines prevent the apoptosis of cancer tumor cells induced by chemotherapeutics. For instance, it is reported that miR-106a is overexpressed in multidrug-resistant GC cell lines, and by targeting *RUNX3* (a pro-apoptotic gene) it is able to reduce the sensitivity of multidrug-resistant GC cell lines to anticancer drugs and inhibit cell apoptosis[186]. On the other hand, inhibition of miR-106a enhanced the sensitivity of multidrug-resistant GC cell lines to chemotherapeutics[186]. In contrast, miR-15b and miR-16 were found to be downregulated in a human multidrug-resistant gastric cancer cell line. MiR-15b and miR-16 directly regulate Bcl-2 protein expression, and their ectopic restoration modulated the susceptibility of cancer cells to chemotherapeutic drug-induced[99]. Other miRNAs were also found to be downregulated in multidrug-resistant cell lines, such as miR-185 and miR-218. The re-expression of downregulated miRNAs involved in drug resistance pathways promotes cancer cell apoptosis during treatment.

2.2.2.3 miRNAs as therapeutic targets

As extensively demonstrated in the previous sections, miRNAs are a powerful key element on gene control, being involved in the regulation of multiple genes and pathways determinant for tumor development. Moreover, the same miRNA can be identified in different types of cancer and other diseases, spanning their value as therapeutic targets (see miR-9 example, Table 2.2.).

The current methods to control dysregulated miRNAs are mainly focused on the ectopic expression of tumor suppressor miRNAs; or on the silencing of endogenous oncomiRs, using AMOs, miRNA sponges or miR-Mask methodologies. These strategies are further revised in the next section, emphasizing the use of AMOs for control of aberrant miRNAs.

2.3 Controlling miRNAs activity

It is quite straightforward that to control miRNA activity could be desirable to restore miRNA expression with tumor suppressing activity (gain-of-function) or to block miRNAs with oncogenic activity inhibiting its function (loss-of-function)[187].

2.3.1 Gain-of-function strategies

Gain-of-function strategies mainly rely on either the incorporation of double-stranded chemically synthesized miRNA mimics or on viral vectors to mediate miRNA overexpression. Chemically synthesized miRNA mimics are generally not the exact natural miRNA duplex. The sense strand is altered to be perfectly complementary to the mature miRNA (to increase stability), and should be chemically modified to inactive this now non-natural sense-strand. MiRNA mimics can be designed to target a single mRNA[188] or to incorporate multiple miRNA units for targeting different mRNAs and silence multiple target genes[187,189,190].

Viral vector-mediated miRNA overexpression consists on the use of an integrating vector system, containing short hairpin RNAs (shRNAs) driven by Pol III promoters[187]. Upon delivery, these systems are able to sturdily express the miRNA of interest.

2.3.2 Loss-of-function strategies

The loss-of-function modulating system of miRNAs can be achieved mainly by applying miRNA sponges; miRNA-Masking Antisense Oligonucleotides; or by using antisense oligonucleotides targeting miRNAs (AMOs)[187] (Figure 2.3).

MiRNA-sponge technology consists of the expression of mRNA molecules with multiple binding sites for the target miRNA that will function as a decoy or a "sponge" to trap the desired miRNAs (Figure 2.3 A). That way the endogenous target mRNA will be preserved and able to function normally[191]. This approach is intensively used to inhibit functional classes of miRNAs *in vitro*, but so far its use *in vivo* has been limited[187]. MiRNA sponges are specific to a miRNA target and not to a gene of interest. Using a miRNA sponge to knock down a miRNA or a miRNA seed family could affect all target genes of its targeted miRNAs, leading to undesirable effects.

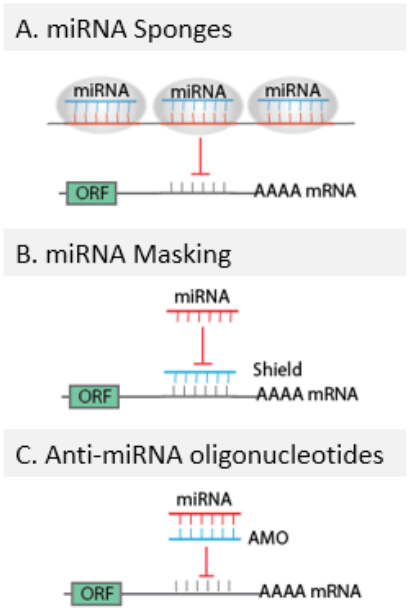


Figure 2.3. Loss-of-function strategies: miRNA sponges (A), miRNA Masking (B) and anti-miRNA oligonucleotides (C).ORF-Open Reading Frame.

MiRNA-Masking Antisense Oligonucleotides technology (miR-Mask, also known as BlockmiR, target protectors or as target site blockers) relies on an inverted approach: instead of blocking the

target miRNA, these molecules shield the mRNA which function is desirable to preserve (Figure 2.3 B). In this way, the miR-Mask are able to block the access of the miRNA to its target mRNA, impeding its action to the target gene. Moreover, miR-mask technology targets the miRNA in a gene-specific manner, i.e. the oligonucleotides are designed to protect the mRNA, and consequently, the expression of the protein of interest, leaving intact the miRNA responsible for the repression which might have other important roles in the system[190]. MiR-Mask is an alternative and valuable supplement to anti-miRNA oligonucleotides technology[187].

Also, this approach that can be further combined with miRNA sponges (sponge-miR-mask technology) to block the access of multiple miRNA members to their binding sites on mRNA, leading to the re-expression of the proteins. A sponge miR-mask is designed to bind by partial complementarity to the 3'UTR of all target mRNAs of a miRNA seed family site of 8 nt. However, sponge-miR-Mask technology has poor gene-specificity, since these molecules might block the expression of all genes associated with the same seed binding site of the miRNA family[187].

One of the most popular approaches to correct aberrant miRNA expression is based on the synthesis of antisense oligonucleotides[192–200] with a complementary sequence (Figure 2.3 C). Antisense oligonucleotides (ASOs) are being used to suppress dysfunctional mRNAs for more than four decades[201], and are currently being used to target miRNAs. In antisense oligonucleotides targeting mRNAs, ASOs mostly stimulate an RNase-dependent degradation of the target RNA. They are designed to harbor continuous DNA monomers along the sequence in order to promote RNase H activity. When applying antisense technology to miRNAs (AMOs), one may consider that the mechanisms through which AMOs act may follow the same pathway of ASOs – the binding of antisense oligonucleotides to miRNA should promote degradation via RNase, in the same way ASOs cleave mRNA. However, it is believed that the anti-miRNAs cause miRNA silencing mostly by steric blocking of the target miRNA. These findings were supported by the work of Davis *et al.*[26], where they tested a designed ASO sequence known to trigger the RNase H-dependent degradation to target the miR-21. The antisense oligonucleotide, despite being effective promoting mRNA degradation, failed to inhibit miR-21 activity, suggesting that the miRNA-ASO duplex may not be accessible to the RNase H.

Targeting aberrant microRNAs with AMOs is a promising approach for post-transcriptional gene control in future cancer therapies. Specific and strong AMOs' recognition and binding to the miRNA target is accomplished through Watson-Crick base pairing, which may be optimized by modifying AMOs at the chemical level.

2.4 The design of Anti-miRNAs

Anti-miR oligonucleotides-based mechanism stands on the complementary base pairing of the oligonucleotide sequence to its target miRNA. AMOs are typically designed to be a perfect match to the miRNA target[202], especially to the seed region of the miRNA, which has been shown to influence anti-miRNA specificity and activity.

In the therapeutics involving antisense oligonucleotides, AMOs must display some desirable characteristics in order to be applied successfully in a biological system. It is important to design and select AMOs with enhanced potency to silence the target miRNA and with increased binding affinity to the target. The potency of the AMOs is intrinsically associated with its capacity to efficiently reduce the expression of the target miRNA. Whereas, the binding affinity is related to the stability of the duplex upon AMO binding to its target, and thus related to the melting temperature (T_m) of the oligonucleotide. A higher T_m value represents an improved binding affinity and a stronger duplex, because more energy is required to destabilize the connection between both molecules. Overall, it is also desirable that the AMOs exhibit improved extracellular and intracellular stability, and thus to be resistant to exo- and endo-nucleases: they should also exhibit improved cellular uptake rates to be efficiently delivered to cells and tissues; and no toxicity or other side effects, such as the knockdown of non-target molecules important to maintain the biological system or the stimulation of undesired auto-immune response[203].

Unmodified DNA oligonucleotides present several disadvantages that preclude their applicability in antisense technologies. As such, several sets of chemical modifications were introduced to improve structural properties of the AMOs.

2.4.1 Chemical modifications – AMOs evolution

The first study reporting the use of antisense oligonucleotides applied to miRNAs used unmodified DNA sequences complementary to several miRNAs, that were injected to *Drosophila* embryos[204]. Antisense oligonucleotides composed only of DNA bases are rapidly degraded in a biological system by endo- and exo-nucleases and fail to connect with the majority of the target miRNA in mammalian cells. The necessity to overcome DNA-AMOs limitations emerged rapidly and a vast array of chemical modifications have been applied to antisense technologies.

Chemical modifications are mainly introduced in the sugar ring, especially at the C2' position, and/or in the backbone of the oligonucleotide structure. Backbone substitutions include either internucleotide linkage modifications or the substitution of the entire backbone for structures analogous to the DNA (Figure 2.4). Internucleotide modifications are often combined with sugar modifications to improve potency and resistance of the oligonucleotide sequence. These modifications will be further discussed in the following sections.

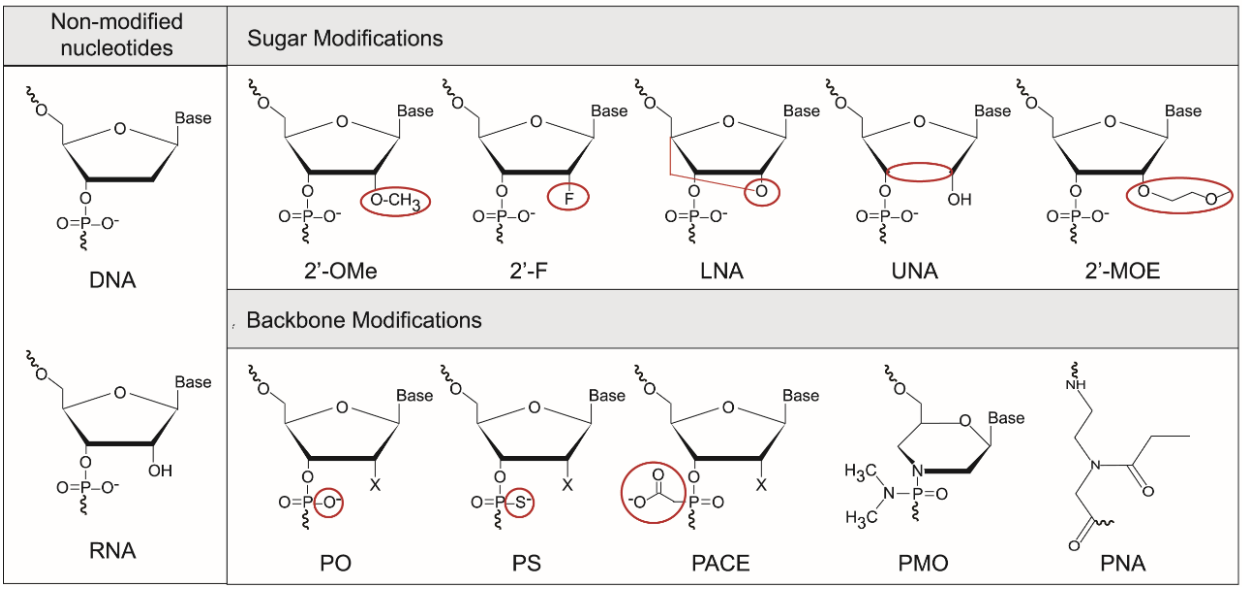


Figure 2.4. Chemical modifications applied in the AMOs design. Unmodified nucleotides – DNA: deoxyribonucleic acid, RNA: ribonucleic acid; Sugar modifications - 2'-OMe: 2'-O-methyl, 2'-F: 2'-fluoro-RNA, LNA: Locked Nucleic Acid, UNA: Unlocked Nucleic Acid, and 2'-MOE: 2'-O-methoxyethyl; Backbone modifications – PO: phosphodiester, PS: phosphorothioate, PACE: phosphonoacetate, PMO: Phosphorodiamidate Morpholino Oligomers, and PNA: Peptide Nucleic Acid. In red is highlighted the site and the type of modification.

2.4.1.1 Sugar modifications

Chemically-modified sugars are a remarkable way to enhance binding affinity and nuclease stability. The C2' position defines the conformation of the sugar ring and modifications at this position, that are able to shift the conformation of the sugar moiety from a C2'-endo (southern conformation, typical of DNA duplexes) to a C3'-endo sugar pucker (northern conformation, typical of RNA duplexes), improves the binding affinity of AMOs for RNA complements[205]. Furthermore, in this conformation the 2'-modification is closer to the 3'-phosphate group, conferring higher nuclease resistance to the oligonucleotide[206].

The most popular alterations applied to miRNAs studies involve modification on the 2' carbon of the ribose. It is the case of 2'-OMe, 2'-MOE and 2'-F alterations, that are all reported to confer AMOs increased binding affinity (ordered by increased potency: 2'-OMe ≅ 2'-MOE < 2'-F)[26] and nuclease resistance compared to DNA (Figure 2.4). LNA modification is also very popular among AMO designs, due to their improved performance on the stabilization of the duplex by its locked configuration. All these substitutions can be combined to improve AMOs potency. For instance, MOE/LNA or 2'F/MOE are successful examples of oligonucleotides mixmers with improved binding affinity when compared to oligonucleotides harboring only one type of substitution[26,202] (Figure 2.4).

The first generation modified-AMOs appeared in 2004 and contained a methylated hydroxyl group at the C2 carbon of the sugar ring (2'-OMe RNAs, Figure 2.4)[207,208]. Hutvagner and his co-workers[207] showed that 2'-OMe oligonucleotides are nontoxic and can efficiently suppress *Caenorhabditis elegans*-let-7 miRNA *in vivo*. In the same year, Meister *et al.*[208] also proved that it is possible to control miR-21 activity with 2'-OMe_AMOs by blocking the RISC complex. 2'-OMe oligonucleotides offer several advantages comparing to DNA-counterparts. They increase binding affinity to the target by approximately +0.8 °C/insert[205]. Also, 2'-OMe is a natural modification that occurs in mammalian RNA conferring minimal or no toxicity when used *in vivo*[207]. While 2'-OMe oligonucleotides being more resistant to nuclease activity when compared to DNA counterparts, they are still susceptible to degradation by exonucleases in the serum. Successful inhibition of miRNAs *in vivo* using 2'-OMe-AMOs was only achieved by applying the AMO directly into the cells[207]. In order to overcome this problem, additional non-oligonucleotide-

modifiers can be placed near the both ends of the oligonucleotide sequence to protect it from the attack of nucleases. Lennox *et al.*[209] described a novel nontoxic compound, N, N-diethyl-4-(4-nitronaphthalen-1-ylazo)-phenylamine ("ZEN") placed at or near 5'- and 3'-ends of a phosphodiester (PO) 2′-OMe oligonucleotide complementary to a targeted miRNA. The 2'-OMe-ZEN, with the modifier placed in both ends of the oligonucleotide sequence (dual-ZEN AMO), completely blocks endo- and exo-nuclease attack, and shows increased potency, binding affinity, good specificity and low-toxicity *in vitro* when compared to the unprotected 2'-OMe-PO design. In the same work, the ZEN modifiers were also compared to other non-nucleotide blocking groups (C3 spacer) placed in the same manner in an AMO sequence. Both ZEN and C3 AMO variants showed improved potency when the modification was performed at the 5'-end of the sequence rather than at the 3'-end, and in the case of the C3-AMOs, the binding affinity of the two AMO variants was the same. The 3'-end modification was expected to give a more stable AMO, and therefore increased potency. The opposite outcome led to the speculation that the potency of an AMO depends not only of its binding affinity and nuclease resistance, but also of the role that the 5'-end plays on the ability of the AMO to invade the miRISC complex. Furthermore, the dual-ZEN AMO showed higher potency than the dual-C3 AMO, which offered limited improvement in potency regarding the unmodified 2′-OMe[209].

In a similar line of work, Vermeulen *et al.*[210] demonstrated that flanking a single-stranded 2'-OMe-AMO sequence with double-stranded duplexes capable of forming hairpin structures highly improves the inhibitory effect of the AMO by several fold, possibly by helping the AMO invasion to miRNA–RISC. More recently, it has been reported that cross-linked duplexes flanking the single-stranded AMO inhibited miRNA functions more efficiently than AMOs with normal single or double strands. The interstrand cross-link of DNA or RNA not only contributed to improve 2'-OMe resistance and potency properties, but also to stabilize the duplex avoiding the risk of dissociation into single strands[211].

The 2'-MOE (2'-O-(2-methoxyethyl)) oligonucleotides harbor a methoxyethyl modification at the RNA 2'-OH position (Figure 2.4). This configuration increases nuclease resistance and target binding affinity by approximately +1 °C/insert[205] when compared with unmodified DNA oligonucleotides. Moreover, 2'-MOE oligonucleotides are effective in silencing miRNAs and display improved anti-miRNA activity when compared to 2'-OMe oligonucleotides[26,212]. Esau *et*

al.[212] demonstrated that miR-122 function can be modulated in mice using a 2'MOE-AMO. The inhibition of the miR-122, a miRNA overexpressed in the liver, resulted in the reduction of plasma cholesterol levels, in the increase of hepatic fatty acid oxidation, and in a decrease of hepatic fatty acid and cholesterol synthesis rates.

The miR-122 is associated with Hepatitis C virus (HCV) infection in the liver. Currently, a company called Regulus Therapeutics is validating a 2'MOE-AMO-122 (RG-101) conjugated with an N-Acetylgalactosamine sugar (GalNAc) for the treatment of HCV infection in humans[213,214]. The GalNAc carbohydrate structure shows high binding affinity to the asialoglycoprotein receptor (ASGPR) on hepatocytes, improving cellular uptake[214] and enhancing the potency of RG-101 by up to 10-20 times compared with unconjugated oligonucleotide. In the beginning of 2016, RG-101 entered the phase II of a clinical study, but despite the promising results in phase I, the drug is currently on a clinical hold by the American Food and Drug Administration (FDA). The same company has other promising AMOs to be applied in miRNA therapeutics. Another GalNAc-conjugated oligonucleotide, the RG-125(AZD4076) targeting miR-103/107, is currently in phase I of clinical development. RG-125 is expected to contribute to the treatment of non-alcoholic steatohepatitis in patients with type 2 diabetes/pre-diabetes.

The 2'-Deoxy-2'-fluoro-nucleoside (2'-F) is a RNA mimic with a fluorine 2'-hydroxyl group at the C2 carbon of the ribose (Figure 2.4). Depending on the sequence, oligonucleotides with 2'-F-RNA residues show increased thermal stability of around +1.6 °C/insert[205], which is higher than 2'-OMe-RNA and DNA. 2'-F-AMOs with PO linkages do not have significant resistance to exonucleases, while phosphorothioate (PS) linkages are highly resistant, conferring some protection to 2'-F-RNA AMOs. For *in vivo* applications, 2'-F-RNA can be further conjugated with other modifications, like 2'-MOE substitutions, to confer more stability[27]. In this study, a 2'-F-AMO was able to potently inhibit miR-122 activity, showing a mild dose-dependent immunostimulatory effect in mice. The 2'-MOE modification presents a lower binding affinity than the 2'-F, but the introduction of additional 2'-MOE modifications into the 2'-F/MOE AMO was able to minimize this immune response without affecting anti-miR-122 activity[27]. Nevertheless, the 2'-F-RNA substitution is a potent, and well-tolerated chemical modification that can be used to efficiently silence abnormal miRNAs. In addition, 2'-F-RNA residues are an

effective alternative to LNA-modified oligonucleotides, since they provide a similar thermal stability and nuclease resistance, but at a lower cost[215].

LNA is a 2'-O, 4'-C-methylene-β-D-ribofuranosyl nucleotide where the ribose is locked in a 3' endo/N-type sugar conformation with a methylated bridge between the oxygen at 2' position and the 4'C (Figure 2.4). LNA monomers are also compatible to other RNA and DNA monomers and with PO and PS linkages, respecting the natural base pairing binding. Due to their chemical structure, LNA-modified oligonucleotides have high resistance to nucleases and the highest binding affinity demonstrated so far of +2 to +5 °C/insert when pairing with DNA sequences and +4 to +10 °C/residue when pairing with a RNA strand[216]. The high binding affinity of LNA-AMOs makes it possible to design shorter sequences without compromising efficiency, which are useful to target the seed region of entire miRNAs families with similar biological functions. Obad *et al*.[24] were the first to describe tiny LNA-sequences of 8 nt (so called "tiny LNAs") targeting the seed region of both individual miRNAs and co-expressed miRNA families. Also, systemic administrations of tiny LNAs showed unassisted uptake and long-term knockdown of miR-21 in a breast cancer mouse model, emphasizing the potential use of LNA-AMOs *in vivo*. More recently, Zhang *et al.*[217] successfully applied tiny-LNAs to silence miR-155 in low-grade B-cell lymphoma cells both *in vitro* and *in vivo*. Safe *in vivo* applications of LNA sequences are highly dependent of sequence context, length and an overall optimized design. Shorter sequences had shown lower toxicity *in vivo* and *in vitro,* and are more likely to improve mismatch discrimination[218], whereas long sequences had demonstrated severe cytotoxicity *in vitro*[209].

In terms of market, there are two drugs using LNA-AMO technology currently in clinical trials. The first drug called Miravirsen from Santaris Pharma, was developed to treat HCV infection by targeting miR-122[219] and entered phase 2 of clinical trials. It is presently in an extension study to provide additional long-term safety and efficacy data. Another company (miRagen Therapeutics) entered phase 1 of clinical studies for MRG106-11-101 LNA-antimiR®, which was designed to control the activity of miR-155. In hematological malignancy, miR-155 has key roles in the differentiation, function, and proliferation of blood and lymph cells. *In vitro* tests using the developed AMO successfully inhibited miR-155 activity in lymphoma cells, restoring normal function and reducing aberrant cell proliferation.

Unlocked Nucleic Acid (UNA, Figure 2.4) like LNA is another analogue of RNA, in which the C2′–C3′-bond has been cleaved, resulting in an unlocked configuration of the furanose ring. The UNA inserts additively decrease duplex stability, and depending of the configuration, the T_m can decrease -5 ºC to -10 ºC/modification[220]. However, despite the decrease of T_m, the UNA unlocked configuration makes this molecule very flexible. UNA monomers can be placed strategically within the AMO sequence to enhance mismatch discrimination, making this substitution interesting for detection purposes (further reviewed in the "miRNA detection using AMOs" section).

2.4.1.2 Backbone modifications

Phosphodiester bonds (PO) are the natural internucleotide linkage present in DNA and RNA (Figure 2.4). Oligonucleotides designed to harbor the natural PO bonds are in this way more tolerated *in vivo*, displaying less toxicity. Yet, they are more prone to be cleaved by endo- and exonucleases in mammalian cells. Chemical modifications of these bonds have been extensively studied, and several chemical strategies have been proven very successful for improving nuclease resistance[221–224].

The first described internucleotide linkage modification in antisense oligonucleotides was a phosphorothioate (PS) linkage, where the non-bridging phosphate oxygen is substituted by a sulfur in the phosphodiester bond (Figure 2.4)[221]. PS bonds are more resistant to the activity of exo-and endonucleases and they can be placed throughout the oligonucleotide sequence (to improve endonuclease resistance) or at strategic points within the sequence, leaving some unmodified PO linkages. Generally, the PS linkages should be added near both the 5' and 3' ends[202] to improve the AMO resistance to exonucleases.

The major drawback associated to PS linkages is their prominent attraction to bind to off-target proteins. PS binding to nuclear proteins may be potentially toxic to normal cells and compromise several cell functions[225]. However, the affinity of PS oligonucleotides to serum albumin, reduces plasma clearance and increases the AMOs lifetime in serum from hours to days[226].

Moreover, PS-DNAs present a slightly reduced binding affinity towards complementary RNA molecules in comparison to their corresponding phosphodiester oligodeoxynucleotide. The melting temperature of a heteroduplex is decreased by approximately - 0.5 ºC per insert. Davis *et al.*[26] compared the effect of the PS backbone substitution on anti-miRNA activity. Uniform 2'-MOE and 2'-OMe sequences, with PS or PO backbones, were tested to evaluate their potency to silence miR-21 over time. 2'-MOE-PO-AMO displayed an increased activity compared to 2'-MOE-PS-AMO, being more active in many later time points. The 2'-OMe showed little or no improvement in both designs (PS or PO), due possibly to the poor resistance of 2'-OMe-PO-AMO in cells. The decrease in terms of thermal stability offered by PS oligonucleotides is compensated by a greater hybridization specificity, higher nuclease resistance, and an improved cellular uptake both *in vitro* and *in vivo* as compared with unmodified DNA oligonucleotides. The potency of PS-oligonucleotides can be further enhanced by combining other substitutions, especially sugar modifications.

Other internucleotide linkage modifications used to silence miRNAs include phosphonoacetate (PACE) and thio-PACE. PACE synthesis replaces the nonbridging oxygen for an acetate group in the internucleotide phosphate linkage (Figure 2.4). Thio-PACE is an analog of PACE comprising a PS substitution instead of a PO bond. Both modifications are reported to be completely resistant to nuclease activity and are able to enter the cells without any assistance as neutral esters[227]. In spite of these advantages they show a slight decrease of binding affinity to complementary RNA targets, when compared to PO linkages - 1.3 ºC/insert for PACE duplexes and - 1.8 ºC/insert for thio-PACE (under high salt concentrations)[227]. Threlfall *et al.*[228] tested the potency of 2'-OMe oligonucleotides with PACE and thio-PACE backbones to inhibit miR-122[228]. In most cases, both types of AMOs formed stable duplexes with their target miRNA, showing higher melting temperatures than simple DNA oligonucleotides. Furthermore, single-stranded 2'-OMe thio-PACE oligonucleotides were notably more efficient in the cellular uptake and significantly improved the potency of a 2'-OMe-based anti-miRNA targeting miRNA-122 in the absence of a transfection agent[228].

Phosphorodiamidate Morpholino oligomers (PMOs) are uncharged substitutes of the PO bonds (Figure 2.4), where the morpholine ring is linked through phosphorodiamidate groups instead of phosphates[223]. Given their neutral charge, PMO oligonucleotides are more resistant to nuclease

activity and exhibit a similar or a slightly improved binding affinity for target miRNAs. Morpholino oligonucleotides have proven to be particularly successful as anti-miRNAs in Zebrafish systems[229,230], exhibiting specific and non-toxic inhibition of both pre-miRNA and mature miRNA activity by blocking Drosha or Dicer nucleolytic processing sites[230]. The uptake of this configuration into mammalian cells is challenging, and as such further conjugation with cell-penetrating peptides (CPPs) is required. This allows both the *in vitro* and *in vivo* uptake, enlarging the potential use of PMOs in anti-miRNA studies. It is worth noticing that the uncharged nature of these molecules facilitates their conjugation with charged cationic molecules, such as the CPPs designed to promote the delivery.

Peptide Nucleic Acid (PNA) is an uncharged synthetic DNA analog composed of N-(2-aminoethyl) glycine monomers linked by peptide bonds[224] (Figure 2.4). PNAs follow the natural base-pairing rules and exhibit a significant nuclease resistance, and increased binding affinity towards DNA or RNA targets. PNA is particularly useful in anti-miRNA applications. Fabani and Gait[22] reported that PNA molecules used to silence miR-122 showed improved activity when compared with a 2'-OMe oligonucleotide. Like the PMOs, the cellular uptake of PNA-AMOs is challenging. PNA shows a more hydrophilic profile than lipophilic, which compromises the diffusion of unmodified-PNA molecules through cell membranes[231]. The PNA oligonucleotide designed by Fabani and Gait[22] had an amino-terminal cysteine to facilitate conjugation with a R6-penetratin peptide (CPP). They also tested an unconjugated AMO with four lysine residues to improve solubility. The four lysine residues were sufficient to confer charge, so that the PNA would be able to be delivered into cells using electroporation or CPPs.

2.4.2 Design Strategies of AMOs

Theoretically, the design of complementary anti-miRNAs sequences targeting miRNAs is quite straightforward. Yet, in reality, the whole process might take a long road before reaching a functional and non-toxic anti-miR. While highly dependent on the strategy defined for the study, some design guidelines should be followed to assist in the design of AMOs. The design of a chemically-improved anti-miR oligonucleotide passes through several stages, from the search of target miRNA sequences to the design of the AMO (including the selection of the most adequate chemical structure) and its validation (Figure 2.5).

First, it is necessary to identify the miRNA sequence of interest from databases like TargetScan v7.1[232] or miRBase[233,234]. The search should be directed to the mature sequence of the miRNA and the guided strand. The passenger strand is not an active sequence of miRNA and is generally not considered in AMOs design. Nonetheless, the passenger strand sequence can be used to synthesize a negative control oligonucleotide.

Next, by base-pairing, it is possible to design an anti-miR oligonucleotide sequence fully complementary to the 5' end of the mature miRNA, especially matching the seed region. The designed sequence can have the same length, be shorter or even longer than the target[21,26,207]. Some examples of shorter and longer sequences were already discussed above, such as in the work of Obad *et al.* using tiny LNAs[24], and in the work of Vermeulen *et al.* using longer 2'-OMe-AMOs with flanking nucleotides next to the complementary antisense miRNA region[210]. After selecting the desired AMO sequence, it is also advisable to perform an alignment for the human genome using for instance a Basic Local Alignment Search Tool (BLAST)[235] to check for possible off-targets of the oligonucleotide sequence.

Due to the poor stability of DNA sequences, chemical modifications should be employed into the design of AMOs. From all the evidence stated above, it is possible to sum-up some specific characteristics of the different chemical-modified AMOs (Table 2.3), especially in terms of binding affinity, nuclease resistance, cellular uptake and cytotoxicity. It is also worth mentioning that unmodified AMOs may lead to an ineffective inhibition of the miRNA activity, since they also serve as a passenger strand and thus trigger the dissociation mechanism responsible for miRNA passenger strand unwinding[26]. Nonetheless, and as observed next, it is important to emphasize that the link between the type of AMOs employed and the overall end result is far from being established for most situations.

Overall, some of the most widely used chemical modifications in anti-miRNA technology are LNA, 2'-F-RNA, 2'-OMe, PNA, and PMOs. Moreover, different combinations can be applied to further improve the performance of a certain AMO design. For instance, 2'-OMe oligonucleotides with a PO backbone are easily degraded in the serum by exonucleases, while introducing a PS substitution linkages at each end a 2'-OMe-PO oligonucleotide improves nuclease resistance and is an effective AMOs substitution for a miRNA knockdown *in vivo*[236]. However, when applying a

full sequence PS substitution in a 2'-OMe-AMO, the same outcome is not achieved and the miRNA levels remain unaffected. The reduction on the activity of a PS-AMOs, comparatively to a PO counterpart, can also be explained by the higher binding affinity of PS-AMOs to many proteins. Some of those are able to relocate to the nucleus, moving the PS-AMOs along with them. As a consequence, there is a decrease of available AMOs in the cytoplasm, which may contribute to the inhibition of anti-miRNA activity[236].

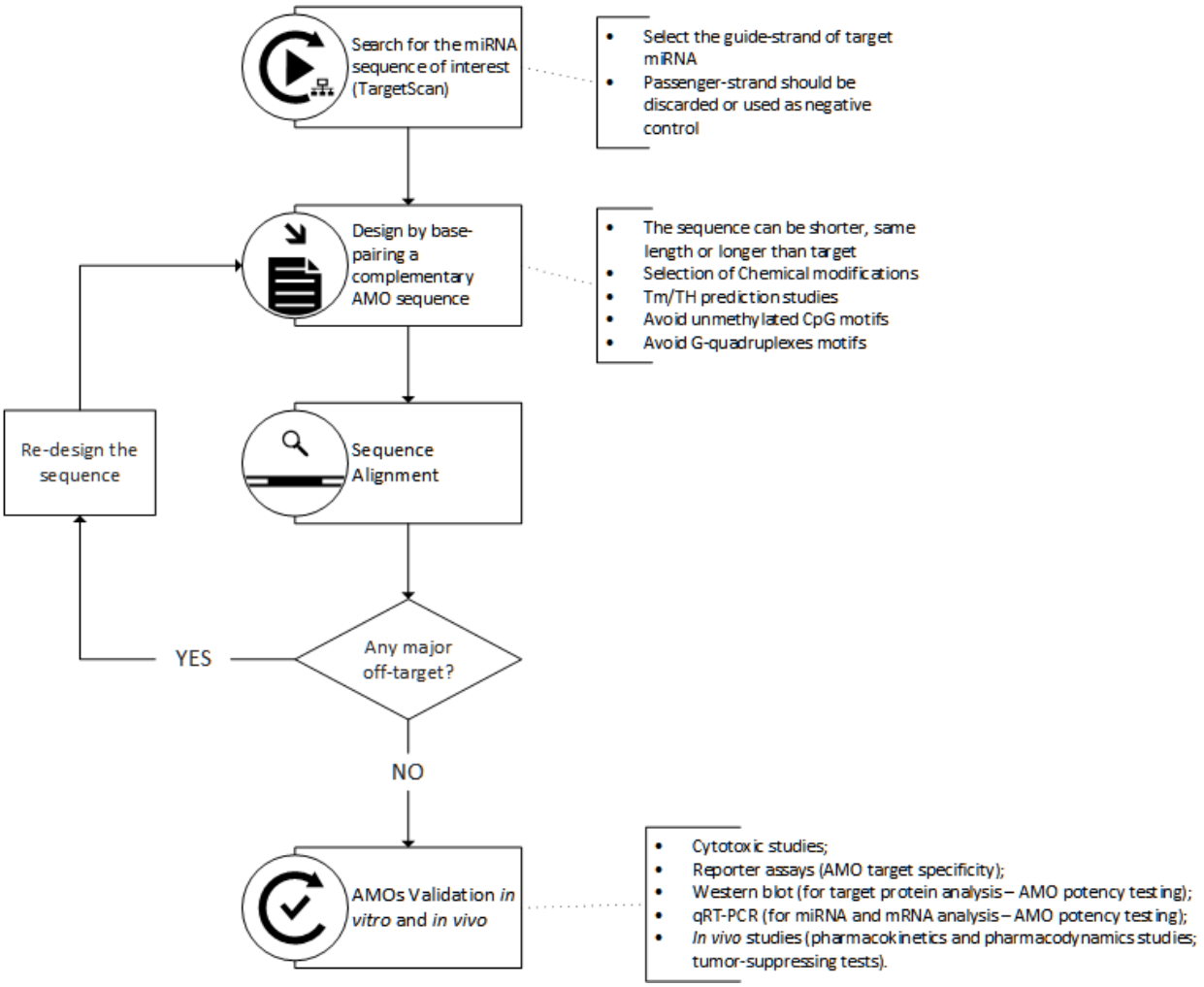


Figure 2.5 AMOs design flowchart: from the identification of target miRNA to the validation of anti-miRNA oligonucleotides.

Another aspect to take into consideration when designing an anti-miR oligonucleotide sequence is the temperature at which the hybridization is desirable to occur. The hybridization temperature (T_H) can be defined as the optimal temperature at which a full (or nearly full) noncovalent binding between the AMO and the target miRNA forming a duplex is observed[237], and at which the AMO do not hybridizes with sequences that contain one or more mismatches. Up to date, there are no mathematical models that accurately predict the optimal T_H for a given oligonucleotide sequence. In order to overcome this and have an estimation of T_H for optimization studies, the melting temperature or mid-transition temperature (T_m) is usually determined as an indicator of T_H[237]. Thermodynamic parameters are well defined for DNA duplexes and in general, the mathematical models to handle the thermodynamics of nucleic acid hybridization (and hence determine the T_m) are available and quite accurate. Different configurations (PNA: RNA; LNA: RNA, etc.) show different thermodynamic parameters and thus different models need to be adapted to predict the thermodynamic parameters of the hybridization[237].

As mentioned before, the PS linkage reduces binding affinity and a complete PS modification lowers the T_m to such extent that the AMO potency is compromised[236]. In spite of some exceptions, it is possible to establish a direct correlation between the increase of the binding affinity and the potency of the AMO to inhibit miRNA activity. However, chemical modifications presenting high T_m values, such as LNA or 2'-MOE/LNA mixmers, may result in an AMO with reduced potency, since they might show self-dimerization effects or form strong secondary structures within the oligonucleotide sequence, which can lower AMO potency. It is believed that there is a threshold in the thermal stability that directly promotes a good potency. After that point, any further affinity increases do not improve potency and higher are the chances of off-target hybridization[48].

Furthermore, other molecules can be applied in the sequence to optimize a specific design in terms of uptake, delivery, and endurance of an AMO, especially when applied *in vivo*. Due to their polyanionic nature, these oligonucleotides do not easily diffuse across cell membranes, and most of the AMOs need to be associated with an efficient delivery system. Applying non-oligonucleotide molecules to the extremities of an AMO protects the sequence from degradation and thus increases the nuclease resistance of these designs[209,236]. Also, it has been reported that adding, for instance, a cholesterol group to the 3'-end facilitates the delivery *in vivo* of the 2'-OMe AMOs containing PS linkages[236,238].

Table 2.3 Properties of the different chemical modifications applied to AMOs

Type of modification	Advantages	Disadvantages	References
PO	▪ Natural backbone structure ▪ Low-toxicity ▪ Inexpensive	▪ Poor stability *in vivo* - Low resistance to exonucleases	201
PS	▪ Increased cellular uptake rate ▪ High nuclease resistance	▪ Non-specific binding to proteins ▪ Slightly lower binding affinity compared with PO	26,221
PACE/thio-Pace	▪ Improved and unassisted uptake ▪ Combination with other modifications to improve thermal stability and binding affinity	▪ Lower binding affinity when compared with other modifications (-1.3 ºC/insert for PACE duplexes and - 1.8 ºC/insert for thio-PACE), but still higher than DNA-AMOs when combined with higher binding affinity modifications such as 2'-OMe	227,228
PMO	▪ High nuclease resistance ▪ Improved thermal stability ▪ Uncharged – easy to conjugate with other molecules	▪ Poor uptake/pharmacokinetic properties	230
PNA	▪ High nuclease resistance ▪ Improved thermal stability ▪ Uncharged – easy to conjugate with other molecules	▪ Poor uptake/pharmacokinetic properties	22,231
2'-OMe	▪ Improved nuclease resistance ▪ Improved thermal stability ▪ Non-toxic	▪ Relatively poor stability *in vivo*: 2′-OMe-PO AMOs are less resistance to exonucleases when compared with other modifications containing a PO backbone	26,205,207,208
2'-MOE	▪ Improved nuclease resistance ▪ Improved thermal stability ▪ Non-toxic	▪ When combined with other T_m-increasing chemical modifications (such as LNA) might form secondary structures within the AMO or present increased self-dimerization effect, lowering the potency of the AMO	26,202,205,212
2'-F	▪ Improved thermal stability ▪ Non-toxic ▪ Lower cost compared with LNA substitution	▪ 2'-F-PO show no resistance to exonucleases	32, 124
LNA	▪ High thermal stability ▪ Increased nuclease resistance ▪ Improved potency and specificity ▪ Improved and unassisted uptake ▪ Mismatch discrimination ▪ Efficient to target miRNA families using tiny-LNA sequences	▪ Low conformational flexibility ▪ T_m-increasing chemical modifications might form secondary structures within the AMO or present increased self-dimerization effect, lowering the potency of the AMO ▪ Might present *in vivo* toxicity	25, 26, 28, 29, 131, 147–149
UNA	▪ Great conformation flexibility ▪ Mismatch discrimination within miRNA families	▪ Poor thermal stability	242

Moreover, other molecules such as cell-penetrating peptides[22,243] can be applied in the extremities of an anti-miR oligonucleotide to promote cellular uptake of otherwise unattractive AMO designs for an *in vivo* delivery purpose. Although CPPs are an attractive way to promote the delivery of oligonucleotides, these molecules are typically conjugated with non-charged PNA and PMOs[244].

Other technical features should be kept in mind when designing antisense oligonucleotides. Generally, oligonucleotides containing unmethylated deoxycytidine-deoxyguanosine (CpG) dinucleotides motifs can trigger immune responses in mammalian systems by activating the toll-like receptor-9 gene (*TLR9*) expressed in immune system cells such as the Lymphocyte B or dendritic cells. For this reason they should be avoided, especially for *in vivo* applications[245,246]. The CG dinucleotide is more frequently found in viral and bacterial DNA than in the human genome, suggesting that it is a marker for the immune system to recognize infection. Nevertheless, AMOs containing these motifs can be applied in situations where it is desirable to induce an immune response for treating cancer, asthma and infectious diseases[246].

The development of new oligonucleotides, more stable and more specific, targeting miRNAs is the investigation focus of many research groups that are continually improving AMOs design and finding new miRNAs that control specific pathways in cancer epigenetics. Improved AMOs could not only be used as a therapeutic tool but also they could be associated with state-of-the-art technologies for the detection of miRNAs in tissues.

2.5 miRNA detection using AMOs

A field breakthrough in the miRNAs technology might pass through the use of AMOs to profile and detect *in vivo* miRNAs known to be involved in cancer processes. The progression of the AMOs technology allied to real-time *in vivo* imaging is, of course, limited by several factors, including the improved specificity and stability of the new generation of oligonucleotides, the optimization of efficient AMO delivery techniques and the advance of support instrumentation that allows the actual live detection of the molecules of interest.

Over the years, several studies have been reported to use LNA oligonucleotides to efficiently target miRNAs, showing the potential of LNA-AMOs in different therapeutic and detection strategies[20,22–24,195]. In the detection field, Válóczi *et al.*[195] developed LNA oligonucleotides with improved sensitivity and high specificity to be applied in northern blot analysis for a highly-efficient detection of miRNAs. With their work, they have opened the precedent to further explore the application of LNA oligonucleotides in other detection methods, like for instance to study of the spatial expression/distribution of miRNAs in cells and tissues by *in situ* hybridization or to study the expression profile of miRNAs by LNA-microarrays.

In situ hybridization (ISH) analysis is a technique that applies antisense oligonucleotides complementary to a specific nucleic acid sequence to determine the precise location of miRNA within the cells. The main difference is that for detection purposes, the synthetic antisense oligonucleotides are linked either to a fluorophore, a radioactively-label or to an antigen-labeled bases so that they can be tracked respectively by fluorescence microscopy, autoradiography, or immunohistochemistry. Currently, the use of LNA-modified oligonucleotides constitute the most promising approach to visualize miRNA expression by i*n situ* hybridization[247–253], but it has only been used *ex-vivo*. It is desirable that the oligonucleotide sequences hybridize at normal body temperature (around 37 ºC) to be prone to be used i*n vivo* and push forward the miRNA detection methods in order to determine spatial and temporal miRNA accumulation in tissues. More recently, UNA modification has proven to be an interesting substitution for mismatch discrimination within miRNAs families. Robertson *et al*.[242] demonstrated the properties of UNA-AMOs for detecting specifically overexpressed miR10b in metastatic breast cancer. UNA oligonucleotides showed increased specificity towards its target and were able to discriminate miR10b from miR10a (presenting 1 mismatch) and from miR10c (presenting 2 mismatches) more efficiently than its DNA counterparts.

There is already some instrumentation in the field of fluorescence microscopy that allows the detection of fluorescence signal by using *in vivo* fluorescent detectors. These detectors are basically labeled-oligonucleotides attached to sophisticated and expensive instrumentation, and a lot of effort is applied in the development of smaller, disposable and low-cost detector systems[254]. Another problematic relies on the sensitivity of the detection methods. Usually, the fluorescence detection requires the high sensitivity devices that allow the measurement of very low levels of

light emitted by the labeled sequences. One example is a prototype developed by Stephen Bellis *et al*.[255] a hybrid platform consisting of a vertical cavity surface emitting laser (VCSEL) to provide the excitation and a photo-diode (APD) to detect the emitted fluorescence. The APD detectors combine the ability to count individual photons, being able to detect low levels of fluorescence, and as a plus are small in size.

Other technologies are now immersing to track and detect in real-time different molecules *in vivo* for biomedical research and clinical applications. Is the case of near-infrared fluorescence Imaging (NIR), a technology recently used in the field of cancer imaging. This technique uses high sensitivity molecular probes labeled with fluorophores in the near-infrared region wavelength (650 nm – 900 nm), that allows relatively deep photon penetration into tissue, minimal tissue auto-fluorescence and higher optical contrast. *In vivo* fluorescence imaging with near-infrared light holds enormous potential for a wide variety of molecular diagnostic and therapeutic applications[256].

Interestingly, using the same principle of the detection techniques stated above, AMOs could be further optimized to be stable *in vivo*, in order to allow miRNA detection in real-time by applying a fluorescence molecule at one end of the sequence. A real-time detection of miRNAs topically in any tissue holds a great promise towards an effective, safe and immediate detection of miRNAs in humans.

2.6 Summary

As exposed in this chapter, miRNAs are involved in the control of several biological pathways, and it is evident that alteration on miRNAs levels has an extensive impact on the synthesis of different proteins associated with different human pathologies, such as cancer.

The development of new technologies to study the function and the mechanisms of regulation of miRNA in human diseases is fundamental. Numerous works show the potential use of AMOs as specific diagnostic biomarkers and/or as a therapy to control aberrant miRNA. The use of AMOs in clinical practice for cancer treatment seems a promising alternative to silence undesirable miRNA function and gene activity. For these reasons, a fully comprehensive study of AMOs

function using different *in vitro* techniques is mandatory. It is also important to associate the *in vitro* results to the *in viv*o studies to validate this strategy as an efficient therapeutic route in cancer treatment. Furthermore, allying the AMO technology to the emerging methodologies for real-time detection holds a great promise towards an effective, safe and immediate detection of miRNAs in humans. *In situ* detection of miRNA accumulation in tumor biopsies may provide a highly valuable approach for prognostic and diagnostic evaluation in a clinical setting.

Accumulating evidences show that miR-9 is overexpressed in gastric cancer and its overexpression may be repressing the tumor suppressor E-cadherin-encoding gene, leading to tumor progression and invasion. This work aims to stablish specifically, as a proof-of-concept, the relationship between miR-9 overexpression and the expression of E-cadherin in GC. In order to achieve the purposed goals, different LNA-based AMOs with a complementary sequence to miR-9 were designed, their cellular uptake and cytotoxicity assessed, and their effects on the expression of miR-9 and of E-cadherin determined. The main results and conclusions of this work are exposed in the following chapters.

Chapter 3

Materials and methods

3.1 Theoretical assessment of a comprehensive model for the hybridization dynamics of molecular probes in FISH

Before the experimental work, a comprehensive study on the hybridization dynamics of MPs in FISH was developed. Each diffusional barrier encounter by the MPs during a FISH procedure (from the hybridization solution until the reaction site within cells) was characterized in terms of characteristic time. The estimation of the order of magnitude of the time required for the MPs to diffuse and react, will allow the determination of the limiting step of the MPs hybridization. Ultimately, would be possible to determine the variables that can be handled to improve molecular probe hybridization, and thus optimizing the different settings in the FISH methodology.

3.2 Cell culture and transfection

In this study, MKN74 (derived from gastric carcinoma), HEK293 (human embryonic kidney 293 cells) and HeLa (derived from cervical cancer) cell lines were used (Figure 3.1). HEK293 and HeLa cells were cultured in Dulbecco's Modified Eagle Medium (DMEM, Gibco, Thermo Fisher Scientific, Inc, UK) supplemented with 10% (v/v) fetal bovine serum (FBS, HyClone, Thermo Fisher Scientific, Inc, UK) and 1% (v/v) Penicillin/Streptomycin (Gibco). MKN74 cells were maintained in RPMI medium 1640 Glutamax I (Gibco) supplemented with 10% (v/v) fetal bovine serum (FBS, HyClone, Thermo Fisher Scientific) and 1% (v/v) Penicillin/Streptomycin (Gibco). All cultured cells were maintained at 37 °C in a humidified 5% CO_2 incubator and the medium was substituted every 2 to 3 days.

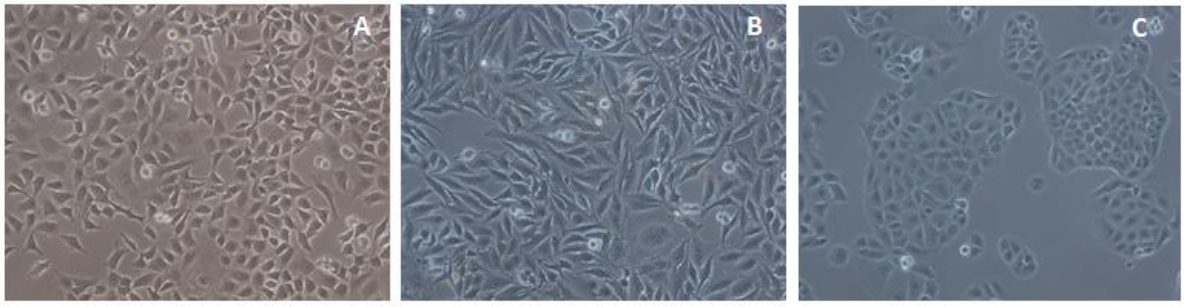


Figure 3.1 Representative images of the different cell lines used in the assay. HEK293 cell line (A); HeLa (B) and MKN74 (C) cell lines; all images were acquired with x100 amplification.

MKN74 cells were transfected in a 6-well plate using Lipofectamine 2000 (Invitrogen, Thermo Fisher Scientific, MA, USA) according to the manufacturer's protocol with some modifications. Briefly, MKN74 were seeded at a low-confluence rate (30%) using RPMI medium supplemented with 10% (v/v) of FBS. On the next day, the medium was discarded and replaced by serum-free Opti-MEM medium (GIBCO) containing the diluted Lipofectamine™ 2000 and the anti-miRNA sequence (1: 1). The complexation was allowed to actuate for 5 min at room temperature. Protein and total RNA was extracted as described below, for qRT-PCR quantification and Western Blot analysis, after 24, 48 and 72 h, post-transfection.

3.3 LNA anti-miR design

The selection of the target sequence was achieved by searching on the database TargetScan v7.1[232] the miR-9 sequence responsible for the silencing of the 3' UTR mRNA that expresses the *CDH1* gene. Complementary LNA-based anti-miR oligonucleotides were then designed taking into consideration optimal sequence length, specificity to the target and theoretical melting temperature.

Overall, three LNA-based anti-miR oligonucleotides were designed with a phosphorothioate backbone (PS): an LNA/DNA anti-miR oligonucleotide sequence (AM_ LNA_PS); another sequence harbouring a 2'O-Methyl substitution and LNA monomers (AM_LNA_2OMe_PS) and a third sequence displaying two amino-LNA monomers conjugated with an palmitoyl molecule (AM_LNA_Pal). Additionally, two oligonucleotide sequences were used as a control: a scramble LNA sequence similar to the LNA/DNA anti-miR sequence designed with 2 mismatches in the seed region (SC_LNA_PS), and a commercial scramble sequence (SC_LNA_PS_Generic).

After the selection of the oligonucleotide sequences, an alignment against the human genome with a Basic Local Alignment Search Tool (BLAST) was performed using the RefSeqRNA database. To the initial anti-miRNA sequence with 23 nucleotides (nt), 1 nt was progressively removed in order to determine the minimum possible length of the sequence without hitting additional off-targets, running a BLAST after each subtraction. Only results with 100% of identity and 100% query coverage were analyzed.

The theoretical melting temperature (T_m) of the AMO sequences was determined using the available online platforms as an indicator of the hybridization temperature (T_H). The T_m predictions for LNA/DNA sequences were evaluated using the Biophysics tool of IDT (available at http://biophysics.idtdna.com/). Predictions for the AM_LNA_2OMe_PS sequence were determined using the 2'OMeRNA/calculator (available at http://rnachemlab.ibch.poznan.pl/calculator1.php).

The LNA control oligonucleotide sequence (SC_LNA_PS) with 2 mismatches was designed by analyzing all possible combinations and by substituting 2 bases in the selected sequence. The sequences that showed low number of hits were analyzed individually to evaluate their targets, in

order to ensure that the hits were not the miR-9 sequence and/or other sequences that could possibly have important roles in cellular functions.

3.4 LNA anti-miR synthesis

All the oligonucleotide sequences used in this study were synthesized at the University of Southern Denmark as described elsewhere[257]. Briefly, the oligonucleotides were synthesized under anhydrous conditions using a standard automated nucleic acid synthesizer (Expedite 8909 instrument, PerSpective Biosystems Inc., MA, USA). LNA monomers were commercially available at Exiqon (Vedbaek, Denmark), and 2'-OMe were available at RiboTask ApS (Odense, Denmark). The amino-LNA nucleoside conjugated with the palmitoyl moiety was synthesized as described by Johannsen *et al.*[258]. Synthesis was performed at the 0.2 - 1.0 μmol scale using a universal polystyrene-based support and the following conditions: trichloroacetic acid in CH_2Cl_2 (3:97) as detritylation reagent; 0.25 M 4,5-dicyanoimidazole (DCI) in CH_3CN as activator; acetic anhydride in THF (9:91, v/v) as cap A solution; N-methylimidazole in THF (1:9, v/v) as cap B solution. A thiolation solution 0.0225 M xanthan hydrate in pyridine/CH_3CN (20:90, v/v) was used for phosphorothioate oligonucleotides. Coupling time was 4.6 min for both monomers. Fluorescein phosphoramidite, FAM (Glen Research, VA, USA) was added in anhydrous acetonitrile (0.1 M) and activated by tetrazole with a 20 min coupling time. The stepwise coupling yields (95-99% per step) were based on the absorbance of the dimethoxytrityl cations (DMT+) released after each coupling step. The cleavage from the support was carried out by using 98% aqueous methanol/ammonia solution 7 N in methanol (1:1), 2 h at room temperature (RT) followed by 32% aqueous ammonia solution, 12 h at 55 °C. All oligonucleotides were purified by reversed-phase HPLC (RP-HPLC) using a Waters 600 system equipped with an XBridge OST C18 (2.5 μm, 19×100 mm) column and an XBridge Prep C18 (5 μm, 10×10 mm) precolumn. After removal of the DMT-group, oligonucleotides were characterized by ion-exchange HPLC (IE-HPLC) on a Dionex system HPLC (VWR) and by matrix-assisted laser desorption ionization time-of-flight mass spectrometry (MALDI-TOF) on a Microflex Maldi (Bruker instruments, Leipzig, Germany). The purified oligonucleotides were precipitated by acetone and their purity (>90%) and compositions were verified by IE-HPLC and MALDI-TOF analysis, respectively.

3.5 Cellular uptake

Cellular uptake of the FAM_AM_LNA_PS sequence was monitored by FISH as described by Guimarães *et al.*[259] with modifications. MKN74 cells were cultured in a 24-well plate until reaching 70% of confluence. Then, the medium was discarded and the cells were fixed using a 4% paraformaldehyde solution, followed by a fixation with 50% ethanol. Each fixation was performed for 10 min at RT. After the fixation, it was added a hybridization solution containing the FAM_AM_LNA_PS at a final concentration of 5, 50 and 100 nM. Plates were then incubated at 37 ºC for 2 hours. Two types of hybridization solutions were tested: one containing 50% (v/v) formamide (Across Organic, NJ, USA), 10% (v/v) dextran sulphate (Fisher Scientific, MA, USA), 0.1% (v/v) Triton-X (Panreac, Barcelona, Spain), 5 mM of EDTA disodium salt 2-hydrate (Panreac), 50 mM Tris-HCl (Fisher Scientific NJ, USA), 10 mM NaCl (Panreac); and another containing urea (VWR BHD Prolabo, Haasrode, Belgium) with different concentrations (0.5 and 2 M) in 900 mM of NaCl (Panreac). After hybridization, the solution was discarded and it was added a pre-warmed washing solution containing 5 mM Tris Base (Fisher Scientific), 15 mM NaCl (Panreac) and 1% Triton X (Panreac) for 30 minutes at 37 ºC. Coverslips were recovered from the plate and were mounted in a microscopic slide. For each experiment two negative controls were made: one using the same hybridization conditions, but without any oligonucleotide sequence in the solution, and another containing the scramble sequence (FAM_SC_LNA_PS).

For the assay using AMOs directly into the culture medium, after the seeding of the MKN74 cells at low confluence (30%), the medium was removed and the hybridization solution containing 0.5 M of urea and the FAM_AM_LNA_PS at a final concentration of 100 nM was added for 10 min. Afterwards, the medium was reestablished and the hybridization took place for an additional 2, 4, 8 and 48 h, at 37 ºC in a 5 % CO_2 incubator. Then, cell slides were fixated and washed as described above. The microscopic slides were mounted using VECTASHIELD Antifade Mounting Medium with DAPI (Vector Laboratories, CA, USA). For image acquisition, an AxioImager Z1 (Carl Zeiss, Germany) epifluorescence microscope was used with a medium grid for optical sections of the fluorescent image. The FAM fluorochrome attached to the oligonucleotides was excited at 488 nm wavelength and the exposure time was fixed for all the preparations.

3.6 Image Quantification

FISH images were analyzed using the ImageJ software (National Institutes of Health, MD, USA). Data was plotted as mean of arbitrary fluorescence units (AFU), representing the difference between the mean of fluorescence intensity of each sample and the background intensity values. Western Blot images were analyzed using the Quantity One® 1-D software v4.6.6 (Bio-rad), and data was normalized to an endogenous control (GAPDH). The background values were obtained by measuring a blank region from each FISH and Western Blot image.

3.7 Viability assay

The different cell lines were seeded at 1.6 x 10^5 cells/well in 96-well plates and left 24h to duplicate. Cells were then incubated with different concentrations (0.5 nM to 100 nM) of LNA-AMOs diluted in Phosphate Buffer Saline 1X (PBS), for 24 h, 48 and 72 h. Cell viability was assessed by MTT (3-(4, 5-dimethylthiazolyl-2)-2, 5-diphenyltetrazolium bromide) assay using the CellTiter 96® AQueous One Solution Cell Proliferation Assay (Promega Corporation, WI, USA) according to the manufacturer's instructions. As a negative control, untreated cells exposed to the same conditions were used. Experiments were performed in triplicate.

3.8 Total RNA extraction

Total RNA from each sample was extracted using the mirVana™ miRNA isolation kit (Invitrogen, Thermo Fisher Scientific, MA, USA), according to the manufacturer's protocol. Shortly, the samples were lysed followed by an acid-phenol chloroform extraction. Total RNA was collected and small RNAs were purified by precipitation with ethanol. Small RNAs were immobilized on glass-fibre filters, washed and eluted with 30 to 60 μL of nuclease-free water. RNA yield and purity were determined by measuring the absorbance at 260 and 280 wavelengths in a NanoDrop® Spectrophotometer (ND-1000; Fisher Scientific). Absorbance ratios (A260: A280) between 1.8 and 2.0 were considered optimal.

3.9 Reverse transcription

The synthesis of single-stranded cDNA from total RNA samples for miRNA amplification was obtained using the TaqMan® MicroRNA Reverse Transcription Kit (Applied Biosystems, CA, USA), according to the manufacturer's protocol. In brief, each reaction consisted on 10 ng of small RNA, 0.15 μL of dNTP Mix with dTTP (100 mM total), 0.19 μL of RNase Inhibitor (20 U/μL), 1.5 μL of 10x RT Buffer, 1 μL of Multiscribe™ RT enzyme (50 U/μL), 3 μL of 5X RT Primers: hsa-miR-9 (RT 583; Applied Biosystems) and RNU48 (RT 001006; Applied Biosystems) and nuclease-free water for a final volume of 15 μL. The reaction was performed at 16ºC for 30 minutes, 42ºC for 30 minutes followed by 85ºC for 5 minutes. The reverse transcriptase reaction for CDH1 mRNA amplification was performed using 200ng of RNA, 1 μL of random hexamer mix (MB129021, Nzytech, Lisbon, Portugal), 1 μL of dNTP Mix with dTTP (100 mM total), 1 μL of RNase Inhibitor (20 U/μL), 2 μL of 10x RT Buffer, 1 μL of Multiscribe™ RT enzyme (50 U/μL) and nuclease-free water for a final volume of 20 μL. Each reaction was carried on a thermocycler according to the following program: 10 minutes at 70 °C, 2 minutes at 4 °C, and 1 hour at 37 °C.

3.10 Quantitative Real-time PCR

qRT-PCR was performed for the relative quantification of miR-9 and of *CDH1* expression, in MKN74 cells after treatment with LNA-based AMOs in the conditions above. The qRT-PCR reaction for amplification of miR-9 was performed using the TaqMan MicroRNA Assays (TM 000583; Applied Biosystems), according to the manufacturer's procedure. For the amplification of *CDH1* mRNA, 0.5 μl of TaqMan Real-Time probe was used in a PCR mixture containing 0.5 μl cDNA, 5.0 μl TaqMan 2X Universal PCR Master Mix No AmpErase® UNG (Applied Biosystems). Reactions were incubated at 95 ºC for 10 min followed by 40 cycles at 95 ºC for 15 s and at 60 ºC for 1 min and run on an Applied Biosystems 7500 Fast Real-Time PCR System. Each sample was amplified in triplicate and normalized to an endogenous control, RNU48 (TM 001006; Applied Biosystems) for miRNA and GAPDH (Human GAPDH Endogenous Control FAM™ Dye/MGB Probe, Non-Primer Limited, Applied Biosystems) for *CDH1* mRNA. The

Applied Biosystems 7500 Fast software was used to analyze the Ct values and the relative amount of miRNA and *CDH1* mRNA were determined using the $2^{-\Delta\Delta Ct}$ method[260].

3.11 Western Blot analysis

Western blot was performed to analyze the effect LNA-AMOs on the expression E-cadherin protein, under the same conditions stated above for the qRT-PCR analysis. MKN74 cells, treated or not with LNA-AMOs were washed three times with ice-cold PBS, and then disrupted using a lysing buffer, containing 1% Triton X-100 (v/v), 1% NP-40 (v/v, pH 7.4), supplemented with phosphatase inhibitor (1: 100) and protease inhibitor (1: 7) during 15 min. Samples were further centrifuged at 14,000 rpm for 20 minutes at 4 °C and the supernatants collected. 20 μg of total protein were mixed with laemmli 4x (Bio-rad, CA, USA), denatured at 95 °C for 5 minutes, and separated on a 10% polyacrylamide gel. Proteins were then transferred onto a nitrocellulose membrane and the membranes were blocked 30 min at RT with 5% dry milk in 0.5% Tween-PBS, followed by incubation at RT during 2 hours with the antibodies in the following dilutions: a mouse monoclonal anti-α-E-Cadherin antibody (1: 1,000) (Clone 36/E-Cadherin, BD Biosciences, CA, USA), and a mouse anti-α-GAPDH antibody (1: 30,000) (sc-47724, Santa Cruz Biotechnology, TX, USA). Blots were then washed 3 times with 0.5% PBS-Tween and incubated with a secondary anti-mouse antibody (1: 20,000) (sc-516102, Santa Cruz Biotechnology) for 2 hours at RT.

3.12 *In vivo* assays

All animal experimentation was performed according to institutional guidelines, with approval of the local institute, and in accordance with the Directive 2010/63/EU regulations.

For this study, 5 to 8 week old nude mice (NIHII(S): nu/nu; male or female) were maintained in standard conditions according to Directive 2010/63/EU and the Portuguese Legislation: Light cycle 12h/12h, *fed ad libitum*, with nesting material such as paper. Mice were monitored daily for general health status, and at least twice a week for tumor volume measurements. Mice were

euthanized at the specific time point described below or whenever the health status of the animal so justifies.

The FAM_AM_LNA_PS oligonucleotide sequence was first tested to assess its potential for *in vivo* detection using fluorescence microcopy. Up to 3 nude mice (NIHII(S): nu/nu) were injected subcutaneously (SC) in two flanks, with $1x10^6$ to $5x10^6$ human cancer MKN45 cells in matrigel (1:1 proportion, total 100 µl administrated via SC), per flank. Following the injection of the tumour cells, the animals were observed at least twice a week for general health status and to measure tumour volume (from when the tumours are not palpable/visible until they are visible or palpable). When tumour volume reached approximately 100-200 mm^3, the animals were then injected intratumorally with PBS (up to 150 µl), in the left-flank tumor, and with the fluorescent AM_LNA_PS oligonucleotide sequence (up to 150 µl), in the right-flank tumor.

The mice were anaesthetized with 1-1.15% (v/v) isofluorane, with controlled concentration of O_2, prior to cancer-cell injection and prior to intratumor injection. After 24h post-AMO injection, the animals were anesthetized with isofluorane prior to *in vivo* imaging. The *in vivo* imaging was acquired using the IVIS Lumina series III (PerkinElmer, MA, USA). After visualization, the mice were humanely euthanized with 4% (v/v) of isofluorane followed by cervical dislocation. Upon euthanasia, necropsies was performed and the tumor was removed, paraffinized for further FISH analysis.

The FISH assay was performed after depparafination and rehydration of the sample. Briefly, three-micrometre thick paraffin cuts were depparafinized using Xylol twice for 10 min each wash, followed by absolute ethanol (twice for 5 min each), and 70% (v/v) of ethanol for 5 min. The samples were rehydrated using distilled water for 5 min. After deparaffinizatin, the FISH assay was performed as described above.

3.13 Statistical Analysis

All data are expressed as means ± standard deviation. Each experiment was repeated at least 3 times. Statistical significance was determined using GraphPad® Prism software v5.0.3. FISH

results were analyzed using one-way analysis of variance (ANOVA) and Tukey's multiple comparisons test, to understand if there are significant differences between the different hybridization conditions tested. MTT, qRT.PCR, and Western Blot results were analyzed using two-way ANOVA and Tukey's multiple comparisons test. Differences in data values were considered significant at p values lower than 0.05, according to three significance levels: $p \leq 0.05$ – significant (*), $p \leq 0.01$ – very significant (**), and $p \leq 0.001$ – extremely significant (***). P values higher than 0.05 were considered not significant (ns).

Chapter 4

Results and discussion

4.1 Theoretical assessment of a comprehensive model for the hybridization dynamics of molecular probes in FISH

FISH is a technique developed in the early ‘80s that allows to detect and localize the presence of specific DNA or RNA sequences within prokaryotic and eukaryotic cells and tissues[261]. The basic principle of the method relies on the complementarity between a fluorescently labeled nucleic acid probe (MP) and a specific nucleic acid sequence that is present inside the cell[262]. A standard FISH procedure includes five steps: fixation, permeabilization, hybridization, washing and finally visualization or quantification of the sample. The fixation/permeabilization of the cells is normally performed together in order to facilitate the uptake of MP by destabilizing the cell wall without lysis or extensive degradation. Hybridization takes place when a specific MP is fully-complementary (or nearly fully-complementary) to the target sequence. After washing non-hybridized or loosely bound MPs are removed, and the hybridized MPs can be detected by using

a fluorescent microscope or quantified by flow-cytometry. FISH may be used both *in vitro* and *in vivo*, where in the latter case, the hybridization solutions is applied directly into the medium, without a prior fixation or permeabilization step[263].

The hybridization step is critical in FISH, as the efficiency of the hybridization is influenced by different factors that need to be taken into account for optimization. Low-fluorescence hybridization signal can result of cell-dependent limitations such as low ribosomal content, inaccessibility of the target site, ribonucleases activity or difficulties in the permeabilization of the cellular envelope or membrane[264]. Optimization of the probe design by using nucleic acid mimics as PNA or LNA can overcome most of these limitations, improving probe specificity and sensitivity[237]. Also, in the case of FISH in fixed cells or tissues, the cellular permeabilization can be further enhanced by using different chemical fixatives to create pores in the cell membrane/envelope. Other parameters, such as the hybridization temperature and composition of the hybridization solution also compromises the success of the hybridization[237,265].

Despite the extended use of FISH in different fields for several decades, a mechanistic approach of the process as a whole is still missing. In their seminal work, Yilmaz *et al.*[266], were able to develop a model to predict the hybridization efficiency in FISH based on the affinity of the probe to the target rRNA. Although their approach quite accurately predicts hybridization efficiency compared to standard prediction methods using the T_m, it only takes into consideration the accessibility of MPs to the rRNA as the limiting step in FISH, excluding other diffusional barriers of the MPs during the process.

For this study, FISH was approached as a particular case of a diffusion-reaction kinetics, similar to other engineering problems that involve diffusion and mass transfer of chemical species within physical and biological systems, and subsequent chemical reaction. For instance, in aerobic bioreactors, the oxygen transfer rate (OTR) and oxygen uptake rate (OUR) are extensively affected by the diffusive and mass transfer coefficients[267]. The oxygen is continuously injected to the system in gas bubbles, from where it needs to be transferred to (and through) the bulk liquid, and then taken up by the microorganisms for maintenance and growth. Like oxygen, MPs in FISH undergo a similar phenomenon during the diffusion from the hybridization solution until the target RNA and subsequent hybridization within the cells. Based on literature models, it was estimated the characteristic time associated with the hybridization process of different DNA-MPs for each

diffusional barrier. As different cell-types impose distinctive barriers for diffusion, it was considered in this approach both bacterial, including gram-negative and gram-positive bacteria, and animal cells. The final goal is to assess which of the diffusional or reaction steps take longer and hence contribute more for the 30-90 minutes that typically lasts a FISH procedure.

4.1.1 The journey: from the medium to the target RNA site

The transport of chemical species within physical systems are ubiquitous to different engineering disciplines, such as the chemical and biological engineering. Taking as an example oxygen transport in bioreactors, it is possible to make an analogy to the transport of MP from the bulk solution to the reaction site within the cells (Figure 4.1).

In bioreactors, the oxygen is transferred from the gas bubbles until it reaches the cells for uptake (Figure 4.1A) [267,268]. This way, the first interfaces are related to the transfer of the oxygen from the gas bubbles to the liquid phase (gas-liquid interface), and the oxygen diffusion through the bulk liquid until the microorganisms (liquid-cell interface). The subsequent interfaces are related to the cellular uptake of oxygen from the bulk to the cytoplasm, and its transport within the cytoplasm to the reaction site. In this model, the variation of the dissolved oxygen concentration with time in the bioreactor is dependent of the OTR and OUR.

The OTR in a bioreactor depends on the liquid side mass transfer coefficient for a specific surface area, kLa, and the driving force in terms of concentrations. The OUR depends essentially on the cellular growth, i.e. on the cellular demands for oxygen and different methods can be applied to calculate it, such as the dynamic technique, where the volumetric uptake rate is determined by measuring the dissolved oxygen concentration after interrupting the oxygen flow[267].

Analogously to the oxygen transfer, for the MP to reach its target, it first has to diffuse from the bulk solution, going through the cellular membrane/envelope and cytoplasm until it reaches the RNA site for hybridization. This process is based on a concentration gradient over time (Figure 4.1 B).

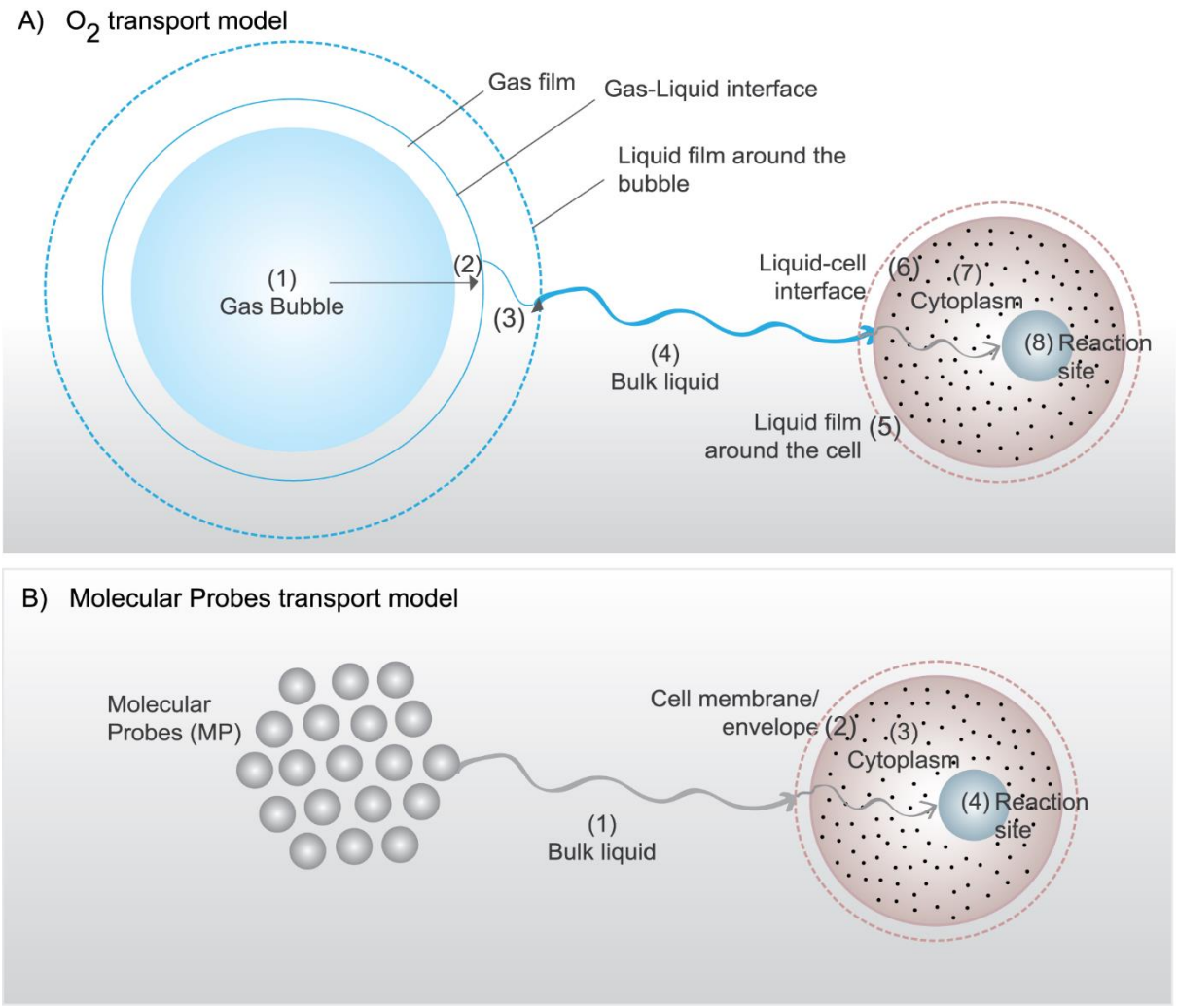


Figure 4.1. Analogy between the oxygen transfer model and the diffusion/reaction model. (A) Oxygen transfer from the gas bubble to the cell cytoplasm and subsequent reaction: (1) Transfer from the interior of the bubble to the gas–liquid interface; (2) Movement across the gas–liquid interface; (3) Diffusion through the relatively stagnant liquid film surrounding the bubble; (4) Transport through the bulk liquid; (5) Diffusion through the relatively stagnant liquid film surrounding the cells; (6) Movement across the liquid–cell interface; (7) Transport through the cytoplasm till the site where the reactions take place; (8) Biochemical reactions involving oxygen consumption. Adapted from Blanch and Clark10; (B) Molecular probe transport model in FISH: (1) MP diffusion through the medium until the cell membrane; (2) Membrane uptake of MP; (3) Cytoplasm diffusion within the cells until the nucleus; (4) Reaction between MP and target RNA.

It is important to notice that, in contrast to oxygen, MPs are not continuously added to the system. Instead, the quantity of MP applied is significantly higher than the number of cells/RNA available

for reaction, in order to ensure a high concentration gradient during the process and a successful hybridization. In fact, the hybridization solution typically contains more than 10^{15} MP molecules and an *Escherichia coli (E. coli)* cell suspension contains around 10^7 molecules of RNA available for hybridization (*E.coli* contains about 55 000 ribosomes per cell in moderate growth conditions at 30 ºC). These values were obtained considering a standard *in vitro* FISH procedure, consisting of 20 µL of hybridization solution with 200 nM of MP and 20 µL of cell suspension with 10^7 cells/mL [269]. Furthermore, the steps regarding the oxygen transfer from the interior of the bubble to the gas-liquid interface to the bulk (Figure 4.1A, step 1-3) are not applicable in a probe diffusion scenario, as the MPs are already in suspension. Additionally, in the oxygen transport models, a liquid film around the cells/solid particle is considered (Figure 4.1A step 5 and Figure 4.1B step 2). The film theory is the simplest theory for interfacial mass transfer that assumes the existence of a stagnant film, also called unstirred layer, near every interface. It represents the resistance to mass transfer that might occur near an interface, and it is almost always hypothetical since the motion of the fluid occurs even in a solid interface[270]. Due to the lack of available data for MP' concentrations in the interface, an overall process, where the cellular membrane/envelope is the first barrier for MP diffusion from the bulk solution to the cytoplasm of the cells can be considered instead (Figure 4.1B, step 2).

The oxygen transport in bioreactors could lay the foundation for modeling the MP transport in a FISH process. Ideally, the analogy would allow to further develop a mathematical model based on the transfer and uptake rate for the MPs. However, adding to the differences highlighted above between both processes, oxygen transport is generally calculated using Equation 1:

$$\frac{dC_{O_2}}{dt} = k_L a \cdot (C^*_{O_2} - C_{O_2}) - q_{O_2} \cdot C_X \qquad \text{(Eq. 1)}$$

Where k_La is the volumetric oxygen mass transfer coefficient in cell free medium (s^{-1}), C_{O2} the concentration of O_2 (kgm^{-3} or $molm^{-3}$), C^*_{O2} the relative to equilibrium concentration of oxygen in each phase, C_x is the cell concentration (kgm^{-3}), and q_{O2} is the specific oxygen uptake rate (mol O_2 $kg^{-1}s^{-1}$).

Table 4.1 Direct comparison between the different steps proposed in the oxygen uptake model and the MP diffusion model, presented in this work

Oxygen model	MP model
1. transfer from the interior of the bubble to the gas–liquid interface	Not applicable. MPs are solid particles assumed to be dissolved in the bulk liquid
2. movement across the gas–liquid interface	Not applicable. MPs are solid particles assumed to be dissolved in the bulk liquid
3. diffusion through the relatively stagnant liquid film surrounding the bubble	Not applicable. MP assumed to be dissolved in the bulk liquid
4. transport through the bulk liquid	Applicable. Considered in the general transfer rate of the MP
5. diffusion through the relatively stagnant liquid film surrounding the cells	Applicable, but there is not enough data to calculate the concentration gradient specifically in this interface. Instead, a global transfer process from the bulk to inside the cells was considered.
6. movement across the liquid–cell interface; diffusion through the solid to the individual cell	Applicable. Diffusion of the MPs through the cell membrane and envelope
7. transport through the cytoplasm till the site where the reactions take place	Applicable. Transport through the cell cytoplasm until the reaction site
8. biochemical reactions involving oxygen consumption and production of CO2 or other gases;	Applicable. Reaction between the MPs and their target RNA
9. transfer of the produced gases in the reverse direction	Not applicable.

In Eq. 1, the first term of the equation corresponds to the OTR and the second to the OUR. Different methods can be applied in order to calculate the OUR, such as the dynamic method, where the volumetric uptake rate is determined by measuring the dissolved oxygen concentration after interrupting the oxygen flow. Under those conditions, the previous equation (Eq. 1) can be simplified to obtain Eq.2 and to determine q_{O2}.

$$\frac{dC_{O_2}}{dt} = -q_{O_2} \cdot C_X \qquad \text{(Eq. 2)}$$

In the case of MP transport, there is not enough data to determine these coefficients individually. Consequently, all the steps defined for the diffusion of the MP (Table 4.1) were modulated in terms of characteristic time for diffusion having in mind the physiologic differences between gram-positive and gram-negative bacteria, and animal cells. The characteristic time is defined as an estimation of the order of magnitude of the time required for a process to reach the equilibrium. One common example of characteristic time applied in chemical engineering problems is for instance the residence time in well-stirred tanks[271]. In here, the characteristic time will give an estimation of the limiting step for diffusion, and provide further insights on under what circumstances the FISH process needs to be approached as a diffusional problem or a reaction kinetics problem.

In the following sections, the characteristic time associated to the transport through the bulk liquid, the diffusion across the cell membrane/envelope and in the cytoplasm, and finally the reaction of the MPs to their target RNA, was calculated for 10 and 40 base pairs (bp) DNA-MPs. The diffusion of the MPs through the cell membrane/envelope is further characterized taking into account the cellular differences between *E. coli*, *Bacillus subtilis* (*B. subtilis*) and HeLa cells, as respective models of gram-negative bacteria, gram-positive bacteria and animal cells.

4.1.2 Diffusion of the MPs in the bulk liquid

In order to calculate the characteristic time in the bulk solution, i.e. the time necessary for a MP to reach a cellular interface, it was first determined the diffusion coefficient of this phase and then applied the mean-square displacement of a molecule in the medium (MSD). The molecular displacement is intrinsically associated to diffusion. Diffusion can be defined as a time-dependent random molecular movement by which matter is transported. This random "walk" is commonly known as Brownian motion - named after the observations of the botanic Robert Brown in the beginning of the nineteen century – and it is the base of the diffusional process[272]. Simply put, without molecular displacement there is no diffusion.

The Brownian motion was mathematically explained almost 100 years after Brown's initial observations by the seminal work of Einstein in 1905[273]. Einstein demonstrated that the molecules

move due to constant forces subjected by other particles in the surrounding medium, causing their motion in a random pattern.

Starting with an example of one-dimension (along the x axis), mathematically the Brownian motion can be seen as a continuous-time process in which a molecule moves a distance δ with equal probability (p=0.5) to the right or to the left at each time step τ (Figure 4.2 A). This means that, after a sufficiently large amount of time (t=nτ), the mean displacement of the molecule is zero with variance $\delta^2 t/\tau$ (Figure 4.2 B).

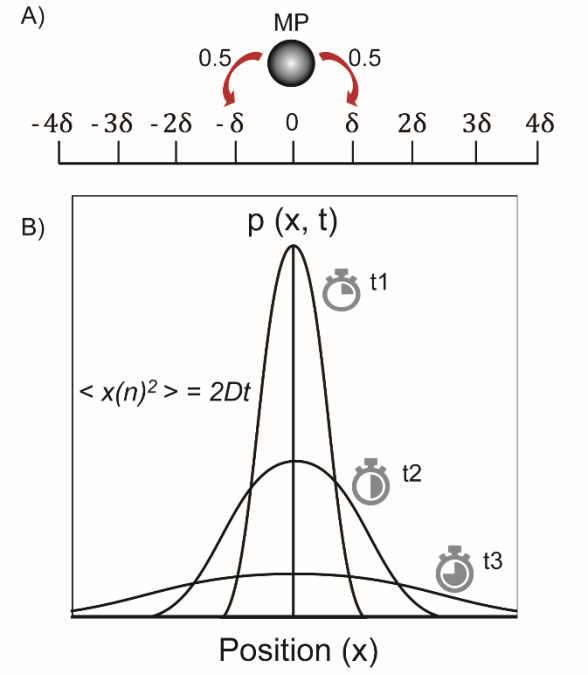


Figure 4.2. Representation of the Brownian motion in one-dimension. A) MP random walk along th x axis with equal probability to move a distance δ or – δ at each time-step. B) Probability (p(x,t)) to find a particle in a time interval at a distance δ from its origin.

During the time-scale of the experiment the molecule has experienced movement, and the distance travelled from its starting point is given by MSD after n time-steps ($<x\ (n)^2>$)[274]. The MSD is directly proportional to time, and is described by the following equation:

$$< x\ (n)^2 > = 2dD_0t \qquad \text{(Eq. 3)}$$

Where x is the average displacement of a molecule over time, d represents the dimension in which diffusion occurs (2d=2, 4 or 6 for one-, two- or three-dimensions, respectively), D_0 is the diffusion coefficient, and t is the time interval of the simulation.

The Einstein's molecular theory modulated mathematically the Brownian motion by correlating the diffusion coefficient to the MSD[273], and associating the diffusion coefficient to measurable molecular properties (Eq. 4).

$$D_0 = \frac{kT}{6\pi\eta_0 r_p} \quad \text{(Eq. 4)}$$

Where T is the absolute temperature (25 °C, equivalent to 298.12 K), η_0 is the viscosity of the medium, r_p is the hydrodynamic radius of the spherical particle, and k is Boltzmann's constant (1.38064852 × 10^{-23} $m^2 \cdot kg \cdot s^{-2} \cdot K^{-1}$). For DNA molecules, the r_p is given by the following correlation (Eq. 5)[275], being the Mw the probe molecular weight.

$$r_{pDNA=}0.024\, M_w^{0.57}\ [nm] \quad \text{(Eq. 5)}$$

Based on these two correlations of Einstein's theory, it is possible to calculate the characteristic time for a three-dimensional diffusion of MPs in the bulk solution.

In order to determine the diffusion coefficient, the Stokes-Einstein equation (Eq. 4) was adapted for non-spherical DNA-MP molecules, which can be modeled as a cylinder of radius 1 nm and length 0.34 nm per base pair[276], and can therefore be considered as a prolate object. The equations for prolate and oblate ellipsoids to model non-spherical solutes were derived by Perrin in 1936[277], as given by the following equation:

$$A(p) = \frac{1}{\sqrt{|1-p^2|}} \begin{cases} \arctan(\sqrt{p^2-1}, & p > 1\ (oblate) \\ \ln(\frac{1+\sqrt{1-p^2)}}{p^2}), & p < 1\ (prolate) \end{cases} \quad \text{(Eq. 6)}$$

Where A(p) is resultant from the angular average of translational and rotational friction factor and p is the ellipsoid aspect ratio, given by the equatorial semiaxis b (1xbp, for a DNA-MP) divided by the polar semiaxis a (0.34xbp, for a DNA-MP).

As a result, it is possible to calculate a translational diffusion coefficient at the dilute limit, $D_t(0)$:

$$D_t(0) = \frac{k_b T}{6\Pi\eta a} A(p) \quad \text{(Eq. 7)}$$

Since the MPs are considered to be anisotropic, the contribution of a rotational diffusion coefficient should be also considered in the diffusion. However, due to the lack of experimental data, only the translational diffusion coefficient was considered, and therefore, D_t was considered equal to D_0.

In a more simple approach, recent works demonstrate that the diffusion coefficient can be determined by considering the DNA mobility in water[278] according to Eq. 8:

$$D_0 = 4.9x10^{-6}[bp\ size]^{-0.72} \quad \text{(Eq. 8)}$$

Where D_0 represents diffusion coefficient and bp size the number of nucleotides present in the DNA. This equation is valid for DNA strands ranging from 21 to 6000 bp, but was developed for double stranded DNA in water. Despite the lack of studies regarding the relationship between single stranded DNA and its size, it has been demonstrated that a rhodamine-labeled 30 bp single-stranded DNA has a diffusion coefficient of $6.2x10^{-11}$ m^2/s in a water solution[279]. This value is in the same order of magnitude as a D_0 of $9.34x10^{-11}$ and $3.44x10^{-11}$ m^2/s calculated by Eq. 8, for 10 bp and 40 bp, respectively.

However, it important to have in mind that the hybridization solution is more viscous than water and that this may affect diffusion. Normally, the hybridization solution contains dextran, which increases the effective viscosity of the medium comparing to water[280], and hence decreasing the motion of MP. As such, in order to have a diffusional range for MPs in the bulk solution, and to test the different approximations stated above, the diffusion coefficients for 10bp and 40 bp DNA-MPs were calculated using eq. 7 and the viscosity values of two 10% (wt/vol) dextran-hybridization solutions: one containing a low molecular weight dextran of 10 kDa (with a viscosity

of 2 mPa.s at 30 ºC)[281] and another containing 500 kDa dextran (with a viscosity of 57.2 mPa.s, at 25 ºC)[280] . The dextran of 500 kDa is used in particular cases to enhance probe hybridization rate by increasing artificially the MP concentration due to the reduction of the available physical space[280,282,283]. Since Eq. 8 does not take into consideration physicochemical parameters as the viscosity, the diffusion coefficient for a 500 kDa hybridization solution was calculated using the Stokes-Einstein equation adapted for non-spherical DNA-MP molecules (Eq. 7). These values were further compared with the diffusion coefficient obtained with equation 8.

As a result for a 10bp MP the diffusion coefficients obtained using Eq. 7 were respectively were respectively, $2.35x10^{-10}$, $1.05x10^{-10}$ and $3.67x10^{-12}$ m^2/s in water, and in 10 kDa and 500 kDa dextran solution. While for the 40 bp MP, the coefficients were respectively, $1.07x10^{-10}$, $4.76x10^{-10}$ and $1.66x10^{-12}$ m^2/s in water, and in 10 kDa and 500 kDa dextran solution. The diffusion coefficients using the MP size-dependent diffusion equation 8 were respectively $9.34x10^{-11}$ and $3.44x10^{-11}$ m^2/s for 10bp and 40 bp MP.

Accordingly, the viscosity of a solution delays the diffusion a specific particle in the medium, as the 500 kDa dextran solutions presents lower diffusion coefficient values when compared with a less viscous solution of 10 kDa and water. Nonetheless, these values were used to calculate the characteristic time of a high-viscous hybridization solution and to modulate the MP diffusion in an extreme scenario. In the case of the 10 kDa hybridization solution, the MP-size-dependent equation (Eq. 8) provides similar values when comparing to the values obtained using equation 7. The molecular weight of the dextran used in the hybridization solution can be a limiting factor for diffusion in FISH. Particularly for gram-positive bacteria, low-viscosity solutions have shown to provide a better result in terms of fluorescent signal[280]. Moreover, the diffusion coefficients calculated for the 10 and 40bp-MPs in the bulk solution using equation 8 were similar to the ones determined by Robertson *et al.*[275] for similar-length linear DNA molecules in buffer solutions (specifically, $9.7x10^{-11}$ m^2/s for an 11 bp-DNA molecule and $4.37x10^{-11}$ m^2/s for a 45 bp-DNA molecule). For those reasons, it was chosen to use Eq. 8 to calculate the characteristic time of MPs in the bulk solution taking as a model a hybridization solution containing 10 kDa dextran.

To determine the MSD, and calculate the characteristic time ($t=MDS/6D_0$, equation 3 adapted for 3D), it was assumed that the MPs and the cells are homogeneously distributed in the bulk solution.

That way, the total volume of the bulk was divided by the number of cells present in solution, assuming that each cell occupied a defined geometrical volume (Figure 4.3).

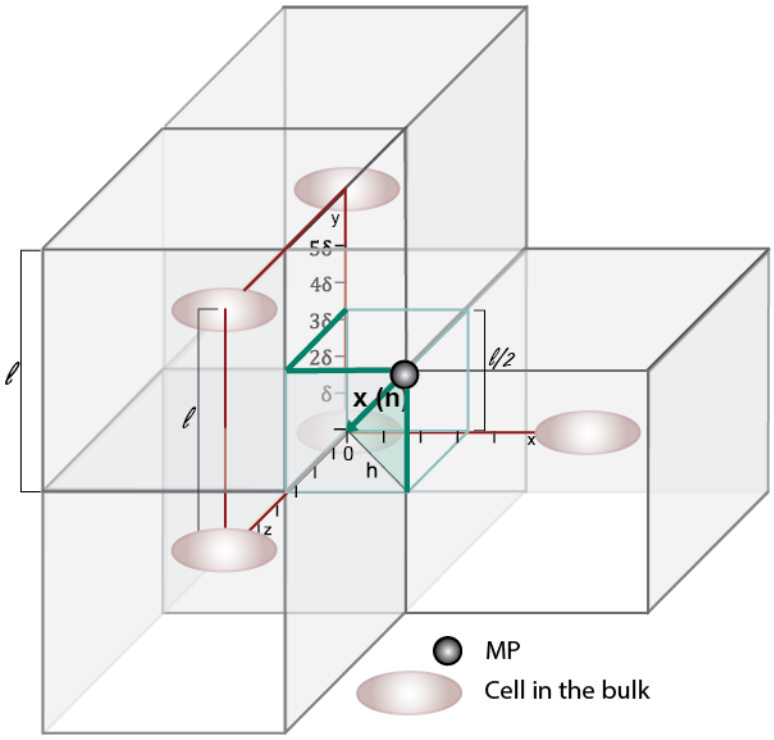


Figure 4.3. Schematic representation of the MP diffusion in the bulk. ℓ is the mean distance between the cell-centers, where the maximum distance for a MP to encounter a cell is $\ell/2$. This distance was further corrected by removing the diameter of each cell-type, considering the cell in the center of the cube, in a vertical or in a horizontal orientation (for non-spherical cells). Considering a three-dimensional movement of MPs, the mean square displacement ($< r(n)^2 >$) is the hypotenuse of Pythagoras's theorem for the given geometric volume ($r(n)^2 = ((l/2)^2 + h^2)$).

Taking the cube root of this number, it is possible to determine the mean distance between the cell-centers (ℓ), where the maximum distance for a MP to encounter a cell is $\ell/2$. This distance was further corrected by removing the diameter of each cell-type, considering the cell in the center of the cube, in a vertical or in a horizontal orientation (for non-spherical cells) (Figure 4.3). Considering a three-dimensional movement of MPs, the mean square displacement ($< x^2 >$) is the hypotenuse of Pythagoras's theorem for the given geometric volume ($x(n)^2 = ((\ell/2)^2 + h^2)$).

The distance between each cell equally distributed in the medium is dependent of the size of the cell and its orientation, in the case of a non-spherical cell. As such, in here, the different layers of the cells were individually characterized, using representative organisms – E. coli for gram-negative bacteria, B. subtilis for gram-positive bacteria and HeLa for animal cells. Rod-shaped cells can be considered to be spherocylinders with radius r and total length L, while spherical cells are modeled as spheres with radius r (as further demonstrated in the next section in Table 4.3). Bacterial cells often present a rod-shape and in here Hela cells were considered spherical cells. Since the cell-size of the models selected for gram-positive and –negative is similar, an average L and r size for bacterial cells was used instead (Table 4.3).

By combining the diffusion coefficients calculated using Eq. 7 and 8 with Eq. 3 it was possible to determine the characteristic diffusion times for the different cells and MP sizes.

In the bulk solution, using equation 8, a 10 bp MP takes around 5.55 seconds (s) to encounter a bacterial cell and 1.84 s to encounter an animal cells, while a 40 bp MP takes around 15 s and 5 s, respectively (Table 4.2).

Table 4.2 Characteristic diffusional times in the bulk solution

MP size (bp)	Type of cell	Characteristic diffusion time (s)		
		Using Eq. 8	Using Eq. 7	
			$D_{10kDa\ dextran}$	$D_{500kDa\ dextran}$
10 bp	Gram-negative	5.58	4.97	142
	Gram-positive	5.53	4.92	141
	HeLa	1.84	1.64	46.9
40 bp	Gram-negative	15.1	10.9	313
	Gram-positive	15.0	10.8	310
	HeLa	4.99	3.61	103

These values are similar to the ones obtained using equation 7 for a 10 kDa dextran solution, validating once more the use of this approximation to calculate characteristic diffusion times for solution with low viscosity (Table 4.2). In the case of solutions with higher viscosity, other

approximations should be applied, as equation 7, to determine the characteristic diffusion time. In a 500 kDa dextran solution, using equation 7, a 10 bp MP takes around 140 seconds (s) to encounter a bacterial cell and 47 s to encounter an animal cells, while a 40 bp MP takes around 310 s and 103 s, respectively (Table 4.2).

Additionally, by applying equation 8 and 3, it is possible to calculate the different characteristic times in the bulk solution for different cell sizes and cellular concentrations, as shown in figure 4.4.

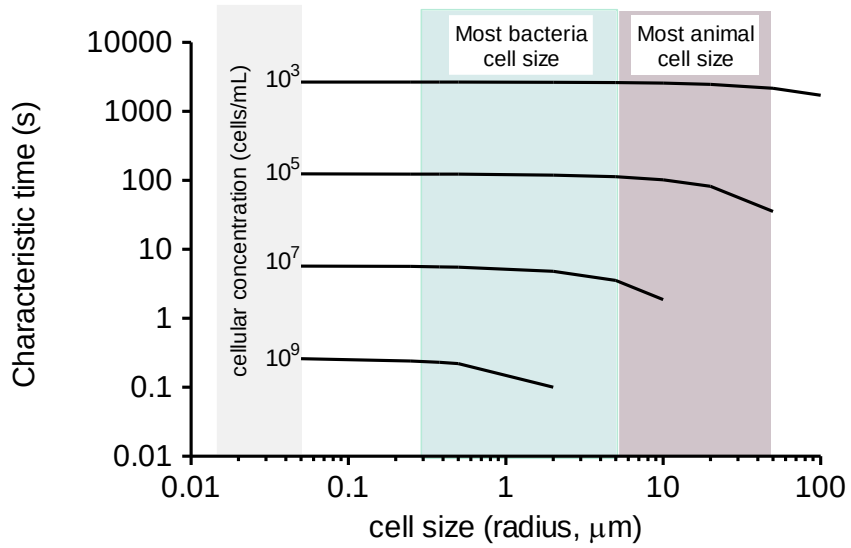


Figure 4.4. Variation of the diffusional characteristic time (s) of a 10bp MP with the cellular size of most bacteria and animal cells (in radius, μm) and the bulk cellular concentrations (cells/mL). These values were calculated considering a 20 μl of hybridization solution with 200 nM of MP and 20 μl of cell suspension.

As expected in the bulk solution, besides the viscosity of the medium, the size of the MPs and the different cells also influences the diffusional time. Animal cells are approximately 20 times larger than bacterial cells, and thus the probability of a MP to encounter a cell in the same bulk volume is higher, resulting in a faster characteristic time. It is important to notice that this also means that for less concentrated samples the characteristic time associated to the bulk diffusion will also increase (Figure 4.4).

4.1.3 Diffusion of the molecular probes through the cell membrane and envelope

Apart from differing in shape and size, the boundaries of cells are constituted by structures with different layers and composition (Figure 4.5). For instance, animal cells present only a cytoplasmic membrane, which is a phospholipidic barrier. Bacterial cells have a different composition at the cell envelope, differing from gram-positive or gram-negative bacteria. The gram-negative bacteria cell envelope is constituted by an outer membrane, followed by the periplasmic space that comprises a thin peptidoglycan layer, and the inner cytoplasmic membrane, a phospholipid bilayer (Figure 4.5)[284]. The periplasmic space normally presents a higher viscosity compared to the cytoplasm due to the presence of small molecules and it is often considered as a "crowded" space[285]. The gram-positive bacteria cell envelope does not have an outer membrane and the peptidoglycan layer is thicker than the one present in gram-negative bacteria, covering the cytoplasmic membrane (Figure 4.5). Both bacterial and mammalian cells have in their membrane proteins channels and other components that are responsible for structure and transport of molecules (Figure 4.5). It is a complex structural and functional system, and a comprehensive review about this subject can be found in Santos *et al.* work [286]. The structural and chemical differences at the membrane level affect the diffusion between different organisms. Table 4.3 summarizes the average dimensions of each barrier for the different cell models defined in here. For bacterial cells the capsule was not considered and the values displayed for the other barriers should be considered as indicative, since the dimensions r and L depend on the growth phase, temperature and available nutrients of the cell, among other variables[287].

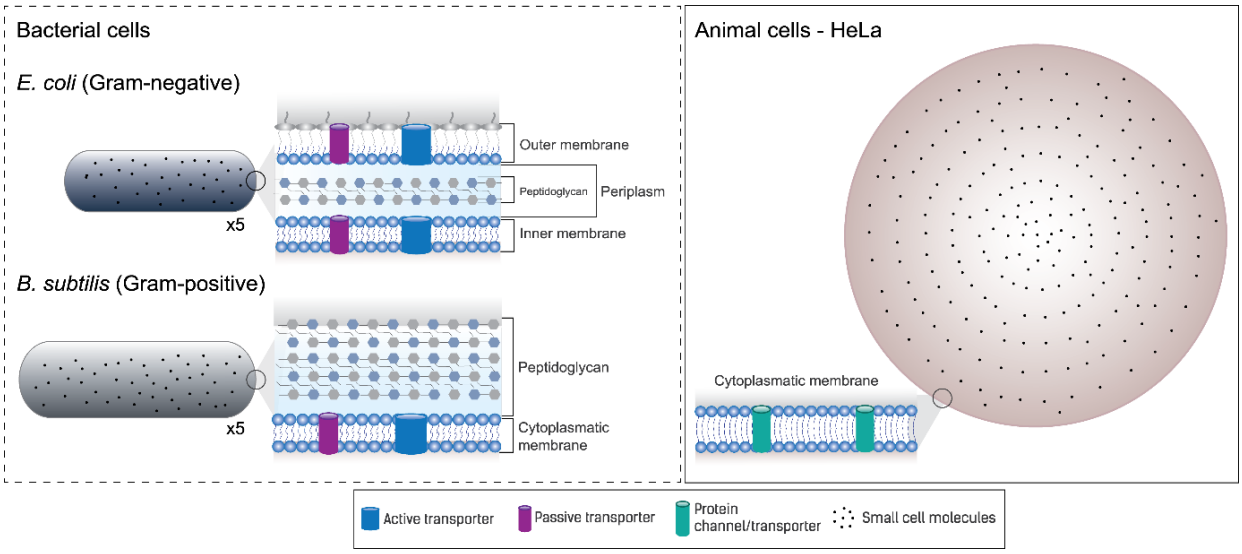


Figure 4.5. Cellular membrane differences between gram-negative and gram-positive bacteria, and animal cells. The schematic representation is at scale considering the cell sizes displayed in Table 3. The bacterial cells are represented 5 times bigger than their real size.

The thickness of each layer was set based on the average of available experimental values. In theory, a lipid bilayer has a thickness of around 4 nm[288]. However, and most likely due to the extra constituents of the outer membrane, such as proteins and lipopolysaccharides (LPS)[284], in gram-negative cells the outer membrane is sometimes considered to be thicker than the cytoplasmic membrane. In here, the core size of the bilayer was considered, keeping in mind that the diffusion in this layer may be slower than in the inner membrane.

To facilitate the interpretation, the different layers were grouped in terms of composition or diffusional mechanisms. The first barrier discussed is the lipid membrane, which in the case of an animal cell, is the first barrier for the MPs. The lipid membrane, is a phospholipid bilayer, similar in composition to the cytoplasmic membrane of gram-positive and gram-negative bacteria. The outer membrane of gram-negative cells is also included in the lipid membranes section.

Table 4.3 Size of the different layers for Bacteria and animal cells, using E. coli as a model for gram-negative bacteria, B. subtilis for gram-positive and HeLa for animal cells

Parameter	Gram negative bacteria (nm) *E.Coli*	Gram positive bacteria (nm) *B. subtilis*	Animal cell HeLa (nm)	Reference
Cell radius [r]	380	490	10 100	[269,289,290]
Total cell length [L]	1940	2500	-	[289,291]
Inner membrane thickness	3.8	3.5	3.5	[292]
Outer membrane thickness	3.5	-	-	[293]
Periplasm thickness	13	-	-	[294]
Peptidoglycan thickness	6.4	35.4 ± 8.2	-	[295,296]

The next barrier discussed, in the case of gram-negative bacteria, is the periplasm followed by the peptidoglycan layer. In the latter, the case of gram-positive peptidoglycan is also included, which despite being the first physical barrier for the MP, is in terms of structure and chemical composition similar to the gram-negative layer, only varying in thickness[284].

4.1.3.1 Molecular diffusion in lipid membranes

As mentioned above, and in spite of composition differences that might affect the MP diffusion, in here the cytoplasmic membrane of gram positive bacteria, both membranes (outer and inner membrane) of gram-negative bacteria, and the membrane of animal cells are approached in the same manner.

Considering the importance of nucleic acids diffusion in lipid membranes, there is a remarkable lack of studies for modeling this process, either in bacteria or animal cells. In one of the few existing studies, the diffusion time of DNA probes in lipid membranes has been estimated by following the formation of endosomes after injecting DNA into the outer side of a liposome. For

an oligonucleotide of 21 bp, the process takes around 1 second[297]. For *in vivo* hybridization, this value should be considered as the lowest bound, because it is well known that proteins and other molecules can obstruct and bind to MPs, decreasing drastically the diffusion coefficient at the membrane. Although no exact equation is available to model this process for the probe of 10 and 40 bp, this information can be used as the indication of the characteristic time a MP can take to go through the membrane.

4.1.3.2 Molecular diffusion in the periplasm of gram-negative bacteria

In gram-negative bacteria, the periplasm is located between the outer and cytoplasmic membrane and is about 13-25 nm in thickness[298]. Besides the peptidoglycan layer, the periplasmic space contains a high concentration of other small molecules like amino acids and peptides that contributes to the increase of the viscosity in this interface[299]. As a result, the periplasm is considered a gel-like matrix and the molecular diffusion in this "crowded" system diverges from a normal Brownian motion (as described in the bulk), and each molecule experiences an effective viscosity during movement. There is limited information about particle diffusion through the periplasm, especially for nucleic acids. Most studies report lateral diffusion of proteins in different membrane layers. Is the case of the work of Mullineaux *et al.*[285], which explores the lateral diffusion of the globular Green Fluorescence Protein (GFP) in the cytoplasm, periplasm, and plasma membrane of *E. coli*. They established that the diffusion in the periplasm (D_{peri}) is about three times smaller than in the cytoplasm (D_{cyto}), but highlighted that in terms of physical properties, the periplasm is a relatively fluid environment, comparable to the cytoplasm. For these reasons, it was assumed that D_{peri} is in the same order of magnitude as D_{cyto}, which values were 7.3×10^{-11} and 1.6×10^{-11} m^2/s, respectively for 10 bp and 40 bp (the determination of D_{cyto} is provided in the section relative to the diffusion of MP in the cytoplasm). Using D_{cyto} and Eq. 3, the 10 bp probe would take 3.8×10^{-7} s to diffuse through the periplasm, while the 40 bp probe, with a larger radius, would take 1.8×10^{-6} s.

4.1.3.3 Molecular diffusion in the peptidoglycan

The peptidoglycan layer is structurally similar in gram-negative and -positive bacteria, mostly varying in thickness. Gram-negative bacteria have a thin peptidoglycan layer, where in gram-positive bacteria the peptidoglycan can be up to 100 nm thick[284]. Overcoming this layer is crucial for a successful FISH procedure, especially in gram-positive bacteria, where longer hybridization times are applied when compared to gram-negative bacteria (normally the FISH procedure takes approximately 120 min from the detection of gram-positive bacteria and 60 min for gram-negative)[280]. Due to the thickness of the peptidoglycan, it is particularly important to proceed to the permeabilization of fixed gram-positive bacteria, or to the enzymatic hydrolysis of the peptidoglycan prior to the hybridization of large molecular probes, in order to have a detectable fluorescence signal[300].

Since there is not data in the literature related to the diffusion coefficient of MPs in the peptidoglycan barrier, the difference between the commonly used experimental hybridization times in FISH for gram-negative and gram-positive bacteria was used to calculate the diffusional coefficient of the layer. In terms of envelope composition, possibly the most significant difference between gram-negative and gram-positive bacteria is the peptidoglycan barrier, and thus the time difference of the experimental hybridization between the two, most likely corresponds to the difference on the thickness of the peptidoglycan. As such, for gram-positive bacteria, a diffusion coefficient of 3.5×10^{-19} m^2/s was obtained, which corresponds to a characteristic diffusional time of 4524 s (75 min). In the case of gram-positive bacteria, the peptidoglycan layer has been considered as one of the most relevant barrier in microbial FISH experiments, but in any case this value is likely to be an overestimation[300].

4.1.4 Transport through the cell cytoplasm until the reaction site

Similar to the periplasm, the cytoplasm is considered a crowded system due to the high concentration of other molecules in the medium. In fact, it is estimated that the macromolecular concentration in the cytoplasm is about 400 mg/mL, 30-40 % of its volume[301,302]. The presence of these molecules increases the viscosity of the medium, slowing down approximately ½ to $^1/_5$ the

diffusion of small molecules (M_w ~ 170 -5,500 KDa) when compared to the diffusion in free water ($D_{cyto} < D_{free\ water}$)[303].

Golding and Cox[304] were the first to introduce the notion that in crowded environments, particles are subjected to a sub-diffusing motion, by examining the motion of fluorescently-labeled mRNA molecules inside E. *coli* cells. They have demonstrated that RNA molecules move discontinuously in *E. coli* cells, with periods of almost localized motion, separated by fast "jumps" to a new position. This type of diffusion is defined as an anomalous diffusion, contrasting to the normal Brownian diffusion.

In the cytoplasm the molecular motion follows an anomalous diffusion due to the crowding, and the diffusion coefficient for any particle of interest can be obtained by applying Eq. 9.

$$\ln\left(\frac{D_0}{D_{cyto}}\right) = \ln\left(\frac{\eta}{\eta_0}\right) = \ln(A) + \left(\frac{\xi^2}{R_h^2} + \frac{\xi^2}{r_p^2}\right)^{-a/2} \qquad \text{(Eq. 9)}$$

where D_0 is the diffusion coefficient of a macromolecule in water of viscosity η_0, D_{cyto} is the diffusion coefficient of the same macromolecule in the cytoplasm, η is the effective viscosity experienced by the macromolecule when crossing the cytoplasm, rp is the hydrodynamic radius of the MP, and ξ, Rh, A, and *a*, are fitting parameters. ξ is an average distance between the surfaces of proteins, Rh is an average hydrodynamic radius of the biggest crowders, A and *a* is a constant of the order of 1. D_0 can be calculated using Eq. 8, and the diffusion coefficient in the cytoplasm for any particle of interest can be obtained by applying Eq. 9. The fitting parameters for the cytoplasm of *E. coli* cells are as follows: ξ = 0.51 ± 0.09 nm, rp = 42 ± 9 nm, ln(A)=0, and a = 0.53 ± 0.04[305]. Regarding animal cells, the fitting parameters obtained for HeLa cells are ξ = 5 ± 4 nm, Rh = 86 nm, Aη_0= 0.9 mPa·s and a = 0.49 ± 0.22[306].

This way, by applying Eq. 9 it was possible to determine D_{cyto} for 10 bp and 40 bp MPs, which was respectively equal to 7.3×10^{-11} and 1.6×10^{-11} in bacteria, and 1.5×10^{-10} and 5.6×10^{-11} m^2/s in animal cells. Using these values, and applying the MSD equation of 3D, the correspondent characteristic times for diffusion of MPs in the cytoplasm were 2.14×10^{-3} and 1.01×10^{-2} s for gram-

negative bacteria, $2.14x10^{-3}$ and $1.01x10^{-2}$ s for gram-positive bacteria, and $2.79x10^{-2}$ and $7.65x10^{-2}$ s for animal cells.

These values, were obtained assuming that the RNA is located in the center of the cells, and as such the maximum distance displaced by the MPs is the radius (in the case of HeLa cells) or half of the total length of the cell (L) (Table 4.3). As it can be observed, the D_{cyto} was higher in animal cells than in bacteria, which is in agreement with the evidence that bacteria have a more crowded cytoplasm than animal cells[307].

4.1.5 Reaction of MP with RNA molecules available at the reaction site

The reaction between a nucleic acid sequence and their target RNA site is limited either by the diffusion until the site or the chemical reaction of both molecules. When the reaction is the limiting step, the time taken for the reaction to occur is longer than the time for diffusion ($t_{reaction} >> t_{diffusion}$). When the reverse case happens, the diffusion is the limiting step, which means that the 2 molecules react immediately at their first encounter. The pathway that the MPs undergo in this step is basically translated in the velocity of the two processes.

The DNA-MP hybridization reaction kinetics, where a single-stranded DNA MP species (A) binds to a target RNA (B) to form a duplex (AB), can be expressed as[308]:

$$A + B \underset{k2}{\overset{k1}{\rightleftharpoons}} AB$$

And the reaction rate of AB formation is given by

$$\frac{d[AB]}{dt} = k_1[A][B] - k_2[AB] \qquad \text{(Eq.10)}$$

where [A], and [B] are the concentrations of the reactants A and B, [AB] is the concentration of the product AB, k_1 is the association reaction constant of second order kinetics ($M^{-1}s^{-1}$), and k_2 is the dissociation reaction constant of first order (s^{-1}). The total concentration of the two reactants is given by:

$A_0 = [A] + [AB]$, and $B_0 = [B] + [AB]$

Many hybridization reactions are carried out with excess of MP to maximize the fluorescence signal and the reaction speed. As demonstrated before, the MPs are in excess comparing to the available RNA molecules for hybridization, such that A0 >> B0, and in this case the reaction kinetics becomes pseudo first order. The reaction rate equation for pseudo-first order kinetics can be expressed as:

$$\frac{d[AB]}{dt} = k_1 A_0 (B_0 - [AB]) - k_2 [AB] \quad \text{(Eq.11)}$$

At initial condition, [AB] = 0 and integrating the above first order equation is possible to obtain:

$$[AB] = B_0 \frac{A_0}{K + A_0} (1 - e^{-(K + A_0) k_1 t}) \quad \text{(Eq.12)}$$

Where K denotes equilibrium dissociation constant defined as k_2/k_1. The characteristic time scale of the reaction was calculated using Eq. 12, knowing the association and dissociation constant values (available in the literature) and assuming a complete hybridization, i.e. all the available RNA molecules are hybridized with the MPs. In this setting, [B] = 0, and [AB] = [B_0]. At t=0, it was considered [A] = 200 nM, and [B] = 1.03×10^{-6} M (4×10^6 ribosomes) for HeLa cells and [B] = 3.54×10^{-14} M (3×10^4 ribosomes) for *E. coli* cells[309]. It was assumed that there was a homogeneous distribution of probes and RNA in all cells, as a simplification, and, based on the literature, that approximately 60% of the mass of the ribosomes is constituted by ribosomal RNA[310].

Regarding the kinetic parameters, it was not possible to find values for the specific MP sizes chosen for this study. It was used instead the following values: $k_1 = 2.9 \times 10^6$ $M^{-1}s^{-1}$ and $k_2 = 0.3$ s^{-1}) for a 16 bp DNA probe, which are values for HeLa cells[311]. Using these values and the Eq. 12, it was possible to obtain the characteristic time of the reaction, which is approximately of 0.02 s for HeLa cells, and 9.8×10^{-4} s for *E. coli* cells.

4.1.6 Summary

The determination of a characteristic time is of great value in chemical engineering, and specifically in FISH it could help defining the limiting step in the hybridization process of MPs, defining the problematic of the hybridization efficiency either as an equilibrium problem or a kinetic problem. In here, the characteristic time in each barrier encountered by the MPs in a FISH procedure from the bulk solution until the reaction site was determined, taking into account the chemical and physical differences between bacterial and animal cells. The obtained characteristic times are summarized in Table 4.4.

Overall, the determined limiting step for diffusion in bacterial cells is the peptidoglycan layer whereas for animal cells the membrane does not impose a significant barrier for diffusion and therefore the limiting step for the diffusion of MPs is more likely to be in the bulk solution or in the hybridization reaction step.

Table 4.4 Summary of the characteristic times given for 10bp and 40 bp MPs in each diffusional barrier

	Characteristic time (s)					
	Gram negative bacteria (*E.coli*)		**Gram positive bacteria (*B. subtilis*)**		**Animal cell (HeLa)**	
Diffusional Barriers	**10 bp**	**40 bp**	**10 bp**	**40 bp**	**10 bp**	**40 bp**
Bulk solution	5.6 - 142	15.1 -313	5.5-141	15.0-310	1.8-46.9	5.0-103.2
Cell membrane/envelope						
- **Lipid membranes**	1.00*	1.00	1.00	1.00	1.00	1.00
- **Periplasm**	3.85×10^{-7}	1.81×10^{-6}	-	-	-	-
- **Peptidoglycan**	2700	2700	4524	4524	-	.
Cytoplasm	2.14×10^{-3}	1.01×10^{-2}	2.14×10^{-3}	1.01×10^{-2}	2.79×10^{-2}	7.65×10^{-2}
Reaction	5.46 (for 16 bp)				4.94 (for 16 bp)	

*value for the inner membrane only

There are a few studies regarding the diffusion of nucleic acids through bacterial and animal cells, and for that reason several adjustments were made to simplify the model presented in here. For

instance, gram-negative outer membrane is considered an asymmetric lipid bilayer, where the inner side is composed by phospholipids and the outer side is a LPS layer. The LPS net negative charge is higher than the usual negatively-charged phospholipids, and it is known to decrease the permeability of the outer membrane to hydrophobic compounds. In *E. coli*, studies showed that it is the outer membrane limits the penetration of PNA, where the LPS is predominately the major barrier for PNA diffusion[312]. The neutral charge of PNA and the relatively high hydrophobicity of this particular nucleic acid compared to charged oligonucleotides was pointed as the probable cause for the PNA limited diffusion in *E. coli* outer membrane. After passing this initial barrier, the molecules face the peptidoglycan layer, which in case of *E. coli*, due to the thickness of the layer, was showed to not impose a significant barrier to PNA passage[312]. This might not be true for gram-positive bacteria, which due to the lack of an outer membrane and LPS as a first protection barrier, they present instead teichoic acids that limit the permeability to hydrophobic compounds and a thicker peptidoglycan layer that may retards significantly the penetration of PNA. In the case of negatively charged nucleic acids, such as LNA, they need to overcome the electrostatic repulsion of the LPS, also negatively charged, in order to cross the outer membrane. Moreover, the outer membrane also presents channel-forming proteins, called porins, which restrict the permeability to hydrophilic compounds and large molecules[313]. The passage of most nucleic acids, which size is around 2–4 kDa, across the outer membrane is very unlikely because porins are only permeable to molecules with 0.7–0.8 nm in diameter and 600 Da in molecular weight.

In the peptidoglycan layer, measurements of the penetration of polysaccharides show that peptidoglycan and its associated anionic polymers provide an open network which is accessible to molecules of molecular weights in the range 30 kDa to 57 kDa. The molecular weight of the MPs used in here is smaller than this range (3 kDa and 12 kDa for 10 bp and 40 bp, respectively), and probably because of the small MP size the diffusion of this molecules is facilitated. The permeability properties of gram-positive cell wall may be dependent upon the nature of the peptidoglycan, particularly its degree of cross-linking and glycan chain length[314]. Moreover, fixation and permeabilization, typically performed in FISH/FIVH, may lead to an alteration to the membrane structure, facilitating the diffusion through this barrier.

All of these particular specifications at the membrane level of bacterial cells were not taken into account in the model, and therefore the characteristic time showed in Table 4.4 cares further optimization, since they might be underestimated specially for the outer membrane of gram-negative bacteria, and overestimated in the case of the peptidoglycan layer.

For animal cells, passive diffusion of nucleic acid mimics is very unlikely because the phospholipid bilayer only allows the passage of small, relatively hydrophobic and uncharged molecules, limiting the uptake of charged molecules of any size[315]. However, there are studies indicating that antisense oligonucleotides may be easily and rapidly internalized by endocytosis, then after transported through multiple membrane-bound intracellular compartments, which may retard cytoplasmic diffusion[316]. Therefore, the phospholipid membrane of mammalian cells might not be a limiting barrier for diffusion of molecular probes, yet their diffusion might be compromised in the cytoplasm and/or bulk solution.

Considering the hybridization reaction of the MPs, the values presented in Table 4.4 were obtained assuming a two-state model, to simplify the system. However, during hybridization the MPs and the target RNA can undergo other configurations (forded or unfolded) as presented in the work of Yilmaz *et al.*[266]. This way, the reaction time might be slower than the one presented in here. Moreover, parameters related to probe affinity, such as Gibbs energy, were not considered in this model, and the model was built only considering the kinetics of the hybridization, not taking into account thermodynamic parameters. The fluorescent intensity of hybridization probes and therefore of the FISH method is influenced by the accessibility and affinity of these molecular probes to their target site. The probe affinity to their target site can be defined thermodynamically by an overall Gibbs free energy change (ΔG^{o}overall). Thermodynamic measurements should be further associated with hybridization kinetics studies in order to obtain a more realistic model of MPs hybridization of MPs in FISH[266,317]. Also, the diffusional time for a MPs to cross the ribosome until reaching the target RNA was not considered, which may affect the overall time in a FISH procedure. Ridgway *et al.*[318], simulated the diffusion and reaction kinetics in a crowded virtual cytoplasm, taking *E. coli* as a model. They stablished that the diffusion time for the largest particles in the cytoplasm to cross a ribosome is roughly around 10^{-7} s and 10^{-6} s.

The development of a more holistic mechanistic model would allow to maximize FISH efficiency helping in the optimization of probe design and probe concentration to apply in different systems.

In future works, these parameters could be further assessed experimentally, using fluorescent microscopy techniques like for instance fluorescence recovery after photobleach (FRAP). FRAP takes advantages of the permanent loss of fluorescent signal of fluorophores when submitted to a beam of intense light (bleaching). After the bleaching of a selected region, the photobleached and the fluorescent molecules of the surrounding areas exchange position, and by the continuing imaging of those regions over time, using a low-intensity light source, it is possible to monitor the movement of both molecules (bleached and fluorescent molecules). The time necessary to recover fluorescence signal in the selected region, or recovery-rate constant, is related to the diffusion coefficient[319]. FRAP has been used to study the motion of fluorescent molecules in solution, on cell surfaces and within the cytoplasm[320,321]. The model presented in here could benefit greatly from well-designed experiments using FRAP to determine the diffusional coefficients in each established diffusional barrier, leading ultimately to an overall diffusion and uptake rate for MPs in FISH in order to better fit the approximation to the oxygen transfer model.

4.2 Anti-miRNA oligonucleotides design and testing

4.2.1 Antisense oligonucleotides design and synthesis

The main goal of this work was to design anti-miR oligonucleotides capable of detecting and silencing miR-9 sequences responsible for E-Cadherin impairment. LNA-based oligonucleotides were selected due to their enhanced properties as AMOs.

Firstly, the miR-9 sequence which targets RNA 3'UTR region encoding the E-cadherin gene was identified. Using the database TargetScan it was possible to define the miR-9 sequence responsible of targeting the 3' UTR site that expresses the *CDH1* gene (Figure 4.6).

	predicted consequential pairing of target region (top) and miRNA (bottom)	seed match
Position 1327-1333 of CDH1 3' UTR hsa-miR-9	5' ...CCUAAAGUGCUGCAG--CCAAAGAC... 3' AGUAUGUCGAUCUAUUGGUUUCU	7mer-1A

Figure 4.6. Representative output of a miR-9 versus gene of interest query using the TargetScan database.

Next, by base complementarity, three main LNA-based AMO sequences were designed with 16 nucleotides targeting the miR-9 (AM_LNA_PS, AM_LNA_2OMe, AM_LNA_Pal, Table 4.5). The AM_LNA_PS sequence is a DNA sequence with an LNA substitution in every 2 nucleotides. The AM_LNA_2OMe, in addition to the LNA substitutions, contains 2'-OMe monomers along the sequence, and the AM_LNA_Pal harbors 2 amino-LNA-palmitoyl monomers within the sequence. AMOs harboring LNA modifications have been reported to show high thermal stability, resistance to nucleases and high efficiency on silencing miRNAs[20,24,240]. LNA substitutions combined with 2'-OMe modifications are known to further improve binding affinity when compared to oligonucleotides with only one type of substitution[239]. The palmitoyl acid has been used to improve cellular uptake of the nucleic acid mimics[258].

Additionally, two control sequences were synthesized, one designed to display two mismatches at the seed region (SC_LNA_PS), and the other is a generic sequence with 19 nucleotides (GN_LNA_PS) available commercially. Furthermore, the AM_LNA_PS and the scramble SC_LNA_PS were labeled with FAM (FAM_AM_LNA_PS and FAM_SC_LNA_PS, respectively, Table 4.5) for cellular uptake and viability assays.

Table 4.5 Anti-miR sequences used in this work and respective theoretical melting temperatures. LNA nucleotide monomers are represented by the symbol + before the nucleotide, 2'-OMe-RNA monomers in small caps letters, DNA nucleotides in capital letters, and palmitoyl-amino-LNA by the symbol, FAM-fluorescein.*

Length (nt)	Name	Type	Sequence (5'-3')*	Predicted T_m (ºC)
16	FAM_AM_ LNA_PS	LNA/DNA	FAM_GC+TAG+ATA+ACC+AAA+GA	57.92
16	AM_ LNA_PS	LNA/DNA	GC+TAG+ATA+ACC+AAA+GA	57.92
16	AM_LNA_2OMe_PS	2'-OMe/LNA	gc+Uag+Aua+Acc+Aaa+Ga	77.60
16	AM_LNA_Pal	DNA/LNA(Pal-LNA(*)	GC*T*AG+ATA+ACC+AAA+GA	73.38[258]
16	FAM_SC_LNA_PS	LNA/DNA	FAM_GC+TAG+ATA+AGC+TAA+GA	51.95
16	SC_LNA_PS	LNA/DNA	GC+TAG+ATA+AGC+TAA+GA	51.95
19	GN_LNA_PS	LNA/DNA	TAA+CAC+GTCT+ATAC+GCC+CA	61.03

All sequences were designed with a PS backbone, which is reported to have increased anti-miRNA activity and enhanced cellular uptake compared to non-modified phosphodiester bonds (PO)[26]. Moreover, theoretical melting temperatures were calculated to guide the design of the AMOs used in this study, in terms of sequence length, number and type of substitutions applied, in order to maintain target specificity and to be functional around 37 ºC, for detection purposes both *in vitro* and *in vivo.*

4.2.2 Screening of the cell lines for miR-9 content

The cell lines used in this study were first tested by qRT-PCR to assess their miR-9 expression levels (Figure 4.7 A). Moreover, since it is expected that miR-9 antagonists induce re-expression of E-cadherin, the expression of E-cadherin expression level was also assessed by western blot (Figure 4.7 B).

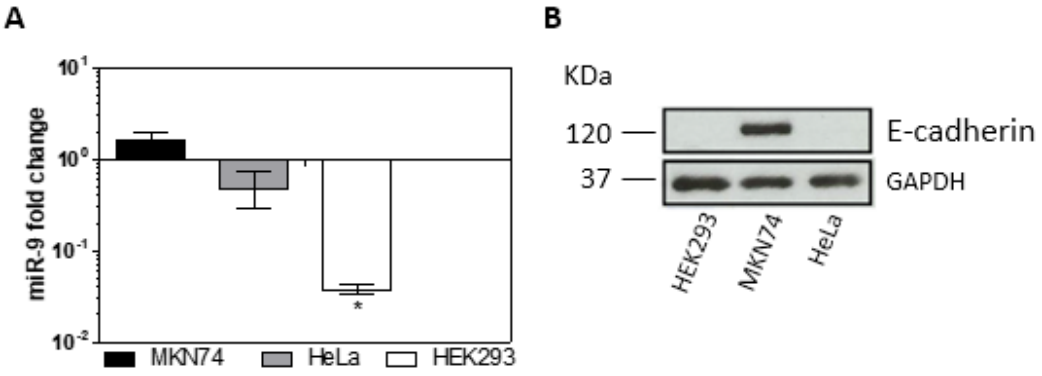


*Figure 4.7. Expression profile of miR-9 (A) and E-cadherin (B) in the cell lines used in this study; * represents a statistically significant difference from the control ($p < 0.05$).*

With exception of the MTT assay, the following experiments were performed using MKN74 cells, since this cell line expresses both miR-9 and E-cadherin (Figure 4.7). This cell line while not presenting a high content on miR-9 expression when compared to other gastric cancer cell models, it presents an unaltered E-cadherin expression, and for that reason it was chosen for this study[118]. In the cell viability studies, all cell lines were used, regardless of miR-9 and E-cadherin expression, to test the cytotoxic effect of AMOs in different tumor cell-types.

4.2.3 Cellular uptake of AMOs and their effect on cell viability

After designing the AMOs, we investigated their ability to enter the cancer cells. For that, the cellular uptake of the FAM_AM_LNA_PS oligonucleotide was monitored by FISH using the miR-9-positive MKN74 cell line.

The first FISH protocol tested comprehended a hybridization solution containing, among other components, 30% (vol/vol) formamide as a destabilizing agent. However, it was not possible to visualize a fluorescence signal even when protocol adjustments, such as hybridization, washing, and fixation time were made. One explanation for this outcome relies on the use of formamide in the hybridization solution. Formamide has been extensively used for over 30 years as an RNA stabilizer to reduce incubation temperature and/or heterologous background hybridization that often occurs with RNA probes[322]. In spite of its advantageous hybridization features, formamide is very toxic and one of the most hazardous chemicals identified by regulatory agencies[323]. Probably due to the high toxicity profile of formamide, the *in vitro* models could not endure the FISH treatment, leading to an unsuccessful hybridization of the LNA oligonucleotides in this study. Several studies report the use of urea in hybridization solution as an alternative to formamide[324–326]. Hybridization buffers containing urea are less toxic and enclose far less chemical compounds comparing to the ones with formamide[265]. Hybridization buffers containing urea are less toxic and enclose far less chemical compounds comparing to the ones with formamide. As an alternative to formamide, a hybridization buffer containing urea in 900 nM of sodium chloride (NaCl) was used in the subsequent FISH assays.

The hybridization was performed using different concentrations of FAM_AM_LNA_PS (5nM, 50nM and 100nM) in 0.5M of urea in 900 nM NaCl. Using urea in the hybridization solution, fluorescence signals were detected for all tested concentrations (FAM_AM_LNA_PS at 5nM, 50nM and 100nM, Figure 4.8 A), with significantly higher intensities at concentrations of 50 nM and 100 nM (50 nM and 100 nM) (Figure 4.8 B).

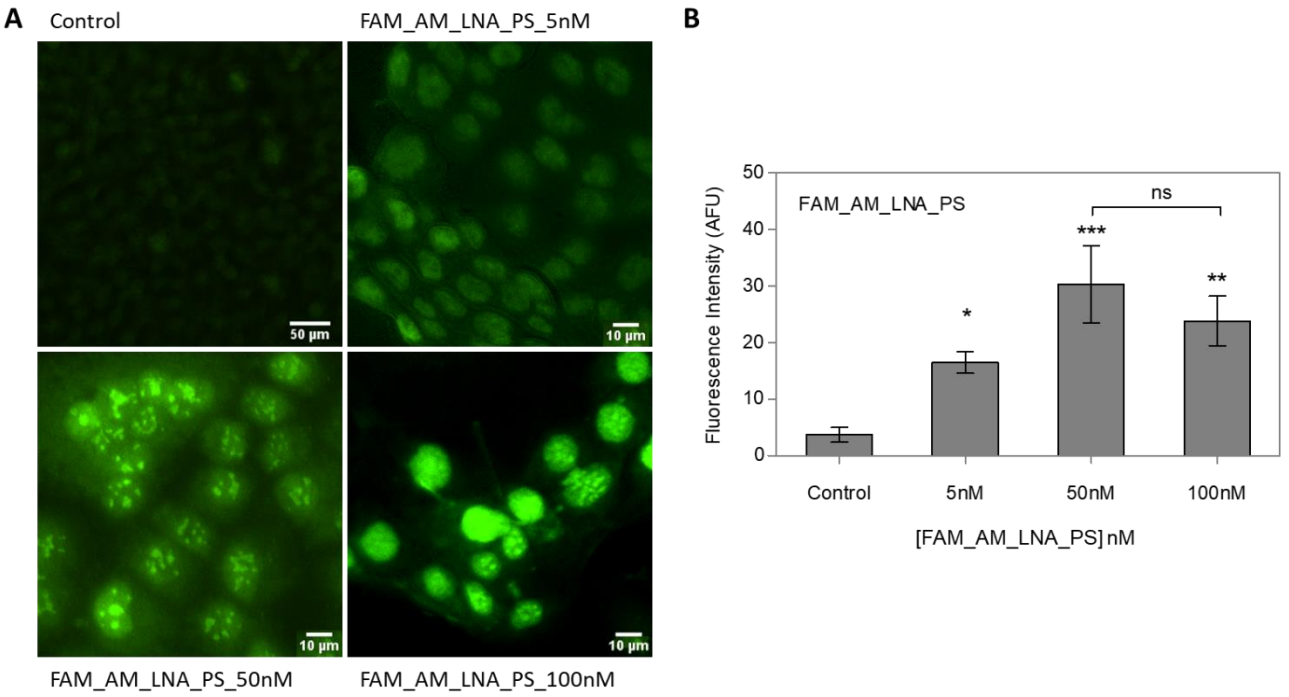


*Figure 4.8. Representative images of the FISH assays using MKN74 cells treated with AM_LNA_PS sequence at different concentrations (FAM_AM_LNA_PS/5nM; FAM_AM_LNA_PS/50nM and FAM_AM_LNA_PS/100nM) in a hybridization solution containing 0.5M of urea. The hybridization step was performed at 37 ºC for 2 hours, followed by a washing step during 30 minutes. Cells without any sequence were used as a negative control (control). All images were acquired using an x200 amplification (A). Average fluorescence intensity for the FAM_AM_LNA_PS sequence at 5nM, 50nM, and 100 nM (B); the fluorescent signal intensity is expressed in arbitrary fluorescent units (AFU); * significantly different from control (*P < 0.05, **P<0.01, ***P<0.001); ns – not significantly different from control (P>0.05).*

As expected, the negative control, i.e. cells without treatment with AMOs, did not display any fluorescent signal (control, Figure 4.8 A). These results highlight the potential of FAM_AM_LNA_PS anti-miR oligonucleotides to enter the cells, allowing the detection by FISH of the target molecule.

The FAM_SC_LNA_PS was used as another negative control at a 50 nM concentration. This concentration was selected based on the results with FAM_AM_LNA_PS, which showed no statistically significant differences between concentrations of 50 nM and 100 nM (Figure 4.8 B).

Using the same FISH settings, the FAM_SC_LNA_PS showed a fluorescence signal in the same range of the lowest FAM_AM_LNA_PS concentration (5 nM, Figure 4.8 B and 4.9 B).

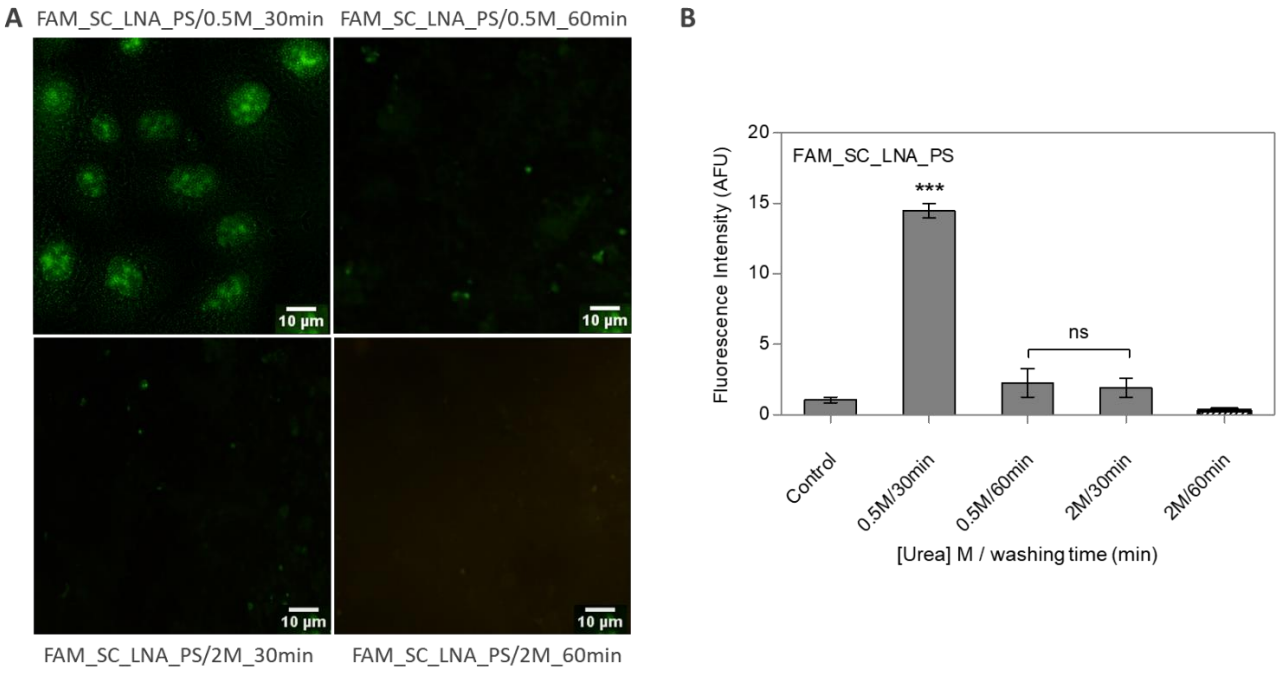


*Figure 4.9 Representative images of the FISH assays using MKN74 cells treated with SC_LNA_PS_50nM sequence at different concentrations of urea in the hybridization solution, and washing times (SC_LNA_PS_0.5M/30min; SC_LNA_PS_0.5M/60min; SC_LNA_PS_2M/30min, and SC_LNA_PS_2M/60min). The hybridization step was performed at 37 ºC for 2 hours. All images were acquired using an x200 amplification (A). Average fluorescence intensity for the SC_LNA_PS sequence using different concentrations of urea in the hybridization solution (0.5M and 2M) and different washing times (30 min and 60 min) (B); the fluorescent signal intensity is expressed in arbitrary fluorescent units (AFU); * significantly different from control (*P < 0.05, **P<0.01, ***P<0.001); ns – not significantly different from control (P>0.05).*

In order to improve AMOs specificity and to eliminate off-target signal, the FISH protocol was adjusted for a longer washing time and and/or higher urea concentration. An extended washing step (Figure 4.9 A, FAM_SC_LNA_PS/0.5M_60min) was sufficient to increase the hybridization stringency and reduce the FAM_SC_LNA_PS signal (Figure 4.9 B).

To further investigate the cellular uptake of AMOs in a setting without carriers or transfection agents, the FAM_AM_LNA_PS and correspondent scramble sequence were added directly in the culture medium.

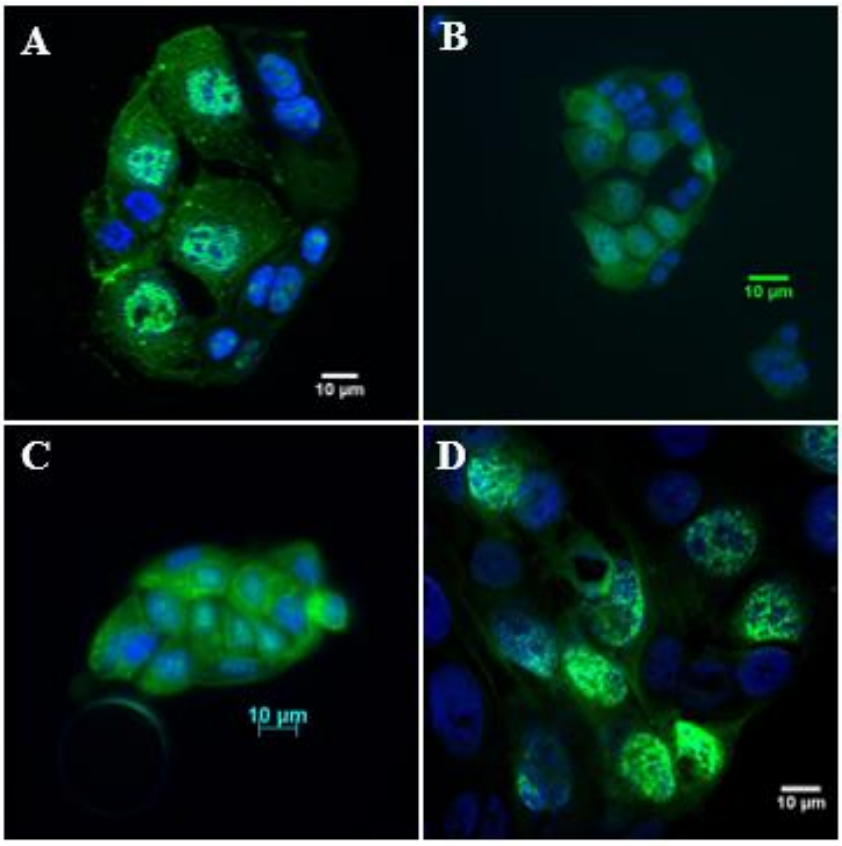


Figure 4.10. FAM_AM_LNA_PS at 100 nM applied directly into the medium after2h (A), 4h (B), 8h (C) and 48h (D) of hybridization. The image was acquired using an x400 amplification and a ZEISS ApoTome.2 with a medium grid for optical sections of the fluorescent image.

Remarkably, a positive fluorescence signal was observed as early as 2h after the AMOs addition (FAM_AM_LNA_PS/naked_2h, Figure 4.10). Furthermore, the fluorescence signal was detected at all time-points, even after 48h of incubation (FAM_AM_LNA_PS/naked_48h, Figure 4.10). Although the signal was not observed transversely in all the cells, it was still possible to detect

fluorescence and to demonstrate that LNA-based AMOs are able to endure in the medium for long periods.

PS-oligonucleotides targeting miRNAs have been shown to be rapidly internalized by cells, both *in vitro* and *in vivo*, in the absence of any carriers, and to interfere with miRNA activity in a process called Gymnosis [327,328]. Gymnotic studies, however, tend to use higher concentrations of AMOs for longer periods of time [327,329]. LNA-based AMOs were able to bind the target miR-9 in the absence of denaturant agents or carriers.

4.2.4 Effect of Anti-miR oligonucleotides in cell viability

After confirming the cellular uptake of the LNA-based AMOs, the effect of AMOs in cell viability was assessed in a panel of cell lines. It was decided to use the sequences labeled with FAM to further evaluate the effect of the fluorochrome in cellular viability. MTT assay results showed that, up to a concentration of 100 nM, FAM_AM_LNA_PS did not significantly reduce cell viability in any of the cell line models used (Figure 4.11 A). These results suggest that LNA-based AMOs are not cytotoxic.

The MTT test was also performed using the FAM_SC_LNA_PS sequence at 5nM and 100nM for 24h and 48h. Since the FAM_AM_LNA_PS did not show significant cytotoxic effect *in vitro*, it was chosen to test the effect of the scramble sequence on cell viability only for the minimum and maximum values of concentration used for the FAM_AM_LNA_PS.

As a result, the FAM_SC_LNA_PS also did not significantly compromise cell viability (Figure 4.10B), reinforcing that LNA-based AMOs are not cytotoxic. Moreover, since both sequences were labeled with FAM and both did not significantly reduced cell viability, this labelling was also considered not cytotoxic.

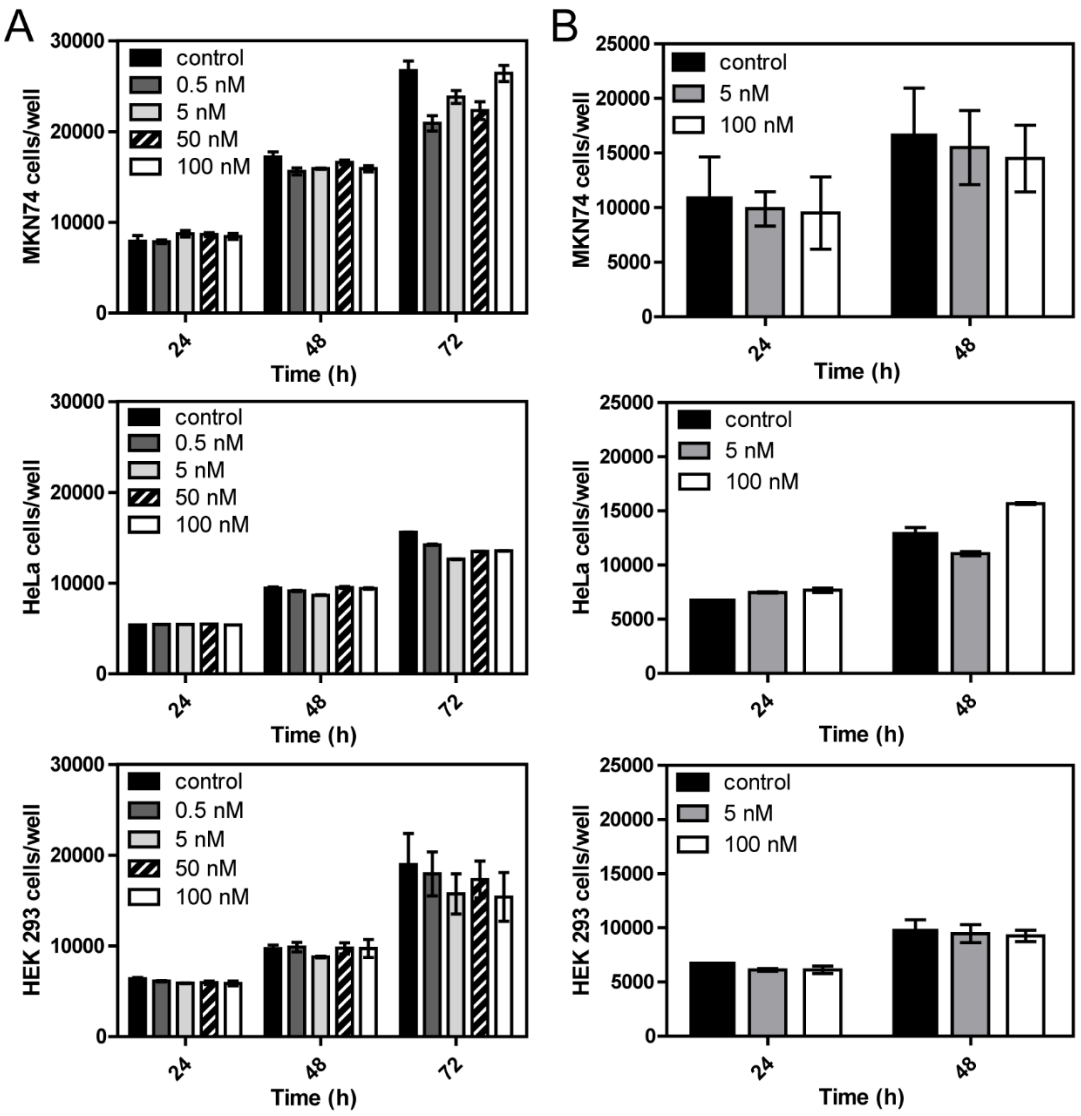


Figure 4.11. MTT viability assay results for the three different cell lines treated with different concentrations of FAM_AM_LNA_PS oligonucleotide sequence (A) and FAM_SC_LNA_PS sequence (B). The control is related to the cells without any Anti-miR oligonucleotide treatment. Error bars correspond to the standard deviation of the mean determined for three independent experiments. No statistically significant differences were found regarding cells treated with AM_LNA_PS or SC_LNA_PS and the control (p>0.05).

Additionally, since is intended to use these sequences *in vivo*, and because the concentration of AMOs applied *in vivo* is normally higher than the ones administrated *in vitro*, the cytotoxic effects of the FAM_AM_LNA_PS on MKN74 cells using higher concentrations (200 nM to 2000 nM) were also tested for 24 and 48 h (Figure 4.12).

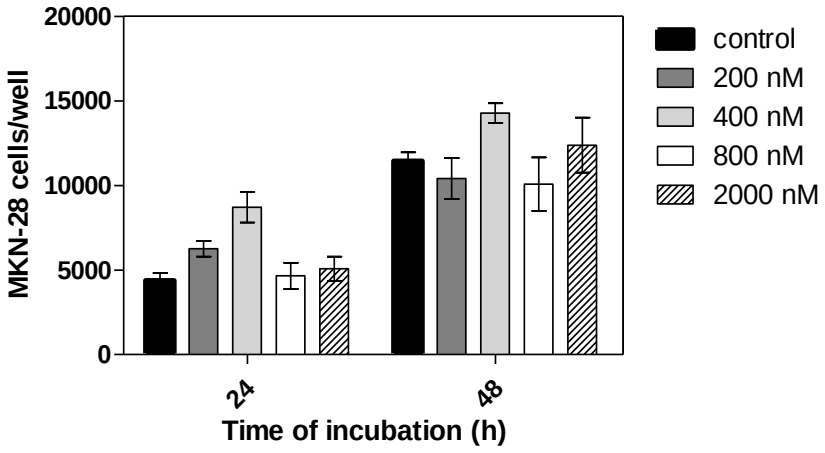


Figure 4.12. MTT viability assay result for MKN74 cells treated with higher concentrations of FAM_AM_LNA_PS sequence. Error bars correspond to the standard deviation of the mean determined for two independent experiments. No statistically significant differences were found regarding cells treated with FAM_AM_LNA_PS or FAM_SC_LNA_PS and the control ($p>0.05$).

The results showed no significant reduction on cell viability at any concentration tested comparing to the control, reinforcing the previous results. Even at high concentrations the AMOs did not showed significant cytotoxic effects on the cell model used. At the end, it was possible to conclude that in general that LNA anti-miR oligonucleotides are not toxic for the cell models, time points and concentration tested.

4.3 Anti-miRNA activity assessment

4.3.1 miR-9 relative quantification

The AM_LNA_PS and two additional chemically modified oligonucleotides (Table 4.5) were used for evaluating the effectiveness of AMOs on the silencing of miR-9.

The SC_LNA_PS sequence had no effect in the expression of miR-9, presenting similar results to the GN_LNA_PS sequence (Figure 4.13), and was thus suitable to function as a negative control.

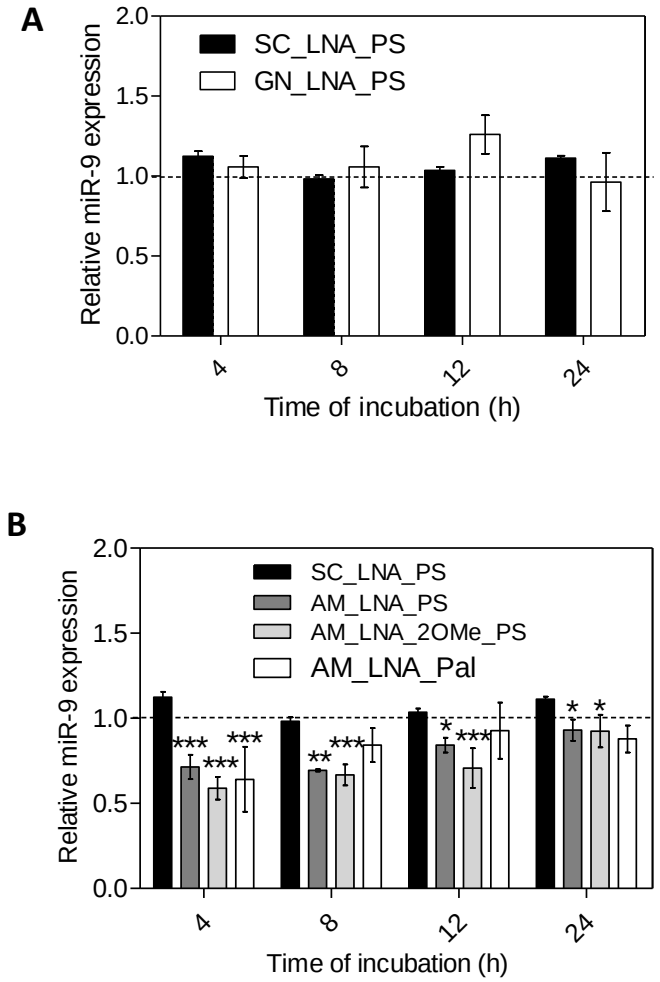


*Figure 4.13. Relative quantification of miR-9 expression by qRT-PCR for the MKN74 cells treated with the control sequences: SC_LNA_PS and GN_LNA_PS (A) and AM_LNA_PS, AM_LNA_2OMe_PS, AM_LNA_Pal_PS (B) sequences. Error bars correspond to the standard deviation of the mean determined for three independent experiments. *significantly different from control (*P < 0.05, **P<0.01, ***P<0.001).*

All the anti-miRNA oligonucleotide designs showed some silencing effect on the miR-9 expression levels. The AM_LNA_PS conformation significantly decreased the miR-9 expression

in the first 8h of incubation. After that time-point, cells started to recover miR-9 content until basal levels (Figure 4.13 B).

The AM_LNA_2OMe_PS conformation influenced the expression of miR-9 during a longer period. A decrease of miR-9 expression levels is visible after 4h, which is maintained up to 12h of incubation (Figure 4.13 B). After that point, there is an increase of miR-9 expression levels, until the basal miRNA level, as a response of the cell to regain miR-9 content after external-stimulated repression.

The AM_LNA_Pal_PS design shows only a repression on miR-9 expression levels at the 4 hour time-point. After that, there is an increase of miR-9 expression almost to a basal level until the end of the experiment (Figure 4.13 B).

LNA-modified AMOs have been reported to specifically inhibit miRNAs leading to up-regulation of the target proteins[20,21,23,239]. The 2'OMe modification associated with LNA monomers is known to display increased potency and stability on silencing aberrant miRNAs[22]. Accordingly, the AM_LNA_2OMe_PS used herein showed a more extensive effect on repressing miR-9 levels, when compared with the other configurations.

The palmitic acid conjugation has been reported to facilitate cellular uptake due to their lipophilic properties[330]. However, it has also been shown that palmitoyl residues do not offer stabilization through electrostatic interactions, and thus the conjugation of 2'-amino-LNA monomers with a palmitoyl moieties show poor duplex stabilization[258]. In fact, oligonucleotides with three palmitoyl-modifications, despite of still being able to form a duplex with RNA, the resulting duplex is severely destabilized when compared to unconjugated 2'-amino-LNA modifications[258]. For this reason, the palmitoyl-amino-LNA (AM_LNA_Pal) was probably not able to form stable duplexes at later time points and consequently was only able to act to its target on the first 4h of incubation.

All the LNA-based AMOs configurations tested were able, to some extent, to repress miR-9 expression at early time points and at low-dosing administration of oligonucleotide. There is some evidence that the PS-AMOs internalization occurs via the endosomal pathway, through which the oligonucleotides might meet the miRNA somewhere within, blocking its action[329]. This silencing

mechanism is still not yet validated for all cell types and miRNAs. Nevertheless, it seems that the PS-AMOs do not necessarily need to be released from endosomes to act upon their target miRNA. This mechanism might explain the fact that the AMOs tested in this study were able to silence the target miRNA in such a short period of time.

4.3.2 *CDH1* relative quantification and E-cadherin expression

All the conformations tested have transversely followed the same pattern between the results obtained by mRNA qRT-PCR and protein quantification. Only the AM_LNA_Pal oligonucleotide sequence after 8h of incubation has (Figure 4.14 A) shown a significant decay on the relative content of *CDH1* mRNA, which was not verified on the protein expression at the same and following time points (Figure 4.14 B). The reason for this result is not very clear. Probably due to the tight regulation of the MKN74 cells, as the cellular machinery is trying to regain miR-9 function by overproducing the miRNA to compensate the effect of the anti-miR sequence, it might have destabilized the expression of *CDH1* mRNA.

In general, for all the AMOs conformation tested, it was not visible an inversely proportional variation on *CDH1* mRNA relative expression level as a possible consequence of the miR-9 silencing. The slight increase in *CDH1* mRNA expression level along time could be explained by the fact that it was only tested a low-dose of AMOs and in a relatively short period of time. Also, the AMOs tested despite designed to target specifically the miR-9 loci responsible for E-cadherin impairment, might also target other miR-9 forms as well. As a consequence, the decrease of miR-9 content might be more extensive than the effect on the *CDH1* mRNA expression level. Another factor to have in consideration is that at this early stage we believe the AMOs only meet the miRNA in the endosomes, and probably due to this do not reach all the miR-9 available content. Therefore, the AMOs tested in this study might present higher potency on silencing the target miRNA in a setting using a broader delivery system, higher AMOs concentration and/or longer incubation periods.

Regarding the protein expression, it was observed a delay between the effect on the relative content of *CDH1* mRNA and the consequent impact on the protein expression, due to the normal time-gap between mRNA re-expression and initiation of the protein translation.

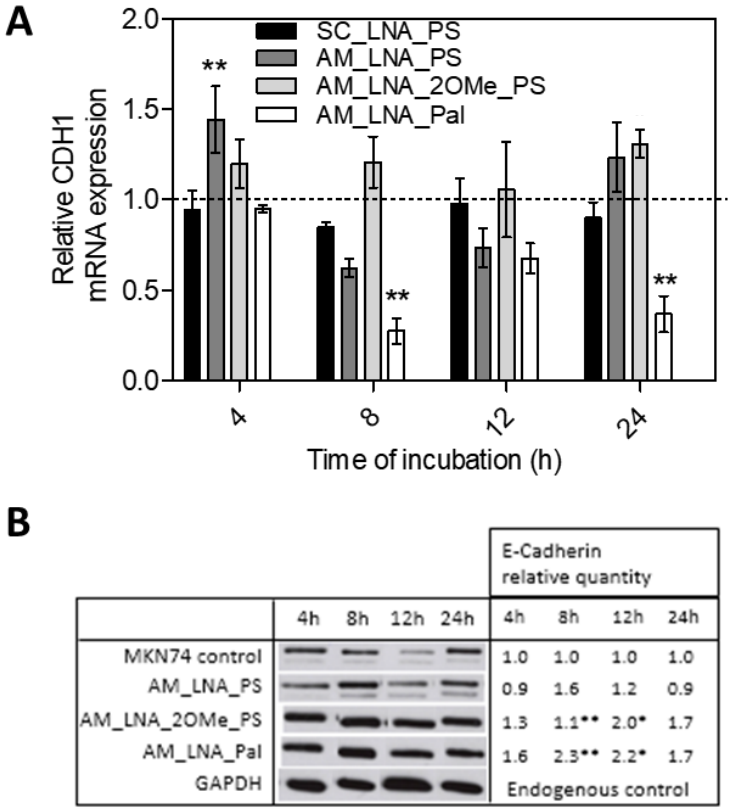


*Figure 4.14 Relative quantification of CDH1 mRNA levels by qRT-PCR for the MKN74 cells treated with AM_LNA_PS, AM_LNA_2OMe_PS, AM_LNA_Pal_PS and SC_LNA_PS sequences after 4, 8, 12 and 24h of incubation (A). E-Cadherin protein level measured by western blotting, extracted from MKN74 cells subjected to the same conditions above (B). All the results were normalized against the situation without any treatment (MKN74 WT) and the respective endogenous control; *significantly different from control (*P < 0.05, **P<0.01, ***P<0.001).*

When analyzing the results by western blot (Figure 4.14 B), it is evident some effect on the E-cadherin expression in comparison with the MKN74 control in all the situations. In cells treated with the AM_LNA_PS oligonucleotide, there is a slight increase in E-cadherin expression after 8h of incubation, which then remains stable in the following time points. These results are in accordance with the qRT-PCR data, with a small delay between the *CDH1* mRNA relative content

and the consequent effect on the protein expression (Figure 4.14 B). In cells treated with the AM_LNA_2OMe_PS and AM_LNA_Pal, the level of E-cadherin seems to increase at all time points, especially at 8h and 12h where a significant increase of protein expression is observed (Figure 4.14 B).

The use of AMOs to control miRNA expression is a promising alternative to silence undesirable miRNA function and to control gene activity. All the sequences tested were able to silence the expression of upregulated miR-9 using a cancer cell model. Even though the results on the E-cadherin expression were not so straightforward, there is a slight increase on protein expression. Overall, the LNA_2OMe_PS oligonucleotide sequence seems to be the design with more promising results on the silencing of miR-9.

Furthermore, the designed AMOs might present higher potency on silencing the target miRNA in a setting using a broader delivery system, higher AMOs concentration and/or longer incubation periods. Also, these sequences could be further improved and modified to target other overexpressed miRNAs within GC and in other human disorders.

4.4 *In vivo* detection of miR-9

The promising results of AMOs tested in vitro led the way for the *in vivo* testing. The FAM_AM_LNA_PS was used in nude mice, to test its potential to detect the target miRNA in xenograft-subcutaneous tumors. Human gastric MKN45 cancer cell line was used for the *in vivo* assays, since this cell line, besides expressing miR-9, shows high tumorigenic capacity and is able to form rapidly consistent solid tumors[331]. Unfortunately, it was not possible to detect a specific fluorescence signal using the developed AMO *in vivo*. The images obtained using IVIS microscope showed an intense fluorescent signal (intense red) uniformly through the animal (Figure 4.15 A), which seems to be caused due to the high autofluorescence of biological tissues. To test this hypothesis, an *in vitro* assay was performed using the *in vivo* conditions in a 24-well plate. In this setting, it was possible to visualize a specific fluorescence signal in the IVIS microscope (Figure 4.15 B) and to discriminate the positive fluorescent signal of MKN45 cells incubated with the FAM_AM_LNA_PS (Figure 4.14 B, red square) from the control situation using MKN45 cells

incubated with a PBS solution (Figure 4.15 B, white square). This result evidences the fact that at the emission wavelength of fluorochrome used to label the FAM_AM_LNA_PS (488 nm) it is not possible to discriminate a positive fluorescence signal from the tissue natural autofluorescence. Biological structures present a natural autofluorescence arising from endogenous fluorophores, when cells and tissues are excited by UV/Vis radiation of suitable wavelength. The majority autofluorescencing molecules in animal cells such as NAD(P)H, collagen or melanin present an emission fluorescence spectrum ranging from 305[222] up to 560 nm[332]. As such, fluorescent molecules for *in vivo* imaging should be labeled with fluorochromes with an emission spectrum starting from 600 nm.

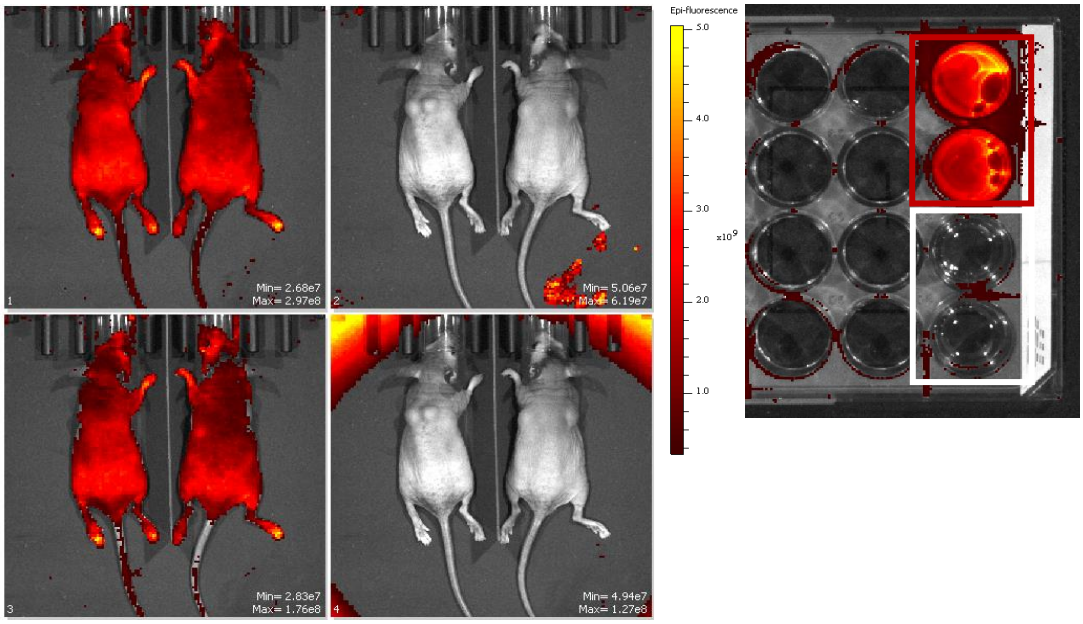


Figure 4.15. In vivo imaging using AM_LNA_PS sequence at 2µM in a hybridization solution containing 0.5M of urea in 900 mM of NaCl (A). MKN45 cell in a 24-well plate incubated with FAM_AM_LNA_PS sequence at 2µM (red square); the white square is the control with MKN45 cells incubated a PBS solution (B). The imagens were acquired using an IVIS Lumina series III microscope. The scale bar indicates the epi-fluorescence intensity: dark red corresponds to high fluorescence signal and yellow low fluorescence signal.

Also, since it is possible to detect fluorescence at 488 nm in the plates using IVIS imaging system, it is believed that the lack of a specific fluorescent signal might not be due to a sensitivity limitation

of the equipment. IVIS® spectrum living image system enables the fluorescence detection to the pmol of labeled-oligonucleotides[333] and has been successfully used on the *in vivo* detection of miRNA expression in tumors using miRNA nanosensors[334].

After euthanasia, the tumors were colected to perform a FISH assay on deparafinized tumor sections. There was no visible difference between the FISH samples compared with the *in vivo* imaging results. In fact, there is still a strong fluorescence signal in the tumors treated with a control solution containing PBS (Figure 4.16 A) when compared with the tumors treated with the AMO (Figure 4.16 B).

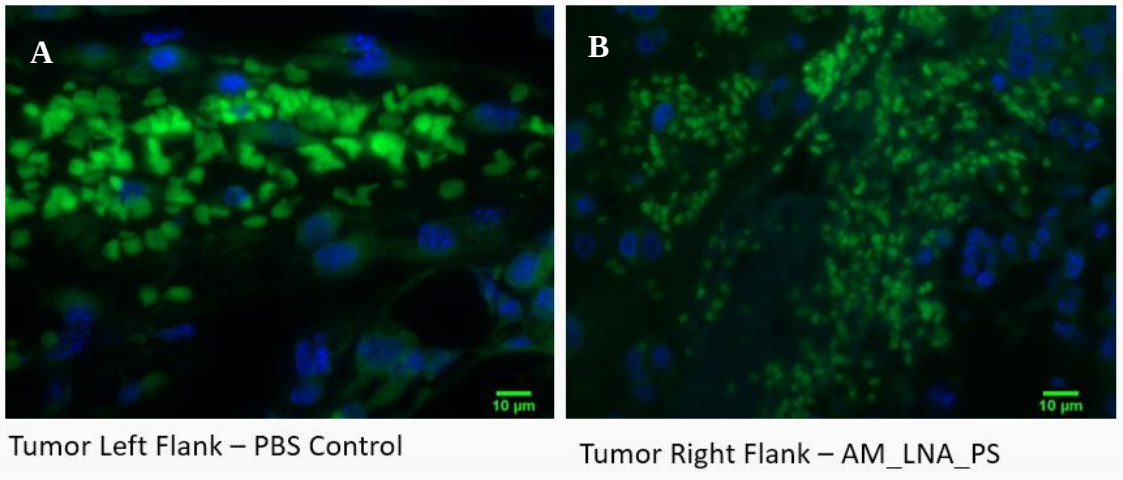


Figure 4.16. Representative images of FISH in depparafinized tumors. The left tumor corresponds to the control situation with PBS (A) and in the right tumor an AM_LNA_PS at 2µM in a hybridization solution containing 0.5M of urea was administrated (B). The images were acquired using an x200 amplification using a ZEISS ApoTome.2. All images were taken at equal exposure times, with overlapping of the DAPI channel, to stain the nucleus.

This result reinforces the fact that fluorochromes with an emission spectrum at 488 nm wavelength might not be suitable to be used in an in vivo approach. Nonetheless, from the results using the 24-well plate, there is evidence that the developed AMOs might be able to detect the target miRNA in an *in vivo* situation.

Chapter 5

Concluding remarks and future perspectives

5.1 General conclusions

The main goal of this work was to design LNA-based AMOs to target the miR-9 in GC. Overexpressed miRNAs are often associated with the downregulation of many tumor suppressing proteins, and are thus implicated in the pathogenesis of several human diseases, including cancer. Due to the accumulating evidence of miR-9 overexpression in a panel of 37 GC specimens, and that its overexpression might influence the expression of E-cadherin, the AMOs developed in here were designed to specifically bind to the miR-9-5p region that targets the *CDH1* 3'UTR mRNA. In this work, by targeting overexpressed miR-9 in GC cell lines using AMOs, it was expected to promote the normal function of *CDH1*-encoding mRNA and this way reestablish the expression of E-cadherin. In addition to the therapeutic approach, this study also aimed to explore the potential of AMOs combined with the FISH technology to effectively detect *in vitro* and *in vivo*

overexpressed miRNAs and their relevance to function as miRNA markers involved in different human diseases.

In order to achieve the proposed goals, three LNA-based-AMOs were designed taking into consideration the enhanced miRNA silencing properties of LNA and 2'-OMe substitutions, as well their improved binding affinity and serum stability; A third sequence was designed containing a palmitoyl acid moiety, which is believed to improve cellular uptake. A PS backbone modification in all the sequences was also selected, mostly due to its improved *in vitro* and *in vivo* cellular uptake properties, and resistance to exonucleases when compared to unmodified oligonucleotides.

Before moving to a treatment based approach, the ability of AMOs to provide a fluorescence signal that can be used as a diagnostic marker was evaluated. Herein, after optimization of a standard FISH protocol, it was possible to detect a specific FISH signal using the FAM_LNA_PS at 50 nM in a hybridization buffer containing urea instead of formamide. The urea-based hybridization solution has provided a strong and specific fluorescence signal, especially when combined with longer washing periods (60 min). Additionally, the ability of AMOs to diffuse through the cell membrane and bind to the miRNA in the absent of a carrier or a denaturant solution was evaluated by adding AMO directly to the culture media, in a process called Gymnosis. Fluorescence signal was observed as soon as after 2h of incubation with the AM_LNA_PS sequence. Further tests on cellular viability have shown that AMOs were not toxic to any of the three cell-lines tested.

In terms of the therapeutic application of the designed AMOs, all the sequences were able to silence the expression of overexpressed miR-9 in MKN74 cells, and it was observed a slight increase on E-cadherin expression. Overall, the LNA_2OMe_PS oligonucleotide sequence seems to be the design with more promising results on the silencing of miR-9.

Moreover, the *in vivo* studies in mice models, despite of the tissue autofluorescence, showed promising results towards the *in vivo* detection and silencing of miR-9 using the AMOs designed in this work, since it was possible to specifically detect miR-9-positive tumor cells in a 24-well plate.

Regarding the diffusion and hybridization dynamics study of MPs in FISH, it was possible to estimate the characteristic time associated with the hybridization process of different molecular probes for each diffusional and cellular barriers, including the reaction time associated with the formation of the duplex MPs:RNA. For bacterial cells, the limiting step for diffusion is likely to be the peptidoglycan layer (2700-4524 s), whereas for animal cells the limiting step is more likely to be the diffusion of the MP through the bulk medium (1.8 s to 103.2 s depending on the size of the MP and the viscosity of the solution) followed by the hybridization reaction time (5 s). The hybridization dynamics model provided here may serve as a basis to optimize FISH protocols and as a conceptual background for the interpretation of FISH as a specific case of a diffusion-reaction process.

In Summary, the therapeutics involving AMOs is a promising approach to silence undesirable miRNA function and gene activity implied in several human pathologies. For that reason, there is an intense effort to optimize the design of AMOs in order to validate this strategy as an efficient therapeutic route in cancer treatment. Currently, three LNA-AMO-based drugs are undergoing clinical trials: one called Miravirsen developed by Santaris Pharma to control the activity of miR-122 associated with Hepatitis C virus (HCV) infection[219]; and two others from miRagen Therapeutics to inhibit miR-155 (MRG-106) and miR-92a (MRG-110, S95010) involved respectively, in blood cancers and in acute cardiovascular diseases. Despite the promising results, no therapeutic strategy has been yet fully developed and validated. Nevertheless, the AMO technology could reach far beyond the therapeutics, and be associated with real-time detection systems for an effective, safe and immediate detection of miRNAs in humans, as demonstrated here by FISH. *In situ* detection of miRNA accumulation in tumor biopsies may provide a highly valuable approach for prognostic and diagnostic evaluation in a clinical setting. Furthermore, little is still known on how the biological systems regulate miRNAs expression in the different human diseases[335]. The double role of miRNAs requires a more intense study in order to develop reliable, specific and safe technologies to fully control miRNA expression. The AMOs technology is indeed a great tool, not only to detect and silence aberrant miRNAs, but also to help unraveling the mechanisms behind miRNA biogenesis and function.

5.2 Future perspectives

This study has demonstrated the potential of LNA-based anti-miRNA sequences to successfully detect and silence overexpressed miR-9 in a gastric cancer model. Despite the promising results, the AMO sequences designed in here could be further optimized by using an improved delivery system, higher AMOs concentration and/or longer incubation periods. Furthermore, the design of LNA-based AMO sequences could also be improved and adapted to target other overexpressed miRNAs within GC other human disorders.

For instance, in gastric cancer, *H. pylori* is considered as a Group 1 carcinogen infection, since it increases the susceptibility to GC. Recent studies have demonstrated that several miRNA, including let-7, miR-17/92, miR-21, miR-106b-93-25 cluster, miR155, miR-194, miR-196, miR-204, miR-222, and miR-223 are dysregulated in *H. pylori*-positive patients, suggesting that *H. pylori* may regulate miRNA activity[336–339]. As an example, miR-204 is reported to be downregulated in patients with *H. pylori*-associated gastritis. MiR-204 targets a metalloproteinase, encoded by the *MMP9* gene, which is responsible for the wound healing delay of the intestinal epithelium, and thus the overexpression of *MMP9* aggravates the inflammatory process[336]. It is coming to light that the infection machinery of *H. pylori* takes advantage of endogenous miRNAs to promote chronic inflammation and cancer progression. *H. pylori* has been under intense study amid the research groups involved in this thesis, either by exploring the virulence factors associated with the bacteria, or by the development of rapid detection methods and alternative therapeutic approaches using nucleic acid mimic oligonucleotides. Unravelling the mechanism through which *H. pylori* controls the expression of miRNAs may lead to alternative and directed therapies that avoid the problematic associated with the increased resistance to antibiotics in the eradication of *H. pylori*. Moreover, miRNAs can be used as potential biomarkers in the diagnosis of *H. pylori*-induced infection.

Regarding the *in vivo* detection, the AMOs should be redesigned and other fluorochromes with emission spectra closer to infrared should be attached, in order to avoid autofluorescence background of the tissues[340]. Further additions to this work include a more detailed *in vivo* study, comprehending, for instance, a biodistribution assay to test the specificity of the AMOs to localize the desired tissue, and a time concentration versus tumor-silencing activity assay[341–343], to test the

duration effect of anti-miRNA sequences and their ability to reduce the developed tumor (Figure 5.1).

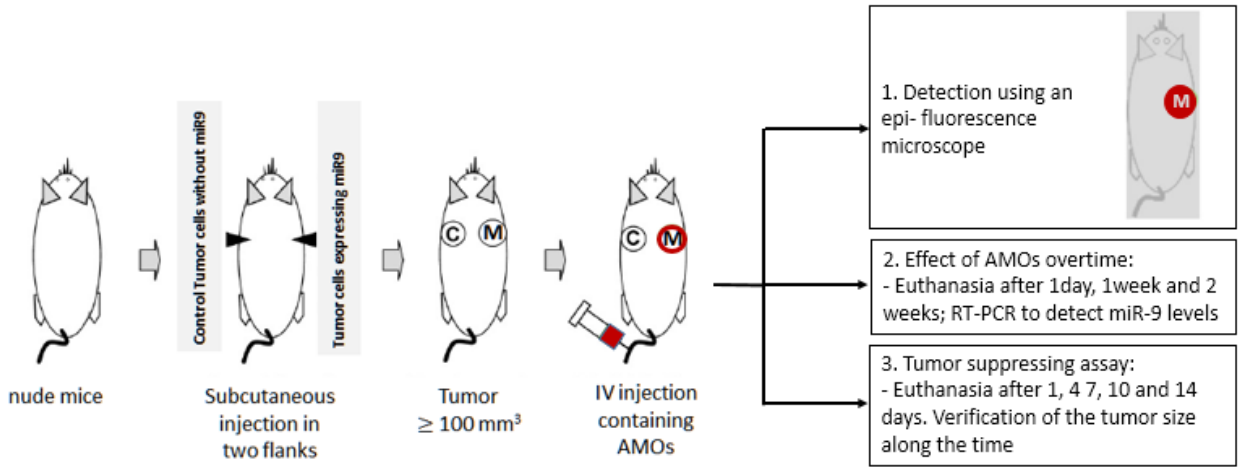


Figure 5.1 Experimental modelling of an in vivo assay proposed for future work. Nude mice are first subcutaneously inoculated with miR-9-negative human cancer cells in one flank (C) and miR-9-positive human cancer cells in the other flank (M). After tumor growth (tumor size at least 100 mm^3), the developed AMOs are injected intravenously (IV) in order to test 1) the potential of the AMO to specifically target the miR-9-positive tumor localized in one of the flanks (M) – biodistribution assay; 2) the effect of AMOs along time to silence the target miR-9, monitored by RT-PCR; and 3) the tumor suppressing effect of the administrated AMO, i.e. the capacity of the AMO reduce the tumor size along time.

Additionally, other systems can be integrated to further optimize *in vivo* imaging of miRNAs. For instance, the use of quencher-fluorophore based systems such as molecular beacons have been used for *in vivo* miRNA detection[344,345]. Molecular beacons with an emission peak at longer wavelength can lead to better tissue penetration, enhancing the fluorescence signal and decreasing the background noise. Magnetic resonance imaging (MRI) has also been employed for imaging of miRNAs, where magnetic nanoparticles were used to provide a non-invasive and effective system, for miRNA detection[346,347]. In the case of miRNA detection in fixed tissues, autofluorescence can be reduced by applying a photobleaching treatment prior to microscopic visualization, using for instance Sudan Black B, to quench background autofluorescence and improve resolution of the fluorescence signal[348]s.

Finally, the comprehensive study of the diffusion and hybridization dynamics of molecular probes in FISH, allowed to take the first steps on the development of a more holistic mechanistic model to maximize FISH efficiency. In future works, these parameters could be further developed to better fit the approximation to the oxygen transfer model and ultimately lead to an overall diffusion and uptake rate for MPs in FISH.

References

1. Ferlay J, Soerjomataram I, Ervik M, Dikshit R, Eser S, Mathers C, Rebelo M, Parkin DM, Forman D, Bray, F. GLOBOCAN 2012 v1.0, Cancer Incidence and Mortality Worldwide: IARC CancerBase No. 11 [Internet]. *Lyon, France: International Agency for Research on Cancer* (2013). Available at: http://globocan.iarc.fr. (Accessed: 8th February 2017)

2. Figueiredo, C. *et al.* in (eds. Tegtmeyer, N. & Backert, S.) 277–304 (Springer International Publishing, 2017). doi:10.1007/978-3-319-50520-6_12

3. Thiery, J. P., Acloque, H., Huang, R. Y. J. & Nieto, M. A. Epithelial-Mesenchymal Transitions in Development and Disease. *Cell* **139,** 871–890 (2009).

4. Christofori, G. Snail1 links transcriptional control with epigenetic regulation. *EMBO J.* **29,** 1787–1789 (2010).

5. David, J. M. & Rajasekaran, A. K. Dishonorable discharge: The oncogenic roles of cleaved e-cadherin fragments. *Cancer Research* **72,** 2917–2923 (2012).

6. Berx, G. & van Roy, F. Involvement of members of the cadherin superfamily in cancer. *Cold Spring Harbor perspectives in biology* **1,** (2009).

7. Van Roy, F. & Berx, G. The cell-cell adhesion molecule E-cadherin. *Cellular and Molecular Life Sciences* **65,** 3756–3788 (2008).

8. Paredes, J. *et al.* Epithelial E- and P-cadherins: Role and clinical significance in cancer. *Biochim. Biophys. Acta - Rev. Cancer* **1826,** 297–311 (2012).

9. Berx, G. *et al.* E-cadherin is a tumour/invasion suppressor gene mutated in human lobular breast cancers. *EMBO J.* **14,** 6107–15 (1995).

10. Barber, M. *et al.* Mechanisms and sequelae of E-cadherin silencing in hereditary diffuse gastric cancer. *J. Pathol.* **216,** 295–306 (2008).

11. Guilford, P. *et al.* E-cadherin germline mutations in familial gastric cancer. *Nature* **392,** 402–405 (1998).

12. Corso, G. *et al.* Somatic Mutations and Deletions of the E-Cadherin Gene Predict Poor Survival of Patients With Gastric Cancer. *J. Clin. Oncol.* **31,** 868–875 (2013).

13. Carvalho, J. *et al.* Lack of microRNA-101 causes E-cadherin functional deregulation through EZH2 up-regulation in intestinal gastric cancer. *J. Pathol.* **228,** 31–44 (2012).

14. Ma, L. *et al.* miR-9, a MYC/MYCN-activated microRNA, regulates E-cadherin and cancer metastasis. **12,** 247–256 (2010).

15. Wang, M. *et al.* miR-17-5p/20a are important markers for gastric cancer and murine double minute 2 participates in their functional regulation. *Eur. J. Cancer* **49,** 2010–21 (2013).

16. Song, J. H. & Meltzer, S. J. MicroRNAs in pathogenesis, diagnosis, and treatment of gastroesophageal cancers. *Gastroenterology* **143,** 35–47.e2 (2012).

17. Katada, T. & Ishiguro, H. microRNA expression profile in undifferentiated gastric cancer. *… J. Oncol.* 537–542 (2009). doi:10.3892/ijo

18. Wan, H.-Y. *et al.* Regulation of the transcription factor NF-kappaB1 by microRNA-9 in human gastric adenocarcinoma. *Mol. Cancer* **9,** 16 (2010).

19. Nedaeinia, R. *et al.* Locked nucleic acid anti-miR-21 inhibits cell growth and invasive behaviors of a colorectal adenocarcinoma cell line: LNA-anti-miR as a novel approach. *Cancer Gene Ther.* **23,** 246–253 (2016).

20. Elmén, J. *et al.* LNA-mediated microRNA silencing in non-human primates. *Nature* **452,** 896–9 (2008).

21. Elmén, J. *et al.* Antagonism of microRNA-122 in mice by systemically administered LNA-antimiR leads to up-regulation of a large set of predicted target mRNAs in the liver. *Nucleic Acids Res.* **36,** 1153–62 (2008).

22. Fabani, M. & Gait, M. miR-122 targeting with LNA/2′-O-methyl oligonucleotide mixmers, peptide nucleic acids (PNA), and PNA–peptide conjugates. *Rna* 336–346 (2008). doi:10.1261/rna.844108.and

23. Ørom, U. A., Kauppinen, S. & Lund, A. H. LNA-modified oligonucleotides mediate

specific inhibition of microRNA function. *Gene* **372,** 137–41 (2006).

24. Obad, S. *et al.* Silencing of microRNA families by seed-targeting tiny LNAs. *Nat. Genet.* **43,** 371–8 (2011).

25. Gaglione, M. *et al.* PNA-based artificial nucleases as antisense and anti-miRNA oligonucleotide agents. *Mol. Biosyst.* **7,** 2490–9 (2011).

26. Davis, S., Lollo, B., Freier, S. & Esau, C. Improved targeting of miRNA with antisense oligonucleotides. *Nucleic Acids Res.* **34,** 2294–304 (2006).

27. Davis, S. *et al.* Potent inhibition of microRNA in vivo without degradation. *Nucleic Acids Res.* **37,** 70–7 (2009).

28. Bartel, D. P. MicroRNAs: genomics, biogenesis, mechanism, and function. *Cell* **116,** 281–297 (2004).

29. Winter, J., Jung, S., Keller, S., Gregory, R. I. & Diederichs, S. Many roads to maturity: microRNA biogenesis pathways and their regulation. *Nat. Cell Biol.* **11,** 228–234 (2009).

30. Kozlowski, P. & Starega-Roslan, J. Structures of microRNA precursors. *Curr. Perspect. microRNAs* 1–16 (2008).

31. Fire, A. *et al.* Potent and specific genetic interference by double-stranded RNA in Caenorhabditis elegans. *Nature* **391,** 806–811 (1998).

32. Basyuk, E., Suavet, F., Doglio, A., Bordonné, R. & Bertrand, E. Human let-7 stem-loop precursors harbor features of RNase III cleavage products. *Nucleic Acids Res.* **31,** 6593–6597 (2003).

33. Borchert, G. M., Lanier, W. & Davidson, B. L. RNA polymerase III transcribes human microRNAs. *Nat. Struct. Mol. Biol.* **13,** 1097–1101 (2006).

34. Denli, A. M., Tops, B. B. J., Plasterk, R. H. A., Ketting, R. F. & Hannon, G. J. Processing of primary microRNAs by the Microprocessor complex. *Nature* **432,** 231–5 (2004).

35. Gregory, R. I. *et al.* The Microprocessor complex mediates the genesis of microRNAs. *Nature* **432,** 235–240 (2004).

36. Han, J. *et al.* Molecular basis for the recognition of primary microRNAs by the Drosha-DGCR8 complex. *Cell* **125,** 887–901 (2006).

37. Kim, V. N. MicroRNA precursors in motion: exportin-5 mediates their nuclear export. *Trends Cell Biol.* **14,** 156–159 (2004).

38. Lund, E., Güttinger, S., Calado, A., Dahlberg, J. E. & Kutay, U. Nuclear export of microRNA precursors. *Science (80-.).* **303,** 95–98 (2004).

39. Koscianska, E., Starega-Roslan, J. & Krzyzosiak, W. J. The role of Dicer protein partners in the processing of microRNA precursors. *PLoS One* **6,** e28548 (2011).

40. Zhang, H., Kolb, F. A., Brondani, V., Billy, E. & Filipowicz, W. Human Dicer preferentially cleaves dsRNAs at their termini without a requirement for ATP. *Eur. Mol. Biol. Organ. J.* **21,** 5875–5885 (2002).

41. Provost, P. *et al.* Ribonuclease activity and RNA binding of recombinant human Dicer. *Eur. Mol. Biol. Organ. J.* **21,** 5864–5874 (2002).

42. Fareh, M. *et al.* TRBP ensures efficient Dicer processing of precursor microRNA in RNA-crowded environments. **7,** 13694 (2016).

43. Chendrimada, T. P. *et al.* TRBP recruits the Dicer complex to Ago2 for microRNA processing and gene silencing. *Nature* **436,** 740–744 (2005).

44. Gregory, R. I., Chendrimada, T. P., Cooch, N. & Shiekhattar, R. Human RISC couples microRNA biogenesis and posttranscriptional gene silencing. *Cell* **123,** 631–640 (2005).

45. Chekulaeva, M. & Filipowicz, W. Mechanisms of miRNA-mediated post-transcriptional regulation in animal cells. *Curr. Opin. Cell Biol.* **21,** 452–460 (2009).

46. Zeng, Y., Wagner, E. J. & Cullen, B. R. Both natural and designed micro RNAs can inhibit the expression of cognate mRNAs when expressed in human cells. *Mol. Cell* **9,** 1327–1333 (2002).

47. Doench, J. G., Petersen, C. P. & Sharp, P. A. siRNAs can function as miRNAs. *Genes Dev.* **17,** 438–442 (2003).

48. Lennox, K. a & Behlke, M. a. Chemical modification and design of anti-miRNA oligonucleotides. *Gene Ther.* **18,** 1111–20 (2011).

49. Wahle, E. & Winkler, G. S. RNA decay machines: Deadenylation by the Ccr4–Not and Pan2–Pan3 complexes. *Biochim. Biophys. Acta - Gene Regul. Mech.* **1829,** 561–570 (2013).

50. Jonas, S. & Izaurralde, E. The role of disordered protein regions in the assembly of decapping complexes and RNP granules. *Genes Dev.* **27,** 2628–2641 (2013).

51. Jonas, S. & Izaurralde, E. Towards a molecular understanding of microRNA-mediated gene silencing. *Nat. Rev. Genet.* **16,** 421–433 (2015).

52. Djuranovic, S., Nahvi, A. & Green, R. miRNA-Mediated Gene Silencing by Translational Repression Followed by mRNA Deadenylation and Decay. *Science (80-.).* **336,** 237–240 (2012).

53. Huntzinger, E. & Izaurralde, E. Gene silencing by microRNAs: contributions of translational repression and mRNA decay. *Nat. Rev. Genet.* **12,** 99–110 (2011).

54. Wu, L., Fan, J. & Belasco, J. G. MicroRNAs direct rapid deadenylation of mRNA. *Proc. Natl. Acad. Sci. U. S. A.* **103,** 4034–4039 (2006).

55. Beilharz, T. H. *et al.* MicroRNA-mediated messenger RNA deadenylation contributes to translational repression in mammalian cells. *PLoS One* **4,** (2009).

56. Zekri, L., Huntzinger, E., Heimstädt, S. & Izaurralde, E. The silencing domain of GW182 interacts with PABPC1 to promote translational repression and degradation of microRNA targets and is required for target release. *Mol. Cell. Biol.* **29,** 6220–6231 (2009).

57. Huntzinger, E. *et al.* The interactions of GW182 proteins with PABP and deadenylases are required for both translational repression and degradation of miRNA targets. *Nucleic Acids Res.* **41,** 978–994 (2013).

58. Kozomara, A. & Griffiths-Jones, S. MiRBase: Annotating high confidence microRNAs using deep sequencing data. *Nucleic Acids Res.* **42,** (2014).

59. Griffiths-Jones, S., Saini, H. K., Van Dongen, S. & Enright, A. J. miRBase: Tools for

microRNA genomics. *Nucleic Acids Res.* **36,** (2008).

60. Griffiths-Jones, S., Grocock, R. J., van Dongen, S., Bateman, A. & Enright, A. J. miRBase: microRNA sequences, targets and gene nomenclature. *Nucleic Acids Res.* **34,** D140–D144 (2006).

61. Griffiths-Jones, S. The microRNA Registry. *Nucleic Acids Res.* **32,** D109–D111 (2004).

62. Friedman, R. C., Farh, K. K.-H., Burge, C. B. & Bartel, D. P. Most mammalian mRNAs are conserved targets of microRNAs. *Genome Res.* **19,** 92–105 (2009).

63. O'Connell, R. M., Rao, D. S., Chaudhuri, A. A. & Baltimore, D. Physiological and pathological roles for microRNAs in the immune system. *Nat Rev Immunol* **10,** 111–122 (2010).

64. Calin, G. A. *et al.* Human microRNA genes are frequently located at fragile sites and genomic regions involved in cancers. *Proc. Natl. Acad. Sci. U. S. A.* **101,** 2999–3004 (2004).

65. Lu, J. *et al.* MicroRNA expression profiles classify human cancers. *Nature* **435,** 834–8 (2005).

66. Lee, Y. S. & Dutta, A. MicroRNAs in Cancer. *Annu. Rev. Pathol. Mech. Dis.* **4,** 199–227 (2009).

67. Li, F., Liu, J. & Li, S. MicorRNA 106b ~ 25 cluster and gastric cancer. *Surg. Oncol.* **22,** 7–10 (2013).

68. Zhang, W., Dahlberg, J. E. & Tam, W. MicroRNAs in tumorigenesis: a primer. *Am. J. Pathol.* **171,** 728–38 (2007).

69. Tili, E., Michaille, J.-J. & Calin, G. A. Expression and function of micro RNAs in immune cells during normal or disease state. *Int. J. Med. Sci.* **5,** 73–79 (2008).

70. Volinia, S. *et al.* A microRNA expression signature of human solid tumors defines cancer gene targets. *Proc. Natl. Acad. Sci. U. S. A.* **103,** 2257–2261 (2006).

71. Esquela-Kerscher, A. & Slack, F. J. Oncomirs - microRNAs with a role in cancer. *Nat.*

Rev. Cancer **6,** 259–69 (2006).

72. Bandyopadhyay, S., Mitra, R., Maulik, U. & Zhang, M. Q. Development of the human cancer microRNA network. *Silence* **1,** 6 (2010).

73. Lynam-Lennon, N., Maher, S. G. & Reynolds, J. V. The roles of microRNA in cancer and apoptosis. *Biol Rev Camb Philos Soc* **84,** 55–71 (2009).

74. Zhang, B., Pan, X., Cobb, G. P. & Anderson, T. A. microRNAs as oncogenes and tumor suppressors. *Dev. Biol.* **302,** 1–12 (2007).

75. Li, X. *et al.* miRNA-223 Promotes Gastric Cancer Invasion and Metastasis by Targeting Tumor Suppressor EPB41L3. *Mol. Cancer Res.* **9,** 824 LP-833 (2011).

76. Mu, Y. P. *et al.* Association of miR-193b down-regulation and miR-196a up-regulation with clinicopathological features and prognosis in gastric cancer. *Asian Pacific J. Cancer Prev.* **15,** 8893–8900 (2014).

77. Wang, M. *et al.* Circulating miR-17-5p and miR-20a: Molecular markers for gastric cancer. *Mol. Med. Rep.* **5,** 1514–1520 (2012).

78. Li, H. L. *et al.* Clinical significance of upregulation of mir-196a-5p in gastric cancer and enriched KEGG pathway analysis of target genes. *Asian Pacific J. Cancer Prev.* **16,** 1781–1787 (2015).

79. Lo, S.-S. *et al.* Overexpression of miR-370 and downregulation of its novel target TGF[beta]-RII contribute to the progression of gastric carcinoma. *Oncogene* **31,** 226–237 (2012).

80. Xu, Y. J. & Fan, Y. MiR-215/192 participates in gastric cancer progression. *Clin. Transl. Oncol.* **17,** 34–40 (2015).

81. Li, C. *et al.* MiRNA-199a-3p: A potential circulating diagnostic biomarker for early gastric cancer. *J. Surg. Oncol.* **108,** 89–92 (2013).

82. Tsai, M.-M. *et al.* MicroRNA-196a/-196b promote cell metastasis via negative regulation of radixin in human gastric cancer. *Cancer Lett.* **351,** 222–231 (2017).

83. Zheng, B. *et al.* MicroRNA-148a Suppresses Tumor Cell Invasion

and Metastasis by Downregulating ROCK1 in Gastric Cancer. *Clin. Cancer Res.* **17,** 7574 LP-7583 (2011).

84. Xu, Y. *et al.* MiR-21 is a promising novel biomarker for lymph node metastasis in patients with gastric cancer. *Gastroenterol. Res. Pract.* (2012). doi:10.1155/2012/640168

85. Lai, K. W. *et al.* MicroRNA-130b regulates the tumour suppressor RUNX3 in gastric cancer. *Eur. J. Cancer* **46,** 1456–1463 (2017).

86. Naito, Y. *et al.* MicroRNA-145 is a potential prognostic factor of scirrhous type gastric cancer. *Oncol. Rep.* **32,** 1720–1726 (2014).

87. Li, X. *et al.* MicroRNA-107, an oncogene microRNA that regulates tumour invasion and metastasis by targeting DICER1 in gastric cancer. *J. Cell. Mol. Med.* **15,** 1887–1895 (2011).

88. Cho, W. C. S. OncomiRs: the discovery and progress of microRNAs in cancers. *Mol. Cancer* **6,** 60 (2007).

89. CHAN, S., WU, C. & LI, A. miR-21 microRNA expression in human gastric carcinomas and its clinical association. *Anticancer …* **912,** 907–911 (2008).

90. Sui, M. *et al.* Upregulation of miR-125b is associated with poor prognosis and trastuzumab resistance in HER2-positive gastric cancer. *Exp. Ther. Med.* **14,** 657–663 (2017).

91. Liu, T., Tang, H., Lang, Y., Liu, M. & Li, X. MicroRNA-27a functions as an oncogene in gastric adenocarcinoma by targeting prohibitin. *Cancer Lett.* **273,** 233–42 (2009).

92. Naguibneva, I. *et al.* The microRNA miR-181 targets the homeobox protein Hox-A11 during mammalian myoblast differentiation. *Nat. Cell Biol.* **8,** 278–84 (2006).

93. Liu, W. *et al.* miR-221 and miR-222 Simultaneously Target RECK and Regulate Growth and Invasion of Gastric Cancer Cells. *Med. Sci. Monit.* **21,** 2718–2725 (2015).

94. Kim, Y.-K. *et al.* Functional links between clustered microRNAs: suppression of cell-cycle inhibitors by microRNA clusters in gastric cancer. *Nucleic Acids Res.* **37,** 1672–1681 (2009).

95. Wu, Q. *et al.* MiR-150 promotes gastric cancer proliferation by negatively regulating the pro-apoptotic gene EGR2. *Biochem. Biophys. Res. Commun.* **392,** 340–345 (2010).

96. Chen, L., Jiang, M., Yuan, W. & Tang, H. Prognostic value of miR-93 overexpression in resectable gastric adenocarcinomas. *Acta Gastroenterol. Belg.* **75,** 22–27 (2012).

97. Petrocca, F. *et al.* E2F1-Regulated MicroRNAs Impair TGFβ-Dependent Cell-Cycle Arrest and Apoptosis in Gastric Cancer. *Cancer Cell* **13,** 272–286 (2017).

98. Park, S. M., Gaur, A. B., Lengyel, E. & Peter, M. E. The miR-200 family determines the epithelial phenotype of cancer cells by targeting the E-cadherin repressors ZEB1 and ZEB2. *Genes Dev.* **22,** 894–907 (2008).

99. Xia, L. *et al.* miR-15b and miR-16 modulate multidrug resistance by targeting BCL2 in human gastric cancer cells. *Int. J. Cancer* **123,** 372–379 (2008).

100. Nishida, N. *et al.* MicroRNA-125a-5p Is an Independent Prognostic Factor in Gastric Cancer and Inhibits the Proliferation of Human Gastric Cancer Cells in Combination with Trastuzumab. *Clin. Cancer Res.* **17,** 2725 LP-2733 (2011).

101. Xu, Y., Huang, Z. & Liu, Y. Reduced miR-125a-5p expression is associated with gastric carcinogenesis through the targeting of E2F3. *Mol. Med. Rep.* **10,** 2601–2608 (2014).

102. Feng, R. *et al.* miR-126 functions as a tumour suppressor in human gastric cancer. *Cancer Lett.* **298,** 50–63 (2017).

103. Liu, L. Y. *et al.* miR-126 inhibits growth of SGC-7901 cells by synergistically targeting the oncogenes PI3KR2 and Crk, and the tumor suppressor PLK2. *Int. J. Oncol.* **45,** 1257–1265 (2014).

104. Takagi, T. *et al.* Decreased Expression of MicroRNA-143 and -145 in Human Gastric Cancers. *Oncology* **77,** 12–21 (2009).

105. Guo, S. L. *et al.* mir-148a promoted cell proliferation by targeting p27 in gastric cancer cells. *Int. J. Biol. Sci.* **7,** 567–574 (2011).

106. Hashimoto, Y., Akiyama, Y., Otsubo, T., Shimada, S. & Yuasa, Y. Involvement of epigenetically silenced microRNA-181c in gastric carcinogenesis. *Carcinogenesis* **31,**

777–784 (2010).

107. Korpal, M., Lee, E. S., Hu, G. & Kang, Y. The miR-200 Family Inhibits Epithelial-Mesenchymal Transition and Cancer Cell Migration by Direct Targeting of E-cadherin Transcriptional Repressors ZEB1 and ZEB2. *J. Biol. Chem.* **283,** 14910–14914 (2008).

108. Imaoka, H. *et al.* Circulating microRNA-203 predicts metastases, early recurrence, and poor prognosis in human gastric cancer. *Gastric Cancer* **19,** 744–753 (2016).

109. Zhou, X., Li, L., Su, J. & Zhang, G. Decreased miR-204 in H. pylori-Associated Gastric Cancer Promotes Cancer Cell Proliferation and Invasion by Targeting SOX4. *PLoS One* **9,** e101457 (2014).

110. Zhang, L. *et al.* MiR-206 inhibits gastric cancer proliferation in part by repressing CyclinD2. *Cancer Lett.* **332,** 94–101 (2017).

111. Wada, R., Akiyama, Y., Hashimoto, Y., Fukamachi, H. & Yuasa, Y. miR-212 is downregulated and suppresses methyl-CpG-binding protein MeCP2 in human gastric cancer. *Int. J. Cancer* **127,** 1106–1114 (2010).

112. Wu, J. *et al.* Induction of anion exchanger-1 translation and its opposite roles in the carcinogenesis of gastric cancer cells and differentiation of K562 cells. *Oncogene* **29,** 1987–1996 (2010).

113. Xu, Y. *et al.* MicroRNA-335 acts as a metastasis suppressor in gastric cancer by targeting Bcl-w and specificity protein 1. *Oncogene* **31,** 1398–1407 (2012).

114. Ji, Q. *et al.* Restoration of tumor suppressor miR-34 inhibits human p53-mutant gastric cancer tumorspheres. *BMC Cancer* **8,** 266 (2008).

115. Yu, F. *et al.* let-7 regulates self renewal and tumorigenicity of breast cancer cells. *Cell* **131,** (2007).

116. Tazawa, H., Tsuchiya, N., Izumiya, M. & Nakagama, H. Tumor-suppressive miR-34a induces senescence-like growth arrest through modulation of the E2F pathway in human colon cancer cells. *Proc Natl Acad Sci USA* **104,** (2007).

117. Corney, D. C., Flesken-Nikitin, A., Godwin, A. K., Wang, W. & Nikitin, A. Y.

MicroRNA-34b and MicroRNA-34c are targets of p53 and cooperate in control of cell proliferation and adhesion-independent growth. *Cancer Res* **67,** (2007).

118. Rotkrua, P., Akiyama, Y., Hashimoto, Y., Otsubo, T. & Yuasa, Y. MiR-9 downregulates CDX2 expression in gastric cancer cells. *Int. J. Cancer* **129,** 2611–20 (2011).

119. Liu, S. *et al.* MicroRNA-9 up-regulates E-cadherin through inhibition of NF-??B1-Snail1 pathway in melanoma. *J. Pathol.* **226,** 61–72 (2012).

120. Song, Y. *et al.* MicroRNA-9 promotes tumor metastasis via repressing E-cadherin in esophageal squamous cell carcinoma. *Oncotarget* **5,** (2014).

121. Zheng, L. *et al.* microRNA-9 Suppresses the Proliferation, Invasion and Metastasis of Gastric Cancer Cells through Targeting Cyclin D1 and Ets1. *PLoS One* **8,** e55719 (2013).

122. Kogo, R., Mimori, K., Tanaka, F., Komune, S. & Mori, M. Clinical Significance of miR-146a in Gastric Cancer Cases. *Clin. Cancer Res.* **17,** 4277 LP-4284 (2011).

123. Tie, J. *et al.* MiR-218 inhibits invasion and metastasis of gastric cancer by targeting the Robo1 receptor. *PLoS Genet.* **6,** e1000879 (2010).

124. Gao, C. *et al.* Reduced microRNA-218 expression is associated with high nuclear factor kappa B activation in gastric cancer. *Cancer* **116,** 41–49 (2010).

125. Tsukamoto, Y. *et al.* MicroRNA-375 is downregulated in gastric carcinomas and regulates cell survival by targeting PDK1 and 14-3-3zeta. *Cancer Res* **70,** (2010).

126. Zhang, Z. *et al.* miR-21 plays a pivotal role in gastric cancer pathogenesis and progression. *Lab Invest* **88,** 1358–1366 (2008).

127. Zhang, B. G. *et al.* microRNA-21 promotes tumor proliferation and invasion in gastric cancer by targeting PTEN. *Oncol. Rep.* **27,** 1019–1026 (2012).

128. Motoyama, K. *et al.* Clinicopathological and prognostic significance of PDCD4 and microRNA-21 in human gastric cancer. *Int. J. Oncol.* **36,** 1089–1095 (2010).

129. Li, L., Zhou, L., Li, Y., Lin, S. & Tomuleasa, C. MicroRNA-21 stimulates gastric cancer growth and invasion by inhibiting the tumor suppressor effects of programmed cell death

protein 4 and phosphatase and tensin homolog. *J. BUON.* **19,** 228–36 (2014).

130. Gregory, P. A. *et al.* The miR-200 family and miR-205 regulate epithelial to mesenchymal transition by targeting ZEB1 and SIP1. *Nat Cell Biol* **10,** 593–601 (2008).

131. Zhu, W. *et al.* miR-200bc/429 cluster modulates multidrug resistance of human cancer cell lines by targeting BCL2 and XIAP. *Cancer Chemother. Pharmacol.* **69,** 723–731 (2012).

132. Luo, H. *et al.* Down-regulated miR-9 and miR-433 in human gastric carcinoma. *J. Exp. Clin. Cancer Res.* **28,** 82 (2009).

133. Zheng, L. *et al.* microRNA-9 suppresses the proliferation, invasion and metastasis of gastric cancer cells through targeting cyclin D1 and Ets1. *PLoS One* **8,** e55719 (2013).

134. Liu, Q. *et al.* CDX2 expression is progressively decreased in human gastric intestinal metaplasia, dysplasia and cancer. *Mod Pathol* **20,** 1286–1297 (2007).

135. Sahin, A., Velten, M., Pietsch, T., Knuefermann, P., Okuducu, A. F., Hahne, J. C., Wernert, N. No TitleInactivation of Ets 1 transcription factor by a specific decoy strategy reduces rat C6 glioma cell proliferation and mmp-9 expression. *Int. J. Mol. Med.* **15,** 771–776 (2005).

136. Duluc, I. *et al.* Changing intestinal connective tissue interactions alters homeobox gene expression in epithelial cells. *J. Cell Sci.* **110,** 1317 LP-1324 (1997).

137. Zhu, L. *et al.* MicroRNA-9 up-regulation is involved in colorectal cancer metastasis via promoting cell motility. *Med. Oncol.* **29,** 1037–1043 (2012).

138. Wang, J. *et al.* Overexpressions of microRNA-9 and microRNA-200c in human breast cancers are associated with lymph node metastasis. *Cancer Biother. Radiopharm.* **28,** 283–8 (2013).

139. Gwak, J. M. *et al.* MicroRNA-9 is associated with epithelial-mesenchymal transition, breast cancer stem cell phenotype, and tumor progression in breast cancer. *Breast Cancer Res. Treat.* **147,** 39–49 (2014).

140. Sun, J., Fang, K., Shen, H. & Qian, Y. MicroRNA-9 is a ponderable index for the

prognosis of human hepatocellular carcinoma. *Int. J. Clin. Exp. Med.* **8,** 17748–17756 (2015).

141. Hao-Xiang, T. *et al.* MicroRNA-9 reduces cell invasion and E-cadherin secretion in SK-Hep-1 cell. *Med. Oncol.* **27,** 654–660 (2010).

142. Sun, Z. *et al.* MicroRNA-9 enhances migration and invasion through KLF17 in hepatocellular carcinoma. *Mol. Oncol.* **7,** 884–894 (2013).

143. Wang, H. *et al.* miR-9 promotes cell proliferation and inhibits apoptosis by targeting LASS2 in bladder cancer. *Tumor Biol.* **36,** 9631–9640 (2015).

144. Tian, C. *et al.* MicroRNA-9 promotes proliferation of leukemia cells in adult CD34-positive acute myeloid leukemia with normal karyotype by downregulation of Hes1. *Tumor Biol.* **37,** 7461–7471 (2016).

145. Chen, P. *et al.* miR-9 is an essential oncogenic microRNA specifically overexpressed in mixed lineage leukemia-rearranged leukemia. *Proc. Natl. Acad. Sci. U. S. A.* **110,** 11511–6 (2013).

146. Zhu, S. W. *et al.* miR-9 modulates osteosarcoma cell growth by targeting the GCIP tumor suppressor. *Asian Pacific J. Cancer Prev.* **16,** 4509–4513 (2015).

147. Ben-Hamo, R., Zilberberg, A., Cohen, H. & Efroni, S. hsa-miR-9 controls the mobility behavior of Glioblastoma cells via regulation of MAPK14 signaling elements. *Oncotarget* **7,** (2015).

148. White, R. A. *et al.* Epithelial stem cell mutations that promote squamous cell carcinoma metastasis. *J. Clin. Invest.* **123,** 4390–404 (2013).

149. Park, Y. R. *et al.* MicroRNA-9 suppresses cell migration and invasion through downregulation of TM4SF1 in colorectal cancer. *Int. J. Oncol.* **48,** 2135–2143 (2016).

150. Zhu, M., Xu, Y., Ge, M., Gui, Z. & Yan, F. Regulation of UHRF1 by microRNA-9 modulates colorectal cancer cell proliferation and apoptosis. *Cancer Sci.* **106,** 833–839 (2015).

151. Mohammadi-Yeganeh, S., Mansouri, A. & Paryan, M. Targeting of miR9/NOTCH1

Interaction Reduces Metastatic Behavior in Triple-negative Breast Cancer. *Chem. Biol. Drug Des.* **86,** 1185–1191 (2015).

152. Higashi, T. *et al.* miR-9-3p plays a tumour-suppressor role by targeting TAZ (WWTR1) in hepatocellular carcinoma cells. *Br J Cancer* **113,** 252–258 (2015).

153. Zhang, J. *et al.* Comprehensive profiling of novel microRNA-9 targets and a tumor suppressor role of microRNA-9 via targeting IGF2BP1 in hepatocellular carcinoma. *Oncotarget* **6,** (2015).

154. Zhang, J. *et al.* Down-regulation of microRNA-9 leads to activation of IL-6/Jak/STAT3 pathway through directly targeting IL-6 in HeLa cell. *Mol. Carcinog.* **55,** 732–742 (2016).

155. Rodriguez-Otero, P. *et al.* Deregulation of FGFR1 and CDK6 oncogenic pathways in acute lymphoblastic leukaemia harbouring epigenetic modifications of the MIR9 family. *Br. J. Haematol.* **155,** 73–83 (2011).

156. Guo, L.-M. *et al.* MicroRNA-9 inhibits ovarian cancer cell growth through regulation of NF-kappaB1. *FEBS J.* **276,** 5537–46 (2009).

157. Yu, T. *et al.* MicroRNA-9 inhibits the proliferation of oral squamous cell carcinoma cells by suppressing expression of CXCR4 via the Wnt/[beta]-catenin signaling pathway. *Oncogene* **33,** 5017–5027 (2014).

158. Fiaschetti, G. *et al.* Epigenetic silencing of miRNA-9 is associated with HES1 oncogenic activity and poor prognosis of medulloblastoma. *Br. J. Cancer* **110,** 636–47 (2014).

159. Zhang, H. *et al.* microRNA-9 Targets Matrix Metalloproteinase 14 to Inhibit Invasion, Metastasis, and Angiogenesis of Neuroblastoma Cells. *Mol Cancer Ther* **11,** 1454–1466 (2012).

160. Busuttil, R. A. & Boussioutas, A. Intestinal metaplasia: A premalignant lesion involved in gastric carcinogenesis. *J. Gastroenterol. Hepatol.* **24,** 193–201 (2009).

161. Silberg, D. G. *et al.* Cdx2 ectopic expression induces gastric intestinal metaplasia in transgenic mice. *Gastroenterology* **122,** 689–696 (2017).

162. Pucci, B., Kasten, M. & Giordano, A. Cell Cycle and Apoptosis. *Neoplasia* **2,** 291–299

(2000).

163. Cui, Y. *et al.* MiR-29a Inhibits Cell Proliferation and Induces Cell Cycle Arrest through the Downregulation of p42.3 in Human Gastric Cancer. *PLoS One* **6,** e25872 (2011).

164. Zhang, L. *et al.* MiR-206 inhibits gastric cancer proliferation in part by repressing CyclinD2. *Cancer Lett.* **332,** 94–101 (2013).

165. Zhu, W. *et al.* miR-497 modulates multidrug resistance of human cancer cell lines by targeting BCL2. *Med. Oncol.* **29,** 384–391 (2012).

166. Sacconi, A. *et al.* miR-204 targets Bcl-2 expression and enhances responsiveness of gastric cancer. *Cell Death Dis.* **3,** e423 (2012).

167. Takeichi, M. Functional correlation between cell adhesive properties and some cell surface proteins. *J. Cell Biol.* **75,** 464–74 (1977).

168. Shapiro, L. *et al.* Structural basis of cell-cell adhesion by cadherins. *Nature* **374,** 327–337 (1995).

169. Yepes, S. *et al.* Co-expressed miRNAs in gastric adenocarcinoma. *Genomics* **108,** 93–101 (2016).

170. Gumbiner, B. M. & McCrea, P. D. Catenins as mediators of the cytoplasmic functions of cadherins. *J. Cell Sci. Suppl.* **17,** 155–158 (1993).

171. Huang, L., Wu, R.-L. & Xu, A.-M. Epithelial-mesenchymal transition in gastric cancer. *Am. J. Transl. Res.* **7,** 2141–2158 (2015).

172. Ma, L. *et al.* miR-9, a MYC/MYCN-activated microRNA, regulates E-cadherin and cancer metastasis. *Nat. Cell Biol.* **12,** 247–256 (2010).

173. DA SILVA OLIVEIRA, K. C. *et al.* Expression of hsa-miR-9 and MYC Copy Number Variation in Hereditary Diffuse Gastric Cancer. *Anticancer Res.* **37,** 2401–2406 (2017).

174. Iorio, M. V. & Croce, C. M. MicroRNA dysregulation in cancer: Diagnostics, monitoring and therapeutics. A comprehensive review. *EMBO Molecular Medicine* **4,** 143–159 (2012).

175. Etheridge, A., Lee, I., Hood, L., Galas, D. & Wang, K. Extracellular microRNA: a new source of biomarkers. *Mutat. Res.* **717,** 85–90 (2011).

176. Tsujiura, M. *et al.* Circulating microRNAs in plasma of patients with gastric cancers. *Br. J. Cancer* **102,** 1174–1179 (2010).

177. Cai, H. *et al.* Plasma microRNAs serve as novel potential biomarkers for early detection of gastric cancer. *Med. Oncol.* **30,** 452 (2013).

178. Zhou, H. *et al.* Detection of circulating tumor cells in peripheral blood from patients with gastric cancer using microRNA as a marker. *J. Mol. Med. (Berl).* **88,** 709–17 (2010).

179. Rotkrua, P. *et al.* Circulating microRNAs as biomarkers for early detection of diffuse-type gastric cancer using a mouse model. *Br. J. Cancer* **108,** 932–940 (2013).

180. Li, X. *et al.* Identification of new aberrantly expressed miRNAs in intestinal-type gastric cancer and its clinical significance. *Oncol. Rep.* **26,** 1431–1439 (2011).

181. Li, X. *et al.* Survival prediction of gastric cancer by a seven-microRNA signature. *Gut* **59,** 579–585 (2010).

182. Wang, Y. Y. *et al.* Clinicopathologic significance of miR-10b expression in gastric carcinoma. *Hum. Pathol.* **44,** 1278–1285 (2013).

183. Katada, T. *et al.* MicroRNA expression profile in undifferentiated gastric cancer. *Int. J. Oncol.* **34,** 537–542 (2009).

184. Bandres, E. *et al.* microRNA-451 regulates macrophage migration inhibitory factor production and proliferation of gastrointestinal cancer cells. *Clin. Cancer Res.* **15,** 2281–90 (2009).

185. Kim, B.-H., Hong, S. W., Kim, A., Choi, S. H. & Yoon, S. O. Prognostic implications for high expression of oncogenic microRNAs in advanced gastric carcinoma. *J. Surg. Oncol.* **107,** 505–510 (2013).

186. Zhang, Y., Lu, Q. & Cai, X. MicroRNA-106a induces multidrug resistance in gastric cancer by targeting RUNX3. *FEBS Lett.* **587,** 3069–3075 (2013).

187. Wang, Z. *MicroRNA interference technologies*. *MicroRNA Interference Technologies* (2009). doi:10.1007/978-3-642-00489-6

188. Wang, Z. in (ed. Wu, W.) 211–223 (Humana Press, 2011). doi:10.1007/978-1-60761-863-8_15

189. Xia, X. G., Zhou, H. & Xu, Z. Multiple shRNAs expressed by an inducible pol II promoter can knock down the expression of multiple target genes. *Biotechniques* **41,** 64–68 (2006).

190. Wang, Z. in (ed. Wang, Z.) 101–110 (Springer Berlin Heidelberg, 2009). doi:10.1007/978-3-642-00489-6_5

191. Ebert, M. S., Neilson, J. R. & Sharp, P. A. MicroRNA sponges: competitive inhibitors of small RNAs in mammalian cells. *Nat. Methods* **4,** 10.1038/nmeth1079 (2007).

192. Saito, Y. *et al.* Development of a novel microRNA promoter microarray for ChIP-on-chip assay to identify epigenetically regulated microRNAs. *Biochem. Biophys. Res. Commun.* **426,** 33–7 (2012).

193. Zhang, J., Zhao, H., Gao, Y. & Zhang, W. Secretory miRNAs as novel cancer biomarkers. *Biochim. Biophys. Acta* **1826,** 32–43 (2012).

194. Galasso, M., Sana, M. E. & Volinia, S. Non-coding RNAs: a key to future personalized molecular therapy? *Genome Med.* **2,** 12 (2010).

195. Válóczi, A. *et al.* Sensitive and specific detection of microRNAs by northern blot analysis using LNA-modified oligonucleotide probes. *Nucleic Acids Res.* **32,** e175 (2004).

196. Sotillo, E. & Thomas-Tikhonenko, A. Shielding the messenger (RNA): microRNA-based anticancer therapies. *Pharmacol. Ther.* **131,** 18–32 (2011).

197. Grady, W. & Tewari, M. The next thing in prognostic molecular markers: microRNA signatures of cancer. *Gut* **59,** 706–708 (2010).

198. Yin, Y., Li, J., Chen, S., Zhou, T. & Si, J. MicroRNAs as Diagnostic Biomarkers in Gastric Cancer. *Int. J. Mol. Sci.* **13,** 12544–55 (2012).

199. Di Leva, G., Briskin, D. & Croce, C. M. MicroRNA in cancer: new hopes for

antineoplastic chemotherapy. *Ups. J. Med. Sci.* **117,** 202–16 (2012).

200. Iorio, M. V & Croce, C. M. MicroRNA dysregulation in cancer: diagnostics, monitoring and therapeutics. A comprehensive review. *EMBO Mol. Med.* **4,** 143–59 (2012).

201. Zamecnik, P. C. & Stephenson, M. L. Inhibition of Rous sarcoma virus replication and cell transformation by a specific oligodeoxynucleotide. *Proc. Natl. Acad. Sci. U. S. A.* **75,** 280–4 (1978).

202. Lennox, K. a & Behlke, M. a. A direct comparison of anti-microRNA oligonucleotide potency. *Pharm. Res.* **27,** 1788–99 (2010).

203. Neudecker, V., Brodsky, K. S., Kreth, S., Ginde, A. A. & Eltzschig, H. K. Emerging Roles for MicroRNAs in Perioperative Medicine. *Anesthesiology* **124,** 489–506 (2016).

204. Boutla, A., Delidakis, C. & Tabler, M. Developmental defects by antisense-mediated inactivation of micro-RNAs 2 and 13 in Drosophila and the identification of putative target genes. *Nucleic Acids Res.* **31,** 4973–4980 (2003).

205. Freier, S. M. & Altmann, K. H. The ups and downs of nucleic acid duplex stability: structure-stability studies on chemically-modified DNA:RNA duplexes. *Nucleic Acids Res.* **25,** 4429–4443 (1997).

206. Egli, M. *et al.* Probing the Influence of Stereoelectronic Effects on the Biophysical Properties of Oligonucleotides: Comprehensive Analysis of the RNA Affinity, Nuclease Resistance, and Crystal Structure of Ten 2‘-O-Ribonucleic Acid Modifications,. *Biochemistry* **44,** 9045–9057 (2005).

207. Hutvágner, G., Simard, M. J., Mello, C. C. & Zamore, P. D. Sequence-specific inhibition of small RNA function. *PLoS Biol.* **2,** E98 (2004).

208. MEISTER, G. Sequence-specific inhibition of microRNA- and siRNA-induced RNA silencing. *RNA* **10,** 544–550 (2004).

209. Lennox, K. a, Owczarzy, R., Thomas, D. M., Walder, J. a & Behlke, M. a. Improved Performance of Anti-miRNA Oligonucleotides Using a Novel Non-Nucleotide Modifier. *Mol. Ther. Nucleic Acids* **2,** e117 (2013).

210. Vermeulen, A. *et al.* Double-stranded regions are essential design components of potent inhibitors of RISC function. *RNA* **13,** 723–30 (2007).

211. Mie, Y. *et al.* Function Control of Anti-microRNA Oligonucleotides Using Interstrand Cross-Linked Duplexes. *Mol. Ther. - Nucleic Acids* **10,** (2018).

212. Esau, C. *et al.* miR-122 regulation of lipid metabolism revealed by in vivo antisense targeting. *Cell Metab.* **3,** 87–98 (2006).

213. Bhat, B. *et al.* RG-101, a GalNAC-conjugated anti-miR employing a unique mechanism of action by targeting host factor microRNA-122 (miR-122), demonstrates potent activity and reduction of HCV in preclinical studies. *Hepatology* **58,** 1393A (2013).

214. BIESSEN, E. A. L. *et al.* Targeted delivery of oligodeoxynucleotides to parenchymal liver cells in vivo. *Biochem. J.* **340,** 783 (1999).

215. Gene Link. 2'-Fluoro deoxyadenosine (2'-F-A). Available at: http://www.genelink.com/newsite/products/mod_detail.asp?modid=136. (Accessed: 10th January 2018)

216. Campbell, M. A. & Wengel, J. Locked vs. unlocked nucleic acids (LNAvs.UNA): contrasting structures work towards common therapeutic goals. *Chem. Soc. Rev.* **40,** 5680–5689 (2011).

217. Zhang, Y. *et al.* LNA-mediated anti–miR-155 silencing in low-grade B-cell lymphomas. *Blood* **120,** 1678 LP-1686 (2012).

218. You, Y., Moreira, B. G., Behlke, M. A. & Owczarzy, R. Design of LNA probes that improve mismatch discrimination. *Nucleic Acids Res.* **34,** e60–e60 (2006).

219. van der Ree, M. H. *et al.* Long-term safety and efficacy of microRNA-targeted therapy in chronic hepatitis C patients. *Antiviral Res.* **111,** 53–59 (2014).

220. Pasternak, A. & Wengel, J. Unlocked nucleic acid - an RNA modification with broad potential. *Org. Biomol. Chem.* **9,** 3591–3597 (2011).

221. Stein, C. A. & Cheng, Y. C. Antisense oligonucleotides as therapeutic agents--is the bullet really magical? *Science (80-.).* **261,** 1004 LP-1012 (1993).

222. Georgakoudi, I. *et al.* NAD(P)H and collagen as in vivo quantitative fluorescent biomarkers of epithelial precancerous changes. *Cancer Res.* **62,** 682–687 (2002).

223. SUMMERTON, J. & WELLER, D. Morpholino Antisense Oligomers: Design, Preparation, and Properties. *Antisense Nucleic Acid Drug Dev.* **7,** 187–195 (1997).

224. Nielsen, P. E., Egholm, M., Berg, R. H. & Buchardt, O. Sequence-selective recognition of DNA by strand displacement with a thymine-substituted polyamide. *Science (80-.).* **254,** 1497 LP-1500 (1991).

225. Weidner, D. A., Valdez, B. C., Henning, D., Greenberg, S. & Busch, H. Phosphorothioate oligonucleotides bind in a non sequence-specific manner to the nucleolar protein C23/nucleolin. *FEBS Lett.* **366,** 146–150 (1995).

226. Geary, R. S. *et al.* Pharmacokinetic Properties of 2′-O-(2-Methoxyethyl)-Modified Oligonucleotide Analogs in Rats. *J. Pharmacol. Exp. Ther.* **296,** 890 LP-897 (2001).

227. Sheehan, D. *et al.* Biochemical properties of phosphonoacetate and thiophosphonoacetate oligodeoxyribonucleotides. *Nucleic Acids Res.* **31,** 4109–4118 (2003).

228. Threlfall, R. N., Torres, A. G., Krivenko, A., Gait, M. J. & Caruthers, M. H. Synthesis and biological activity of phosphonoacetate- and thiophosphonoacetate-modified 2[prime or minute]-O-methyl oligoribonucleotides. *Org. Biomol. Chem.* **10,** 746–754 (2012).

229. Flynt, A. S., Li, N., Thatcher, E. J., Solnica-Krezel, L. & Patton, J. G. Zebrafish miR-214 modulates Hedgehog signaling to specify muscle cell fate. *Nat. Genet.* **39,** 259–63 (2007).

230. Kloosterman, W. P., Lagendijk, A. K., Ketting, R. F., Moulton, J. D. & Plasterk, R. H. A. Targeted Inhibition of miRNA Maturation with Morpholinos Reveals a Role for miR-375 in Pancreatic Islet Development. *PLOS Biol.* **5,** e203 (2007).

231. Wittung, P. *et al.* Phospholipid membrane permeability of peptide nucleic acid. *FEBS Lett.* **375,** 27–29 (1995).

232. Research, W. I. for B. TargetScan. *v7.1* Available at: www.targetscan.org. (Accessed: 1st March 2017)

233. Griffiths-Jones, S., Grocock, R. J., Van Dongen, S., Bateman, A. & Enright, A. J.

miRBase: microRNA sequences, targets and gene nomenclature. *Nucleic Acids Res.* **34,** D140–D144 (2006).

234. Griffiths-Jones lab, Faculty of Life Sciences, U. of M. miRBase. Available at: http://www.mirbase.org/. (Accessed: 1st March 2017)

235. U.S. National Library of Medicine. BLAST: Basic Local Alignment Search Tool. *V2.6.0: January 09, 2017* Available at: https://blast.ncbi.nlm.nih.gov/Blast.cgi. (Accessed: 1st March 2017)

236. Krützfeldt, J. *et al.* Silencing of microRNAs in vivo with 'antagomirs'. *Nature* **438,** 685–9 (2005).

237. Fontenete, S., Guimarães, N., Wengel, J. & Azevedo, N. F. Prediction of melting temperatures in fluorescence in situ hybridization (FISH) procedures using thermodynamic models. *Crit. Rev. Biotechnol.* **8551,** 1–12 (2015).

238. Krützfeldt, J. *et al.* Specificity, duplex degradation and subcellular localization of antagomirs. *Nucleic Acids Res.* **35,** 2885–92 (2007).

239. Fabani, M. M. & Gait, M. J. miR-122 targeting with LNA/2'-O-methyl oligonucleotide mixmers, peptide nucleic acids (PNA), and PNA-peptide conjugates. *RNA* **14,** 336–346 (2007).

240. Worm, J. *et al.* Silencing of microRNA-155 in mice during acute inflammatory response leads to derepression of c/ebp Beta and down-regulation of G-CSF. *Nucleic Acids Res.* **37,** 5784–92 (2009).

241. Yamamichi, N. *et al.* Locked nucleic acid in situ hybridization analysis of miR-21 expression during colorectal cancer development. *Clin. Cancer Res.* **15,** 4009–16 (2009).

242. Robertson, N. M. *et al.* Unlocked Nucleic Acids for miRNA detection using two dimensional nano-graphene oxide. *Biosens. Bioelectron.* **89,** 551–557 (2017).

243. Oh, S. Y., Ju, Y. & Park, H. A highly effective and long-lasting inhibition of miRNAs with PNA-based antisense oligonucleotides. *Mol. Cells* **28,** 341–345 (2009).

244. Jiang, T. *et al.* Tumor imaging by means of proteolytic activation of cell-penetrating

peptides. *Proc. Natl. Acad. Sci. U. S. A.* **101,** 17867–17872 (2004).

245. Vollmer, J. *et al.* Characterization of three CpG oligodeoxynucleotide classes with distinct immunostimulatory activities. *Eur. J. Immunol.* **34,** 251–62 (2004).

246. Vollmer, J. *et al.* Oligodeoxynucleotides lacking CpG dinucleotides mediate Toll-like receptor 9 dependent T helper type 2 biased immune stimulation. *Immunology* **113,** 212–223 (2004).

247. Chaudhuri, A. D., Yelamanchili, S. V & Fox, H. S. Combined fluorescent in situ hybridization for detection of microRNAs and immunofluorescent labeling for cell-type markers. *Front. Cell. Neurosci.* **7,** 160 (2013).

248. Lagendijk, A. K., Moulton, J. D. & Bakkers, J. Revealing details: whole mount microRNA in situ hybridization protocol for zebrafish embryos and adult tissues. *Biol. Open* **1,** 566–9 (2012).

249. Søe, M. J., Møller, T., Dufva, M. & Holmstrøm, K. A sensitive alternative for microRNA in situ hybridizations using probes of 2'-O-methyl RNA + LNA. *J. Histochem. Cytochem.* **59,** 661–72 (2011).

250. Jørgensen, S., Baker, A., Møller, S. & Nielsen, B. S. Robust one-day in situ hybridization protocol for detection of microRNAs in paraffin samples using LNA probes. *Methods* **52,** 375–81 (2010).

251. Nuovo, G. J. In situ detection of microRNAs in paraffin embedded, formalin fixed tissues and the co-localization of their putative targets. *Methods* **52,** 307–15 (2010).

252. Obernosterer, G., Martinez, J. & Alenius, M. Locked nucleic acid-based in situ detection of microRNAs in mouse tissue sections. *Nat. Protoc.* **2,** 1508–14 (2007).

253. Robertson, K. L. & Thach, D. C. LNA flow-FISH: a flow cytometry-fluorescence in situ hybridization method to detect messenger RNA using locked nucleic acid probes. *Anal. Biochem.* **390,** 109–14 (2009).

254. Moreira, L., Guimarães, N. M. & Azevedo, N. F. in *Bioinspired Materials for Medical Applications* 215–239 (2017). doi:10.1016/B978-0-08-100741-9.00008-5

255. Bellis, S., Jackson, J. C. & Mathewson, A. Towards a disposable in vivo miniature implantable fluorescence detector. in **6083,** 60830N–60830N–8 (2006).

256. Frangioni, J. V. In vivo near-infrared fluorescence imaging. *Current Opinion in Chemical Biology* **7,** 626–634 (2003).

257. Fontenete, S. *et al.* Hybridization-based detection of Helicobacter pylori at human body temperature using advanced locked nucleic acid (LNA) probes. *PLoS One* **8,** e81230 (2013).

258. Johannsen, M. W., Crispino, L., Wamberg, M. C., Kalra, N. & Wengel, J. Amino acids attached to 2′-amino-LNA: synthesis and excellent duplex stability. *Org. Biomol. Chem.* **9,** 243–252 (2011).

259. Guimaraes, N., Azevedo, N. F., Figueiredo, C., Keevil, C. W. & Vieira, M. J. Development and application of a novel peptide nucleic acid probe for the specific detection of Helicobacter pylori in gastric biopsy specimens. *J Clin Microbiol* **45,** 3089–3094 (2007).

260. Livak, K. J. & Schmittgen, T. D. Analysis of Relative Gene Expression Data Using Real-Time Quantitative PCR and the 2−ΔΔCT Method. *Methods* **25,** 402–408 (2001).

261. Langer-Safer, P. R., Levine, M. & Ward, D. C. Immunological method for mapping genes on Drosophila polytene chromosomes. *Proc. Natl. Acad. Sci.* **79,** 4381–4385 (1982).

262. Moter, A. & Göbel, U. B. Fluorescence in situ hybridization (FISH) for direct visualization of microorganisms. *J. Microbiol. Methods* **41,** 85–112 (2000).

263. Fontenete, S. *et al.* Towards fluorescence in vivo hybridization (FIVH) detection of H. pylori in gastric mucosa using advanced LNA probes. *PLoS One* **10,** (2015).

264. Behrens, S., Fuchs, B. M., Mueller, F. & Amann, R. Is the In Situ Accessibility of the 16S rRNA of Escherichia coli for Cy3-Labeled Oligonucleotide Probes Predicted by a Three-Dimensional Structure Model of the 30S Ribosomal Subunit? *Appl. Environ. Microbiol.* **69,** 4935–4941 (2003).

265. Simard, C., Lemieux, R. & Cot??, S. Urea substitutes toxic formamide as destabilizing

agent in nucleic acid hybridizations with RNA probes. *Electrophoresis* **22,** 2679–2683 (2001).

266. Yilmaz, L. S. & Noguera, D. R. Mechanistic approach to the problem of hybridization efficiency in fluorescent in situ hybridization. *Appl. Environ. Microbiol.* **70,** 7126–39 (2004).

267. Garcia-Ochoa, F., Gomez, E., Santos, V. E. & Merchuk, J. C. Oxygen uptake rate in microbial processes: An overview. *Biochemical Engineering Journal* **49,** 289–307 (2010).

268. Clark, D. S.; Blanch, H. W. *Biochemical Engineering.* (Marcel Dekker, New York., 1997).

269. Bakshi, S., Siryaporn, A., Goulian, M. & Weisshaar, J. C. Superresolution Imaging of Ribosomes and RNA Polymerase in Live Escherichia coli Cells. *Mol. Microbiol.* **85,** 21–38 (2012).

270. Cussler, E. L. Diffusion: Mass Transfer in Fluid Systems. *Engineering* **Second,** 580 (1997).

271. Corriou, J.-P. & Azzaro-Pantel, C. in *Green Process Engineering* 27–48 (CRC Press, 2015). doi:doi:10.1201/b18533-4

272. Brown, R. A brief account of microscopical observations made in the months of June, July, and August, 1827, on the particles contained in the pollen of plants; and on the general existence of active molecules in organic and inorganic bodies. *Edinb. New Philos. J.* **5,** 358–371 (1828).

273. Einstein, A. Investigations on the Theory of the Brownian Movement. *Annalen der Physik* **19,** 579 (1905).

274. Siegel, R. a. Random walks in biology. *Journal of Controlled Release* **32,** 201–202 (1994).

275. Robertson, R. M., Laib, S. & Smith, D. E. Diffusion of isolated DNA molecules: Dependence on length and topology. *Proc. Natl. Acad. Sci.* **103,** 7310–7314 (2006).

276. Purohit, P. K. *et al.* Forces during bacteriophage DNA packaging and ejection. *Biophys. J.*

88, 851–66 (2005).

277. Perrin, F. Mouvement Brownien d'un ellipsoide (II). Rotation libre et dépolarisation des fluorescences. Translation et diffusion de molécules ellipsoidales. *J. Phys. le Radium* **7,** 1–11 (1936).

278. Lukacs, G. L. *et al.* Size-dependent DNA mobility in cytoplasm and nucleus. *J. Biol. Chem.* **275,** 1625–1629 (2000).

279. Xu, X.-H. & Yeung, E. S. Direct Measurement of Single-Molecule Diffusion and Photodecomposition in Free Solution. *Science (80-.).* **275,** 1106–1109 (1997).

280. Rocha, R., Santos, R. S., Madureira, P., Almeida, C. & Azevedo, N. F. Optimization of peptide nucleic acid fluorescence in situ hybridization (PNA-FISH) for the detection of bacteria: The effect of pH, dextran sulfate and probe concentration. *J. Biotechnol.* **226,** 1–7 (2016).

281. Algotsson, M. *et al.* Sample preservation method and sample preservation substrate. (2017).

282. Hrabovszky, E. & Petersen, S. L. Increased concentrations of radioisotopically-labeled complementary ribonucleic acid probe, dextran sulfate, and dithiothreitol in the hybridization buffer can improve results of in situ hybridization histochemistry. *J. Histochem. Cytochem.* **50,** 1389–400 (2002).

283. Wahl, G. M., Stern, M. & Stark, G. R. Efficient transfer of large DNA fragments from agarose gels to diazobenzyloxymethyl-paper and rapid hybridization by using dextran sulfate. *Proc. Natl. Acad. Sci. U. S. A.* **76,** 3683–3687 (1979).

284. Silhavy, T., Kahne, D. & Walker, S. The bacterial cell envelope. *Cold Spring Harbor perspectives in biology* **2,** 1–16 (2010).

285. Mullineaux, C. W., Nenninger, A., Ray, N. & Robinson, C. Diffusion of green fluorescent protein in three cell environments in Escherichia coli. *J Bacteriol* **188,** 3442–3448 (2006).

286. Santos, R. S., Figueiredo, C., Azevedo, N. F., Braeckmans, K. & De Smedt, S. C. Nanomaterials and molecular transporters to overcome the bacterial envelope barrier:

Towards advanced delivery of antibiotics. *Adv. Drug Deliv. Rev.* (2017). doi:https://doi.org/10.1016/j.addr.2017.12.010

287. Chien, A.-C., Hill, N. S. & Levin, P. A. Cell Size Control in Bacteria. *Curr. Biol.* **22,** R340–R349 (2012).

288. van Meer, G., Voelker, D. R. & Feigenson, G. W. Membrane lipids: where they are and how they behave. *Nat. Rev. Mol. Cell Biol.* **9,** 112–124 (2008).

289. Katz, A. *et al.* Bacteria Size Determination by Elastic Light Scattering. *IEEE J. Sel. Top. QUANTUM Electron.* **9,** 277–287 (2003).

290. Zhao, L. *et al.* Intracellular water-specific MR of microbead-adherent cells: The HeLa cell intracellular water exchange lifetime. *NMR Biomed.* **21,** 159–164 (2008).

291. Grossman, N., Ron, E. A. & Woldringh, C. L. Changes in cell dimensions during amino acid starvation of Escherichia coli. *J. Bacteriol.* **152,** 35–41 (1982).

292. Mitra, K., Ubarretxena-Belandia, I., Taguchi, T., Warren, G. & Engelman, D. M. Modulation of the bilayer thickness of exocytic pathway membranes by membrane proteins rather than cholesterol. *Proc. Natl. Acad. Sci.* **101,** 4083–4088 (2004).

293. Bayer, M. E. Zones of membrane adhesion in the cryofixed envelope of Escherichia coli. *J. Struct. Biol.* **107,** 268–280 (1991).

294. Graham, L. L., Beveridge, T. J. & Nanninga, N. Periplasmic space and the concept of the periplasm. *Trends Biochem. Sci.* **16,** 328–329 (2017).

295. Beeby, M., Gumbart, J. C., Roux, B. & Jensen, G. J. Architecture and assembly of the Gram-positive cell wall. *Mol. Microbiol.* **88,** 664–672 (2013).

296. Vollmer, W. & Seligman, S. J. Architecture of peptidoglycan: more data and more models. *Trends Microbiol.* **18,** 59–66 (2010).

297. Angelova, M. I. & Tsoneva, I. Interactions of DNA with giant liposomes. *Chem. Phys. Lipids* **101,** 123–137 (1999).

298. Seltmann, G. & Holst, O. in (eds. Seltmann, G. & Holst, O.) 103–132 (Springer Berlin

Heidelberg, 2002). doi:10.1007/978-3-662-04878-8_3

299. Holst, O., Moran, A. P. & Brennan, P. J. in *Microbial Glycobiology* 1–13 (2010). doi:10.1016/B978-0-12-374546-0.00001-8

300. Bidnenko, E., Mercier, C., Tremblay, J., Tailliez, P. & Kulakauskas, S. Estimation of the state of the bacterial cell wall by fluorescent In situ hybridization. *Appl. Environ. Microbiol.* **64,** 3059–62 (1998).

301. Zimmerman, S. B. & Trach, S. O. Estimation of macromolecule concentrations and excluded volume effects for the cytoplasm of Escherichia coli. *J. Mol. Biol.* **222,** 599–620 (1991).

302. Fulton, A. B. How crowded is the cytoplasm? *Cell* **30,** 345–347 (1982).

303. Mastro, A. M., Babich, M. A., Taylor, W. D. & Keith, A. D. Diffusion of a small molecule in the cytoplasm of mammalian cells. *Proc. Natl. Acad. Sci.* **81,** 3414–3418 (1984).

304. Golding, I. & Cox, E. C. Physical nature of bacterial cytoplasm. *Phys. Rev. Lett.* **96,** (2006).

305. Kalwarczyk, T., Tabaka, M. & Holyst, R. Biologistics-Diffusion coefficients for complete proteome of Escherichia coli. *Bioinformatics* **28,** 2971–2978 (2012).

306. Kalwarczyk, T. *et al.* Comparative analysis of viscosity of complex liquids and cytoplasm of mammalian cells at the nanoscale. *Nano Lett.* **11,** 2157–2163 (2011).

307. van den Berg, J., Boersma, A. J. & Poolman, B. Microorganisms maintain crowding homeostasis. *Nat. Rev. Microbiol.* **15,** 309–318 (2017).

308. Kilså Jensen, K., Ørum, H., Nielsen, P. E. & Nordén, B. Kinetics for hybridization of peptide nucleic acids (PNA) with DNA and RNA studied with the BIAcore technique. *Biochemistry* **36,** 5072–5077 (1997).

309. No Title. Available at: http://www.thermofisher.com/pt/en/home/references/ambion-tech-support/rna-tools-and-calculators/macromolecular-components-of-e.html. (Accessed: 1st April 2017)

310. Noller, H. F. RNA structure: reading the ribosome. *Science* **309,** 1508–14 (2005).

311. Schoen, I., Krammer, H. & Braun, D. Hybridization kinetics is different inside cells. *Proc. Natl. Acad. Sci. U. S. A.* **106,** 21649–21654 (2009).

312. Eriksson, M., Nielsen, P. E. & Good, L. Cell permeabilization and uptake of antisense peptide-peptide nucleic acid (PNA) into Escherichia coli. *J. Biol. Chem.* **277,** 7144–7147 (2002).

313. Nikaido, H. Molecular basis of bacterial outer membrane permeability revisited. *Microbiol. Mol. Biol. Rev.* **67,** 593–656 (2003).

314. Lambert, P. a. Cellular impermeability and uptake of biocides and antibiotics in gram-positive bacteria and mycobacteria. *J Appl Microbiol* **92,** 46S–54S (2002).

315. Cooper, G. M. & Hausman, R. E. *The Cell: A Molecular Approach 2nd Edition*. *Sinauer Associates* (2007). doi:NBK9839

316. Koller, E. *et al.* Mechanisms of single-stranded phosphorothioate modified antisense oligonucleotide accumulation in hepatocytes. *Nucleic Acids Res.* **39,** 4795–4807 (2011).

317. Walton, S. P., Stephanopoulos, G. N., Yarmush, M. L. & Roth, C. M. Thermodynamic and Kinetic Characterization of Antisense Oligodeoxynucleotide Binding to a Structured mRNA. *Biophys. J.* **82,** 366–377 (2002).

318. Ridgway, D. *et al.* Coarse-Grained Molecular Simulation of Diffusion and Reaction Kinetics in a Crowded Virtual Cytoplasm. *Biophys. J.* **94,** 3748–3759 (2008).

319. De Los Santos, C., Chang, C.-W., Mycek, M.-A. & Cardullo, R. A. FRAP, FLIM, and FRET: Detection and analysis of cellular dynamics on a molecular scale using fluorescence microscopy. *Mol. Reprod. Dev.* **82,** 587–604 (2015).

320. Schlessinger, J., Axelrod, D., Koppel, D. E., Webb, W. W. & Elson, E. L. Lateral transport of a lipid probe and labeled proteins on a cell membrane. *Science (80-.).* **195,** 307 LP-309 (1977).

321. Carisey, A., Stroud, M., Tsang, R. & Ballestrem, C. in (eds. Wells, C. M. & Parsons, M.) 387–402 (Humana Press, 2011). doi:10.1007/978-1-61779-207-6_26

322. Ausubel, F. M. *et al. Current Protocols in Molecular Biology*. *John Wiley Sons New York N Y* **1,** (1994).

323. National Toxicology, P. Toxicology and carcinogenesis studies of formamide (Cas No. 75-12-7) in F344/N rats and B6C3F1 mice (gavage studies). *Natl Toxicol Progr. Tech Rep Ser* 1–192 (2008).

324. Matthiesen, S. H. & Hansen, C. M. Fast and non-toxic in situ hybridization without blocking of repetitive sequences. *PLoS One* **7,** e40675 (2012).

325. Lawson, T. S., Connally, R. E., Vemulpad, S. & Piper, J. a. Dimethyl formamide-free, urea-NaCl fluorescence in situ hybridization assay for Staphylococcus aureus. *Lett. Appl. Microbiol.* **54,** 263–6 (2012).

326. Simard, C., Lemieux, R. & Côté, S. Urea substitutes toxic formamide as destabilizing agent in nucleic acid hybridizations with RNA probes. *Electrophoresis* **22,** 2679–83 (2001).

327. Souleimanian, N. *et al.* Antisense 2′-Deoxy, 2′-Fluoroarabino Nucleic Acid (2′F-ANA) Oligonucleotides: In Vitro Gymnotic Silencers of Gene Expression Whose Potency Is Enhanced by Fatty Acids. *Mol. Ther. - Nucleic Acids* **1,** e43 (2012).

328. Stein, C. A. *et al.* Efficient gene silencing by delivery of locked nucleic acid antisense oligonucleotides, unassisted by transfection reagents. *Nucleic Acids Res.* **38,** (2009).

329. Järver, P. *et al.* Peptide-mediated Cell and In Vivo Delivery of Antisense Oligonucleotides and siRNA. *Mol. Ther. - Nucleic Acids* **1,** e27 (2012).

330. Polushin, N. N. & Cohen, J. S. Antisense pro-drugs: 5’-ester oligodeoxynucleotides. *Nucleic Acids Res.* **22,** 5492–5496 (1994).

331. Liu, J. *et al.* Spheroid body-forming cells in the human gastric cancer cell line MKN-45 possess cancer stem cell properties. *Int. J. Oncol.* **42,** 453–459 (2013).

332. Gallas, J. M. & Eisner, M. Fluorescence of Melanin-Dependence upon Excitation Wavelength and Concentration. *Photochem. Photobiol.* **45,** 595–600 (1987).

333. Ko, H. Y. *et al.* A color-tunable molecular beacon to sense miRNA-9 expression during

neurogenesis. *Sci. Rep.* **4,** 4626 (2015).

334. Yoo, B. *et al.* In Vivo Detection of miRNA Expression in Tumors Using an Activatable Nanosensor. *Mol. Imaging Biol.* **18,** 70–78 (2016).

335. Ardekani, A. M. & Naeini, M. M. The role of microRNAs in human diseases. *Avicenna Journal of Medical Biotechnology* **2,** 161–179 (2010).

336. Li, X., Wang, L., Li, G., Zheng, X. & Duan, C. Expression of miR-204 and MMP-9 in Helicobacter pylori-associated gastric ulcer. *Int. J. Clin. Exp. Med.* **9,** 7928–7936 (2016).

337. Hayashi, Y. *et al.* CagA mediates epigenetic regulation to attenuate let-7 expression in Helicobacter pylori-related carcinogenesis. *Gut* **62,** 1536 LP-1546 (2013).

338. Shiotani, A. *et al.* H. pylori eradication did not improve dysregulation of specific oncogenic miRNAs in intestinal metaplastic glands. *J. Gastroenterol.* **47,** 988–998 (2012).

339. Oertli, M. *et al.* MicroRNA-155 Is Essential for the T Cell-Mediated Control of Helicobacter pylori Infection and for the Induction of Chronic Gastritis and Colitis. *J. Immunol.* **187,** 3578 LP-3586 (2011).

340. Zhang, X., Bloch, S., Akers, W. & Achilefu, S. Near-infrared Molecular Probes for In Vivo Imaging. *Curr. Protoc. Cytom.* **CHAPTER,** Unit12.27-Unit12.27 (2012).

341. Zeng, Z. *et al.* Specific and sensitive tumor imaging using biostable oligonucleotide aptamer probes. *Theranostics* **4,** 945–952 (2014).

342. Liu, Y., Tseng, Y. & Huang, L. Biodistribution Studies of Nanoparticles Using Fluorescence Imaging: A Qualitative or Quantitative Method? *Pharm. Res.* **29,** 3273–3277 (2012).

343. Fluiter, K. *et al.* In vivo tumor growth inhibition and biodistribution studies of locked nucleic acid (LNA) antisense oligonucleotides. *Nucleic Acids Res.* **31,** 953–962 (2003).

344. Kang, W. J. *et al.* Molecular beacon-based bioimaging of multiple microRNAs during myogenesis. *Biomaterials* **32,** 1915–1922 (2011).

345. Yao, Q. *et al.* Novel molecular beacons to monitor microRNAs in non-small-cell lung cancer. *Mol. Cell. Probes* **26,** 182–187 (2012).

346. Hwang, D. W., Song, I. C., Lee, D. S. & Kim, S. 81-88 Smart magnetic fluorescent nanoparticle imaging probes to monitor MicroRNAs. *Small* **6,** 81–88 (2010).

347. Jo, M. hee *et al.* A reverse complementary multimodal imaging system to visualize microRNA9-involved neurogenesis using peptide targeting transferrin receptor-conjugated magnetic fluorescence nanoparticles. *Biomaterials* **33,** 6456–6467 (2012).

348. Oliveira, V. C. *et al.* Sudan Black B treatment reduces autofluorescence and improves resolution of in situhybridization specific fluorescent signals of brain sections. *Histol. Histopathol.* **25,** 1017–1024 (2010).